

EFFECTS OF CELL ENTRAPMENT IN CA-ALGINATE
ON THE METABOLISM OF YEAST
SACCHAROMYCES CEREVISIAE

Thesis by
Jorge Luis Galazzo

In Partial Fulfillment of the Requirements
for the Degree of
Doctor of Philosophy

Department of Chemical Engineering
California Institute of Technology
Pasadena, California USA

1989

(Submitted November 21, 1988)

© 1989

Jorge L. Galazzo

All Rights Reserved

To Patricia

Paula and Juan Andrés

ACKNOWLEDGEMENTS

I would like to express my gratitude to Jay Bailey, my advisor, for his guidance and support during my work in this project. His enthusiasm and vision helped me to shape my ideas into a coherent form. I hope I will be able to apply all I have learned from him in my future work.

I appreciated the NMR discussions with Frances Arnold. She provided me with some good ideas about how to use NMR. Jackie Shanks shared many of her ideas and techniques with me, which I also appreciated. Thanks are given to the people of the Regional NMR facility at Caltech for their assistance in my training in the NMR technique.

It has been a pleasure to work in the Bailey's research group all this years. Ken Reardon showed me my way around the lab. Alex Seressiotis introduced me into the computer world. I shared my office with several people, but I would like to mention Elis Andersson and Staffan Birnbaum in particular. I have learned many things from them.

The financial assistance of CONICET in my first year of study is acknowledged. I greatly appreciated the economical support that Caltech provided in the last years of my work.

Much love and thanks are given to my dearest ones: Patricia, Paula and Juan Andrés. We have shared many things in this process which helped us to grow as a family. I also acknowledge the influence of Mom and Dad who taught me how to deal with obstacles. Finally, thanks you God.

ABSTRACT

Saccharomyces cerevisiae cells grown in suspension have been immobilized in calcium-alginate beads. Fermentation rates and intracellular composition have been determined under nongrowing conditions in these Ca-alginate entrapped cells and for identical cells in suspension. Glucose uptake and ethanol and glycerol production are approximately two times faster in immobilized cells than in suspended cells. Intermediate metabolite levels such as fructose-1,6-diphosphate, glucose-6-phosphate and 3-phosphoglycerate have been determined by phosphorus-31 nuclear magnetic resonance (NMR) spectroscopy under glucose fermenting conditions. Results show a different sugar phosphate composition in immobilized cells. Also, at steady-state glucose fermentation, the intracellular pH of entrapped cells is lower as indicated by the chemical shift of the intracellular inorganic phosphorus resonance. Carbon-13 NMR shows an increase in polysaccharide production in immobilized cells.

S. cerevisiae cells grown within a Ca-alginate matrix have a specific growth rate 40% lower than the growth rate of similar cells cultivated in suspension. Alginate-grown cells have been used to compare glucose fermentation under nongrowing conditions in suspended and Ca-entrapped cells. Fermentation rate is higher in immobilized cells than in suspended cells. The observed differences in intracellular components between suspended and immobilized cells are qualitatively similar to the differences observed for cells grown in suspension. Ethanol

production rate is 2.7 times faster in immobilized alginate-grown cells than in suspended suspension-grown cells.

These results suggest that cell immobilization is affecting cell metabolism at different levels. Catabolic regulation is altered as indicated in the nongrowing condition experiments. Also, anabolic regulation is altered as suggested by the changes in growth rate observed in cells growing within the immobilization matrix. The combination of these experimental determinations with knowledge of the metabolic pathways involved in *S. cerevisiae* allows the development of a quantitative *in vivo* description of most key pathway enzymes involved in yeast glucose catabolism. The evaluation of flux-control coefficients for all these steps indicates that alginate entrapment of suspension-grown cells increases the glucose uptake rate and shifts the step most influencing ethanol production from glucose uptake to phosphofructokinase. In alginate-grown cells, glucose uptake is limiting ethanol production in both suspended and immobilized cells. There is a 5% decrease in the glucose uptake flux-control coefficient of immobilized cells due to an increment in the glucose uptake rate. This increment increases ethanol production by approximately 100%.

An analysis of the anticipated effects of genetic manipulation to improve the ethanol production rate in yeast *S. cerevisiae* using the framework of the metabolic control theory indicates that in suspended suspension-grown cells the highest improvement is obtained by increasing the activity of glucose transport, whereas in immobilized suspension-grown cells the greatest enhancement is obtained by incrementing the maximum activity of phosphofructokinase. This indicates that the metabolic engineering strategy to be used in order to enhance

any properties in the cell will depend not only on the specific microorganism, but also on the environmental conditions in which it is placed. In conditions where several steps share the flux control in a pathway, a substantial enhancement in pathway rate will be possible only if the activities of all those steps are increased simultaneously.

TABLE OF CONTENTS

Acknowledgements	iv
Abstract	v
List of Figures	xii
List of Tables	xv
CHAPTER 1: Introduction	1
References	8
CHAPTER 2: <i>In vivo</i> nuclear magnetic resonance analysis of immobilization effects on glucose metabolism of yeast <i>Saccharomyces cerevisiae</i>	10
Abstract	11
Introduction	12
Materials and methods	14
Organism	14
Culture and sample preparation.....	14
Nuclear magnetic resonance (NMR) spectroscopy	16
Analyses	17
Results	18
Overall fermentation kinetics.....	18
Assessment of mass transport effects on observed kinetics.....	20
Stimulus-response NMR measurements	23

Analysis of quasi-steady state metabolite concentrations	26
Influence of extracellular pH on fermentation kinetics and intracellular state	32
Discussion	32
Acknowledgements	35
References	36
CHAPTER 3: Study of glucose metabolic kinetics of suspended and immobilized <i>Saccharomyces cerevisiae</i> cells grown in Calcium-alginate beads	39
Abstract	40
Introduction	41
Materials and methods	42
Organism	42
Culture and sample preparation	43
Reactor system	44
Experimental procedure	44
Nuclear magnetic resonance (NMR) spectroscopy	47
Analyses	48
Results	49
Growth rate of immobilized cells	49
Fermentation kinetics of immobilized-grown cells	51
Phosphorus-31 NMR measurements	53
Discussion	58

Acknowledgements	64
References	65
CHAPTER 4: Fermentation pathway kinetics and metabolic flux control in suspended and immobilized <i>Saccharomyces cerevisiae</i>	68
Abstract	69
Introduction	70
Model description	72
Quasi-steady state flux relationships	75
Estimation of <i>in vivo</i> rate parameters for key pathway reactions	76
Metabolic control theory	94
Results and discussion	96
Acknowledgements	102
References	103
CHAPTER 5: Analysis of the potential for improving yeast <i>Saccharomyces cerevisiae</i> fermentation activity by metabolic engineering	107
Abstract	108
Introduction	109
Results	111
Effects of altering the glucose uptake step	112
Effects of altering phosphofructokinase maximum activity	115
Effects of altering ATP consumption rate	118

Discussion	121
References	125
CHAPTER 6: Conclusions	126
APPENDIX A: Application of linear prediction singular value decomposition for processing <i>in vivo</i> NMR data with low signal-to-noise ratio.....	130
Abstract	131
Introduction	132
Materials and methods.....	134
Linear prediction singular value decomposition method.....	136
Results	137
Low cell density experiments.....	137
Short time acquisition experiments.....	141
Discussion	145
Acknowledgements	145
References	146
APPENDIX B: Comparison of intracellular sugar phosphate levels of intact cells and perchloric cell extracts using phosphorus-31 NMR	148
Abstract.....	149
Introduction	150
Materials and methods.....	150
Yeast strains	150

Culture and NMR preparation	151
Assay	151
Data processing	153
Estimation of sugar phosphate concentrations	154
Results	154

LIST OF FIGURES

Figure 2.1: Ethanol concentration as a function of time for suspended and entrapped cells.....	19
Figure 2.2: ^{31}P NMR spectrum of immobilized cells for steady-state glucose fermentation.....	24
Figure 2.3: Transient ^{31}P NMR spectra for a step in glucose concentration for suspended and entrapped cells.....	25
Figure 2.4: Comparison of the downfield region of ^{31}P NMR spectrum of suspended and immobilized cells.....	27
Figure 2.5: ^{13}C NMR spectra of suspended and immobilized cells	28
Figure 3.1: Immobilized cell recirculation reactor	45
Figure 3.2: Cell concentration data for <i>Saccharomyces cerevisiae</i> growing in a recirculation reactor	50
Figure 3.3: Glucose and ethanol concentrations in recirculation medium	52
Figure 3.4: Ethanol production by <i>S. cerevisiae</i> cells.....	55
Figure 3.5: Comparison of ^{31}P spectra of cells resting in starvation buffer	56
Figure 3.6: ^{31}P NMR spectra of <i>S. cerevisiae</i> cells entrapped in Ca-alginate	57
Figure 3.7: ^{31}P spectra of <i>S. cerevisiae</i> cells grown in Ca-alginate beads at steady-state glucose metabolism	59
Figure 4.1: Anaerobic fermentation pathway of <i>S. cerevisiae</i>	74
Figure 4.2: Least-squares fitting for estimation of hexokinase kinetic parameters	79

Figure 4.3: Glycogen synthetase maximum velocity as a function of glucose-6-phosphate <i>in vivo</i> concentration	83
Figure 4.4: pH model dependence of phosphofructokinase allosteric constant	85
Figure 4.5: Comparison of experimental and calculated phosphofructokinase reaction rates	87
Figure 4.6: pH model dependence of pyruvate kinase allosteric constant and phosphoenolpyruvate binding constant.....	90
Figure 4.7: Comparison of experimental and calculated pyruvate kinase reaction rates	92
Figure 5.1: Flux-control coefficients as a function of glucose uptake velocity.....	113
Figure 5.2: Ethanol production rate as a function of glucose uptake velocity.....	114
Figure 5.3: Flux-control coefficients as a function of phosphofructokinase maximum activity.....	116
Figure 5.4: Ethanol production rate as a function of phosphofructokinase maximum activity.....	117
Figure 5.5: Flux-control coefficients as a function of ATPase kinetic constant	119
Figure 5.6: Ethanol production rate as a function of ATPase kinetic constant	120
Figure 5.7: Ethanol production rate for alginate-grown cells as a function of glucose uptake velocity	124
Figure A.1: Low-cell density ³¹ P NMR spectra.....	138
Figure A.2: Percent deviation of metabolite concentrations for the low-cell density data	140
Figure A.3: Comparison of the downfield region of the 15-sec scan data	143

Figure A.4: Percent deviation of metabolite concentrations for the 15-sec scan data.....	144
Figure B.1: <i>In vivo</i> and perchloric acid extract ³¹ P NMR spectra of <i>S. cerevisiae</i> ATCC 18790	155
Figure B.2: Downfield region of <i>in vivo</i> and perchloric acid extract ³¹ P NMR spectra of <i>S. cerevisiae</i> ATCC 18790 cells.....	156
Figure B.3: Downfield region of <i>in vivo</i> and perchloric acid extract ³¹ P NMR spectra of <i>S. cerevisiae</i> D603 cells	157
Figure B.4: <i>In vivo</i> vs. <i>in vitro</i> relative levels of various sugar phosphate compounds	158

LIST OF TABLES

Table 2.I: Substrate uptake and product formation rates for suspended and immobilized cells	20
Table 2.II: Comparison of intermediate metabolite concentrations of cells grown in suspension.....	31
Table 3.I: Substrate uptake and product formation rates for cells grown within a Ca-alginate matrix.....	53
Table 3.II: Comparison of intermediate metabolite concentrations of cells grown in a Ca-alginate matrix.....	58
Table 3.III: Ethanol production ratios as functions of growth and biocatalyst state.....	62
Table 4.I: Experimental data summary for suspension-grown cells.....	72
Table 4.II: ATP, ADP and ATP concentrations	77
Table 4.III: Hexokinase kinetic expression.....	80
Table 4.IV: Glycogen synthetase kinetic expression.....	81
Table 4.V: Phosphofructokinase kinetic expression	84
Table 4.VI: Glyceraldehyde 3-phosphate dehydrogenase kinetic expression.....	88
Table 4.VII: Pyruvate kinase kinetic expression	89
Table 4.VIII: Model parameter values	93
Table 4.IX: Flux-control coefficients of suspension-grown cells	97
Table 4.X: Flux-control coefficients for the branches going to polysaccharide and glycerol	99

Table 4.XI: Concentration-control coefficients of suspension-grown cells	101
Table 5.I: Flux-control coefficient summary	110
Table A.I: Metabolite concentration estimation by FFT and by LPSVD using the low-cell density data	139
Table A.II: Metabolite concentration estimation by FFT and by LPSVD using the 15-sec scan data	142
Table B.I: Comparison of cell extract vs. <i>in vivo</i> determinations	160

CHAPTER 1

INTRODUCTION

The use of immobilized cells as biocatalysts is a widely employed method to produce chemicals that require biotransformations of raw materials. Several processes that use immobilized cells are now well established on an industrial scale, such as the production of L-aminoacids⁽¹⁾ and ethanol.^(1,2)

Cell immobilization has been the subject of several reviews in the literature. Industrial applications of immobilized cells,^(1,2) engineering principles concerning reaction engineering,^(3,4) mass transfer and kinetics,^(5,6) and reactor design,⁽⁷⁾ are among the topics most frequently addressed.

Whole-cell immobilization is defined as "the physical confinement or localization of intact cells to a certain defined region of space with the preservation of some desired catalytic activity."⁽³⁾ The system to confine the cells within a region may be chemical, such as in surface attachment methods, or physical, such as in gel entrapment methods. A classification of cell immobilization procedures based on the utilized immobilization mechanism is given below:⁽³⁾

- attachment to surfaces, either by physical adsorption or by chemical bonds;
- entrapment within porous matrices, such as preformed supports or gel entrapment;
- containment behind a barrier, such as synthetic membranes, microencapsulation, or two-phase emulsions;
- self-aggregation, either by natural cell aggregation or artificially induced (e.g., glutaraldehyde cross-linking).

Immobilized cell systems have desirable properties that are not readily achieved in conventional batch and/or continuous systems employing free cells. Immo-

bilized cells offer the possibility to operate the bioreactor using high cell concentrations and high dilution rates without the risk of "washout." Also, less downstream processing is required because the products leaving the reactor are relatively free of cells. Metabolic manipulation of organisms through environmental control is one of the most attractive attributes of immobilized cell systems.⁽⁸⁾ Cell immobilization decouples cell growth and product formation. Thus, cell metabolism may be more easily controlled with less influence from biosynthetic processes. However, an understanding of the interactions between the cell and the immobilization process is essential. Only then can the biocatalyst designer and formulator be able to conveniently manipulate the cell environment, and thus optimize the output from such systems.

Immobilization can alter the metabolic activity of the cells because physical stresses that closely packed cells exert on one another and on the support are not present in traditional fermentations. Also, biological responses to cell surface contact with the support or with other cells may be involved, as may local concentrations of trace extracellular products. Many investigations on immobilized cells have shown that immobilization sometimes affects cellular metabolism. Growth rate, substrate uptake, and product formation in immobilized cells are often different from those of cells in suspension cultures.⁽⁹⁻¹⁰⁾ Also, cellular composition is affected by immobilization as indicated by larger quantities of reserve carbohydrates and structural polysaccharides found in immobilized cells than in suspended cells.⁽¹¹⁾

When cells are immobilized in a confined space and are allowed to grow, interactions with other cells and/or with the immobilization matrix may affect

cellular morphology and may interfere with the organism reproduction. Morphology alterations have been observed in a system composed of *Escherichia coli* retained between two microporous membranes.⁽¹²⁾ Nutrient medium is circulated on one side of the device, and on the other side the pressure exerted by the cells on the membrane is measured. The specific cell volume of the growing cells has been found to be 25% lower than the volume of similar cells growing in suspension. This indicates that the pressure generated by closely packed growing cells, which in this case increases to 3.3 atm, may be important in cell metabolic regulation.

Usually, the study of immobilized cells has been done by performing a series of experiments and by correlating cause and effect in the observed results. Optimization of the immobilized cell system is then based on those observations. This trial-and-error approach has usually been done using ill-defined systems, which makes extrapolation of the results difficult.

The design of the experimental setup is of critical importance when studying the various parameters that might influence the metabolic regulation of immobilized cells. Mass transfer limitation has to be reduced to a minimum, if not eliminated, in order to analyze the intrinsic cell kinetics of immobilized cells.⁽¹¹⁾ The study of cell metabolic regulation requires the estimation of metabolite concentrations inside the cell.⁽⁸⁾ This is one of the main problems with the study of immobilized cells. Usually the cells have to be released from the immobilization matrix, and then the intracellular components determined.^(11,13) If the metabolism is not blocked during this period, the cell may degrade some of its

components, leading to misinterpretation of the results. Also, this methodology is destructive, and the same sample may not be used in transient experiments.

The development of new experimental techniques,⁽⁸⁾ such as fluorescence measurements^(14,15) and *in vivo* nuclear magnetic resonance (NMR) spectroscopy,⁽¹⁶⁻¹⁸⁾ allows noninvasive, multicomponent determinations of intracellular concentrations. In particular, NMR is very useful for comparing suspended and immobilized cell metabolism since intermediate metabolite levels, and other important variables such as intracellular pH, can be estimated using the intact, immobilized cell matrix.

NMR allows the simultaneous observation of all mobile compounds. This permits the detection of metabolism not predicted beforehand, which may be missed by more conventional methods of analysis. The most suitable nucleus for NMR observation in living cells is phosphorus-31 because it is a natural isotope and most of the more important phosphorylated compounds in the cell may be observed: intracellular inorganic phosphate, extracellular inorganic phosphate, sugar phosphates, ATP, NAD⁺/NADH, and polyphosphates.^(17,18) Another important nucleus used in *in vivo* NMR is carbon-13. The natural abundance of ¹³C is only 1.1%, and enriched compounds are usually employed to enhance signal detection.⁽¹⁹⁾ One of the advantages of ¹³C NMR is that it is possible to detect which pathways are active in the cell under different conditions, using the appropriate labelled substrate.⁽¹⁹⁾ A disadvantage of NMR is its inherent lack of sensitivity.^(20,21) This requires the use of samples with high cell densities compared to that in growing cultures. However, reasonable intracellular concentration estimates from lower cell density samples can be obtained by treating

the NMR data by linear prediction singular value decomposition techniques as is discussed in Appendix A. This will allow NMR analysis of diluted cell samples resembling more closely bioreactor conditions.

The immobilization method used in this work is cell entrapment within a calcium-alginate matrix. The system has been designed to minimize mass transfer limitations in order to study the intrinsic effects of immobilization on cell metabolism. Cell entrapment in Ca-alginate is simple to perform. Also, high cell densities may be obtained in relatively small sample volumes without significant loss of cell viability. Furthermore, cell release from the immobilization matrix is relatively easy to accomplish. This makes possible the quantification of the total cell density within the biocatalyst, and therefore the expression of the results in a per-cell-mass basis.

Saccharomyces cerevisiae is the organism used in this work. It is one of the best characterized yeasts and its biochemistry is well known.^(22,23) This simplifies the identification of any differences between suspended and immobilized cells. The effects of cell entrapment on the glucose metabolism of nongrowing *S. cerevisiae* cells are discussed in Chapter 2. Under these conditions, glucose fermentation kinetics is decoupled from biosynthetic pathways such as DNA, RNA or protein formation. Cell growth within the immobilization matrix is analysed and discussed in Chapter 3 using the same methodology applied in Chapter 2.

The experimental information is used in Chapter 4, combined with knowledge of the metabolic pathways involved in *S. cerevisiae*, to develop a detailed description of the kinetics of glucose metabolism in yeast for *in vivo* con-

ditions. Kinetic representations of hexokinase, phosphofructokinase, glycogen synthetase, glyceraldehyde 3-phosphate dehydrogenase, and pyruvate kinase are included in the model. This quantitative description of the pathway shows the effects of cell immobilization on *S. cerevisiae* glucose catabolism.

In Chapter 5, a strategy to increase yeast fermentation characteristics is discussed using the kinetic model of Chapter 4. The methodology used is general, and it may be used for studying alterations in cell metabolism due to any modifications (environmental or genetic) performed in the cell. It also provides a strategy for the optimal genetic manipulation of a microorganism towards improvement of its productivity and/or any other property of interest.

REFERENCES

1. Linko P., and Linko Y., *CRC Crit. Rev. Biotechnol.*, **1**, 289 (1983).
2. Margaritis A., and Merchant F., *CRC Crit. Rev. Biotechnol.*, **1**, 339 (1983).
3. Karel S., Libiki S., and Robertson C., *Chem. Eng. Sci.*, **40**, 1321 (1985).
4. Venkatasubramanian K., Karkare S., and Vieth W., *Appl. Biochem. Bioeng.*, **4**, 312 (1983).
5. Radovich J., *Biotechnol. Adv.*, **3**, 1 (1985).
6. Engasser J., and Hovath C., *Appl. Biochem. Bioeng.*, **1**, 127 (1976).
7. Buchholz K., In: "*Advances in Biochemical Engineering*", Fiechter J. Ed., pp. 39-71, (1982).
8. Bailey J., Axe D., Doran P., Galazzo J., Reardon K., Seressiotis A., and Shanks J., *Ann. N.Y. Acad. Sci.*, **506**, 1 (1987).
9. Koshcheyenko K., Turkina M., and Skryabin G., *Enzyme Microb. Technol.*, **5**, 14 (1983).
10. Inloes D. S., Smith W. S., Taylor D. P., Cohen S. N., Michaels A. S., and Robertson C. R., *Biotechnol. Bioeng.*, **23**, 79 (1981).
11. P. M. Doran and J. E. Bailey, *Biotechnol. Bioeng.*, **28**, 73 (1986).
12. Fowler J., and Robertson C., "*Nutrient transport and cellular morphology in immobilized cell aggregates*", Engineering Foundation Conference.

- Biochemical Engineering VI, Oct. 2-7th., Santa Barbara, (1988).
13. Hattori R., Hattori T., and Furusaka C., *J. Gen. Appl. Microbiol.*, **18**, 271 (1972).
 14. Zabriskie D., and Humphrey A., *Appl. Environ. Microbiol.*, **35**, 337 (1979).
 15. Scheper T., and Schugerl K., *Appl. Environ. Microbiol.*, **23**, 440 (1986).
 16. Navon G., Shulman R., Yamane T., Ecclesball T., Lam K., Baronotsky J., and Marmur J., *Biochemistry*, **18**, 4487 (1979).
 17. den Hollander J., Ugurbil K., Brown T., and Shulman R., *Biochemistry*, **20**, 5871 (1981).
 18. Shanks J., and Bailey J., *Biotechnol. Bioeng.*, in press, (1988).
 19. Gadian D., In: "*Nuclear Magnetic Resonance and its Application to Living Systems*", Oxford Univ. Press, Oxford, (1982).
 20. Burk S., and Shulman R., *Ann. Rev. Microbiol.*, **41**, 595 (1987).
 21. Fernandez E., and Clark D., *Enzyme Microb. Technol.*, **9**, 259 (1987).
 22. Strathern J., Jones E., Brioach J., (eds.), "*The Molecular Biology of the Yeast Saccharomyces.*", Cold Spring Harbor Lab., (1982).
 23. Rose A., and Harrison J., (eds.), "*The Yeasts*", vol. 1 and 2, Academic Press, London, (1971).

CHAPTER 2

IN VIVO NUCLEAR MAGNETIC RESONANCE ANALYSIS
OF IMMOBILIZATION EFFECTS ON GLUCOSE METABOLISM
OF YEAST *SACCHAROMYCES CEREVISIAE*

ABSTRACT

Fermentation rates and intracellular compositions have been determined for alginate-entrapped *Saccharomyces cerevisiae* and for identical cells in suspension. Glucose uptake and ethanol and glycerol production are approximately two times faster in immobilized cells than in suspended cells. Phosphorus-31 nuclear magnetic resonance (NMR) spectroscopy of fermenting immobilized and suspended cells shows differences in intermediate metabolite levels such as fructose-1,6-diphosphate, glucose-6-phosphate and 3-phosphoglycerate and in internal pH. Carbon-13 NMR shows an increase in polysaccharide production. These data suggest that immobilization has accelerated the rate of glucose transport or of glucose phosphorylation. The effects of immobilization upon cell metabolism are observed in a very short period of time under conditions in which negligible DNA, RNA or protein synthesis takes place.

INTRODUCTION

Environmental control has been shown to be a very convenient method to alter and regulate cell product formation.^(1,2) In particular, cell immobilization enables continuous bioconversion without the requirement of simultaneous cell growth. There is evidence in that immobilization can cause qualitative changes in cellular function and composition.⁽³⁻¹⁰⁾ It is presently impossible to predict whether immobilized cell metabolism will follow the same patterns as in the freely suspended organism. More information is needed on the details of immobilization effects on cell function.

Immobilized cells are usually in contact with a solid surface or matrix and/or with other cells. Such interactions may affect cellular morphology⁽⁴⁻⁶⁾ and may physically constrain reproduction of the organism. Unusual cell morphology has been observed in immobilized yeast entrapped in polyacrylamide gel⁽⁵⁾ and in hollow fiber membranes,⁽⁶⁾ indicating that the pressure exerted by closely packed growing cells on one another and on the support may be important in cell reproduction and function. Specific biological responses based on external receptor interactions with neighboring surfaces or cells may also be involved. Immobilized cells often operate within a chemical environment different from that of the external medium, and this could also influence metabolic kinetics.

Most often, activities and yields for immobilized cells are found to be reduced compared with suspended cells. In some systems, however, rate enhancement occurs. Higher specific rates of productivity and glucose consumption for immobilized cells compared with suspended cells have been reported.⁽⁷⁻¹⁰⁾ Increase in glucose uptake and ethanol production have been found in *Saccharomyces cerevisiae* cells immobilized on crosslinked gelatin.⁽¹⁰⁾ Specific ethanol production was 40-50% greater for immobilized cells than for suspended cells, and the immobilized cells consumed glucose twice as fast as the suspended cells.

Larger quantities of reserve carbohydrates and structural polysaccharides have been found in immobilized cells than in suspended cells,⁽¹⁰⁾ indicating that cellular composition is also affected by immobilization. *S. cerevisiae* grown on a gelatin surface are polyploid⁽¹⁰⁾ and exhibit dynamic responses of reduced pyridine nucleotides different from those of yeast grown in suspension.⁽¹¹⁾

This research provides enhanced experimental detail on the influence of immobilization on metabolic kinetics of fermenting *S. cerevisiae*. Macroscopic determinations of substrate and product concentrations as functions of time after glucose addition are combined with nuclear magnetic resonance (NMR) spectroscopy, a non-invasive technique that allows *in vivo* estimation of intermediate metabolites' concentrations. NMR is particularly useful for comparing suspended and immobilized cell metabolism because intermediate metabolite levels and intracellular pH can be estimated using the intact, immobilized cell matrix.

MATERIALS AND METHODS

Organism

Saccharomyces cerevisiae ATCC 18790, a standard diploid strain, was obtained from the American Type Culture Collection. The stock culture was maintained on yeast extract, peptone and glucose agar plates at 4°C.

Culture and sample preparation

S. cerevisiae cells were grown as described previously⁽¹²⁾ in a rotary shaker at 30°C in a medium of the following composition: 1% yeast extract, 2% peptone, and 2% glucose, adjusted to pH 4.5 with citrate buffer (50 mM). A preculture (4 mL) was inoculated with one loop of cells and cultivated for 12-15 h. The preculture was used to inoculate the main culture (400 mL) in 1-L flasks. Mid-exponential phase cells (50% of growth saturation) were chilled in an ice bath to 4°C under manual shaking. The cells were harvested by low-speed centrifugation at 4°C and washed with 150 mL of wash medium per mL of cell pellet. (0.85 g/L H₂KPO₄, 0.15 g/L HK₂PO₄, 0.5 g/L MgSO₄·7H₂O, 0.5 g/L NaCl in 50 mM MES buffer for the pH 5.5 experiments, and in 50 mM tartrate buffer for the pH 4.5 experiments.)

The cell pellet was either resuspended in resuspension medium (wash medium supplemented with 7.5 mM P_i and 1% CaCl₂) at the desired cell concentration, or used further in the immobilization. For immobilization, the cell

pellet was resuspended in wash medium supplemented with 7.5 mM P_i at twice the desired cell concentration and mixed with an equal volume of 4% Na-alginate. The homogeneous mixture was filled into a cylindric reservoir and compressed nitrogen gas was used to force the solution through a small tube (0.8 mm in diameter). A coaxial tube with a larger diameter (1.8 mm) was used to blow off the alginate droplets into 2% $CaCl_2$ solution at a controlled size by a compressed concentric air stream.⁽¹³⁾ Beads that formed (*ca.* 1 mm in median diameter) were allowed to cure for 0.5 h. Then the beads were washed and stored in re-suspension medium. All samples were kept on ice until they were used (always less than 2 hours).

The samples consisted of 2 mL of cell suspension (cell density *ca.* 0.5 gr_{wet}/mL) or Ca-alginate beads (cell density *ca.* 0.3 gr_{wet}/mL) in 10-mm o.d. NMR sample tubes. In the suspended cell experiments, N_2 gas was bubbled through the cell suspension using the two-bubbler scheme described by den Hollander *et al.*⁽¹⁴⁾ (one bubbler at the bottom of the NMR tube generated small bubbles at a rate of 10 mL/min while a second bubbler generated bubbles above the level of the NMR detection coils at *ca.* 100 mL/min). In the immobilized cell experiments, a perfusion device allowed medium circulation through the NMR tube containing the Ca-alginate immobilized cells. The perfusion device consisted of a threaded 10-mm o.d. NMR tube (Wilmad Glass Co.) in which two capillary tubes were inserted, one in the bottom of the packed bed formed by the beads, and the other in the top of the packed bed. A peristaltic pump circulated the medium to and from a reservoir vessel outside the NMR magnet, in

which N₂ gas was bubbled at *ca.* 300 mL/min. All experiments were conducted anaerobically.

Nuclear Magnetic Resonance (NMR) spectroscopy

NMR spectra were obtained in the Fourier-transform mode on a Bruker WM-500 spectrometer at 20°C. ³¹P NMR spectra were obtained at 202.46 MHz and were accumulated in 3 min blocks (360 scans) using 70° pulses and a repetition time of 0.5 sec. The chemical shifts were measured with glycerol phosphorylcholine (GPC) as internal standard, which resonates at 0.49 ppm from 85% phosphoric acid (0 ppm) with upfield shifts given a negative sign. Peak resonance assignments were made from the literature.^(12,14-16) Intracellular pH was determined from the chemical shift of the intracellular P_i resonance using an NMR titration curve obtained at physiologic ionic strength.^(12,14,16)

For estimation of intracellular concentrations, saturation constants were obtained for each peak, comparing intensities in fully relaxed spectra with intensities in saturated spectra using the actual experimental pulsing conditions as described above. 50 μL of phosphate (1 M) was added at the end of each experiment to convert intensity to concentration. For estimation of intracellular concentrations it was assumed that 1.67 g wet cells contains 1 mL of intracellular volume.⁽¹⁷⁾

¹³C NMR spectra were obtained at 125.76 MHz and were accumulated in 1.5 min blocks using 45° pulses and a repetition time of 0.34 sec. Gated decoupling of protons was employed to suppress nuclear Overhauser enhancement

with a decoupling power during acquisition of 5 W. Chemical shifts were referred to tetramethylsilane through the use of the α -[C-1]glucose resonance at 92.97 ppm as an internal reference. Labelled [^{13}C -1]glucose was obtained from Sigma Chemical Co. and used without further purification.

FIDs (free induction decays) were stored during the course of the experiments in 8K files for ^{31}P and in 16K files for ^{13}C in the Bruker WM-500 computer hard disk and were transferred later to a VAX 11/780 computer where all subsequent processing was performed using the LAB ONE^(TM) NMR1 spectroscopic data analysis software system.⁽¹⁸⁾

Analyses

Samples taken from the reservoir vessel during the NMR immobilized cell experiments were filter sterilized and analyzed for glucose by a Waters Associates high pressure liquid chromatograph with refractive index detector and Waters Associates Carbohydrate column for carbohydrate analysis (solvent 65:35 acetonitrile:water); for ethanol by gas chromatography utilizing a Shimadzu GC-9 chromatograph system equipped with a 2 m glass column packed with Chromosorb 101 (80/100) mesh, the helium carrier gas flow rate was 50 mL/min, the detector temperature was 200°C and the oven temperature was 130°C; and, for glycerol using an analytical kit for triglycerides (Sigma). Data processing of GC and HPLC chromatograms was made using a Shimadzu CR-3A integrator system. Also, suspended cell fermentations were done to mimic the conditions of the NMR experiments but used a lower cell density (*ca.* 0.1 gr_{wet}/mL). Samples

were taken at different times and analyzed for glucose, ethanol and glycerol as before.

RESULTS

Overall fermentation kinetics

In all the experiments reported here, resting cells in buffer were suddenly exposed to glucose solution. Time zero refers to the time of glucose addition. Under these conditions, no cell growth was detected either in the suspended cell experiments or in the immobilized cell experiments. Figure 1 shows ethanol concentration (per cell mass) as a function of time for suspended and immobilized cells. These data indicate that the fermentation rate is constant during this initial interval of the experiment.

The specific rate of ethanol production by the immobilized cells is *ca.* twice the suspended cell ethanol specific productivity. Accordingly, the rate of glucose uptake is also larger for immobilized cells than for suspended cells. Glycerol concentration also increases linearly with time (results not shown). Glycerol production is faster in immobilized cells and varies between 5% and 10% of ethanol production for both suspended and immobilized cells. Experimental values for glucose uptake and ethanol and glycerol production are listed in Table I.

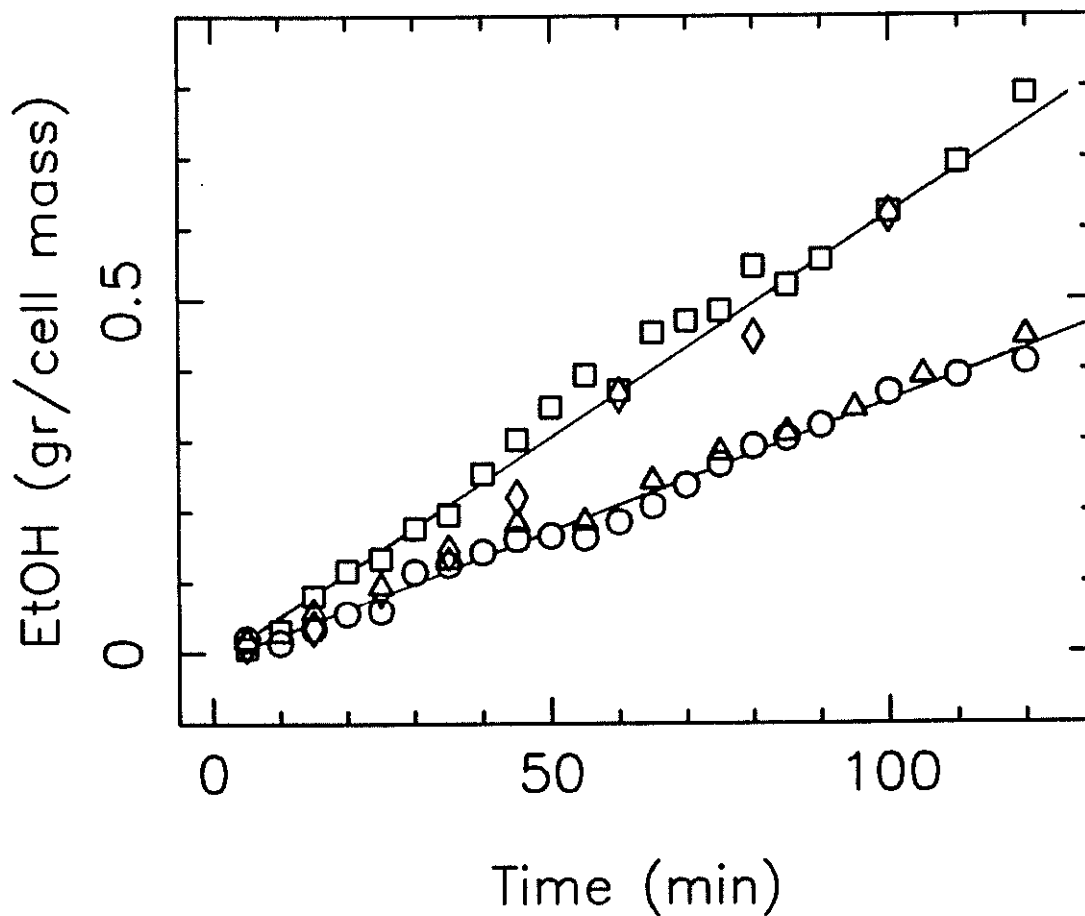


Figure 1: Ethanol concentration as a function of time.

(○, △) suspended cells and (□, ◇) entrapped cells at 20 °C and $\text{pH}^{\text{ex}}=5.5$. 300 mM of glucose was added at time zero to cells in phosphate buffer. Determinations for immobilized cells were performed on samples taken from the recirculating reservoir. Separate fermentations, simulating the NMR experimental conditions, were done for the suspended cell determinations using a cell density of *ca.* 0.1 $\text{gr}_{\text{wet}}/\text{mL}$. Different symbols correspond to two independent experiments.

TABLE I: Substrate uptake and product formation rates for suspended and immobilized cells.

Rates were estimated from the slope of concentration vs. time data and are expressed in mmol per L of cell volume per min, assuming that 1.6 gr of wet cells contains 1.0 mL of cells.⁽¹⁷⁾

pH ^{ex} = 5.5	Suspended cells ($\frac{\text{mmol}}{\text{min L}_{\text{cells}}}$)	Immobilized cells ($\frac{\text{mmol}}{\text{min L}_{\text{cells}}}$)
Glucose uptake	14.5	35.1
Ethanol prod.	26.7	49.0
Glycerol prod.	1.8	3.7

pH ^{ex} = 4.5	Suspended cells ($\frac{\text{mmol}}{\text{min L}_{\text{cells}}}$)	Immobilized cells ($\frac{\text{mmol}}{\text{min L}_{\text{cells}}}$)
Glucose uptake	17.3	38.2
Ethanol prod.	32.2	55.0
Glycerol prod.	1.9	3.8

Assessment of mass transport effects on observed kinetics

One important question that arises in the interpretation of kinetic data for immobilized cells is whether or not mass transfer limitation, either external or within the immobilized cell aggregate, is significant. If negligible mass transfer limitation is present, the observed kinetics are the intrinsic cell kinetics.

In this immobilized cell system there are two regions where mass transfer may influence observed reaction rates. The first is within the cell aggregate where diffusion and bioconversion reactions are taking place simultaneously. Mi-

crosscopy examination of several sectioned immobilized cell beads showed cells uniformly dispersed throughout the matrix as expected based upon the immobilization procedure. Accordingly, it is appropriate to estimate intrapellet mass transfer resistance based on a pseudohomogeneous model with uniform catalytic activity. The other region of possible mass transfer influence is between the bulk fluid phase and the external particle surface. Dimensionless numbers describe relative rate magnitudes in each region. Assuming a spherical homogeneous particle, the pertinent dimensionless numbers are defined as follows:

$$Bi = \frac{\text{film transport rate}}{\text{intraparticle diffusion rate}} = \frac{R \cdot k_s}{D_{es}}$$

and

$$\Phi = \frac{\text{max. observed rate}}{\text{intraparticle diffusion rate}} = \left(\frac{r_{max} \cdot R^2}{D_{es} \cdot S_b} \right)^{1/2}$$

where:

D_{es} = intraparticle diffusion of substrate coefficient

k_s = external mass transfer coefficient

r_{max} = maximum observable rate

R = particle radius

S_b = bulk substrate concentration

Conditions to have negligible mass transfer resistance in both regions are:^(19,20)

$$\Phi < 0.3 \quad \text{and} \quad \frac{\Phi}{Bi} \ll 1$$

The Biot number (Bi) was estimated from the following correlation:⁽²¹⁾

$$Bi = 0.95 Re^{1/2} Sc^{1/3} \quad ; \quad 10 < Re < 10^4$$

where Re is the Reynolds number and Sc is the Schmidt number:

$$Re = \frac{2Ru\rho}{\mu} \quad ; \quad Sc = \frac{\mu}{\rho D_s}$$

and:

u = fluid velocity

ρ = fluid density

μ = fluid viscosity

D_s = substrate diffusivity

Values of glucose diffusion coefficients in water and in 2% calcium alginate were taken from the literature:^(22,23)

$$D_s = 6.8 \times 10^{-6} \text{ cm}^2/\text{sec} \quad \text{and} \quad D_{es} = 6.1 \times 10^{-6} \text{ cm}^2/\text{sec}$$

These immobilized cell experiments were designed so that the mass transfer resistances are negligible. Typical maximal values for the dimensionless numbers above for these experiments are: $\Phi = 0.083$ and $\frac{\Phi}{Bi} = 5.0 \times 10^{-5}$. The values of Φ and $\frac{\Phi}{Bi}$ are far below the suggested thresholds for possible mass transfer interferences. Accordingly, minor uncertainties about the effective diffusion coefficients in these preparations or other parameters do not alter the conclusion of

negligible mass transfer intrusion. Thus, the observed kinetics are the intrinsic cell kinetics.

Stimulus-response NMR measurements

Very useful information can be obtained from a ^{31}P NMR spectrum (Figure 2). Estimates of intracellular (pH^{in}) and extracellular pH (pH^{ex}), and the concentrations of intracellular (P_i^{in}) and extracellular phosphate (P_i^{ex}), sugar phosphates (SP), polyphosphates (PP_i), uridine-diphospho-glucose ($UDPG$), adenosine tri- and diphosphate ($ATP + ADP$), and NAD(H) can be obtained from a single spectrum.^(12,14-16)

After adding glucose to starved cells, intracellular conditions change with time until a quasi-steady state is achieved. Correspondingly, ^{31}P NMR spectra are therefore time-dependent for 5-10 min. Figure 3 shows ^{31}P NMR spectra of suspended *S. cerevisiae* cells in the region between 6 and -1 ppm, over different time intervals after adding glucose to starved cells. Prior to glucose addition the SP resonance is at its basal level and consists mostly of 3-phosphoglycerate. By 3 min after glucose addition, SP rapidly increases and now is mainly composed of contributions from glucose-6-phosphate, fructose-6-phosphate and 3-phosphoglycerate (see below). The P_i^{in} peak decreases and shifts downfield.

By 12-15 min a "steady-state" condition is established during which spectral components corresponding to intracellular species are relatively constant. Figure 4 shows a comparison between suspended and immobilized cell spectra of the downfield region of ^{31}P NMR during this quasi-steady state after feeding glucose.

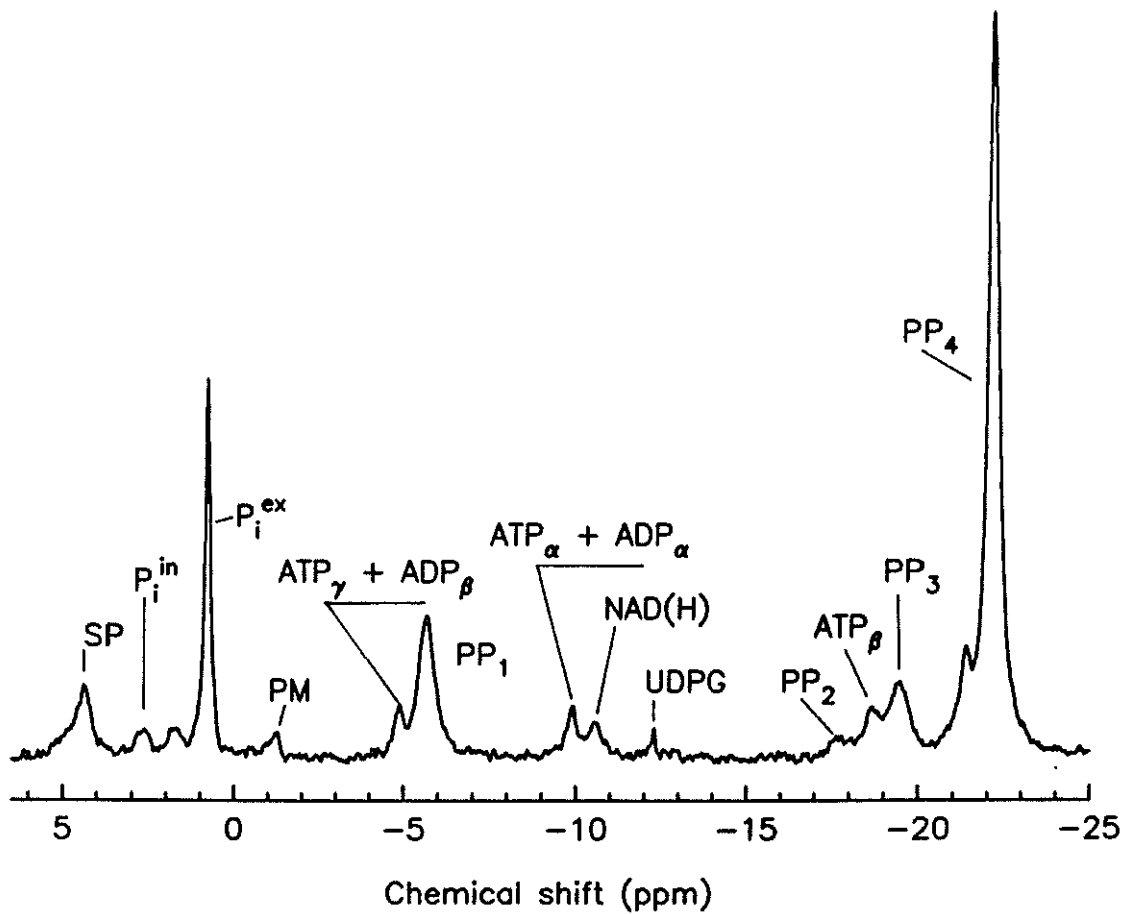


Figure 2: ^{31}P NMR spectrum of immobilized cells for steady-state glucose fermentation.

^{31}P spectra at 202.46 MHz recorded using 70° pulses and 0.5 sec acquisition time. Chemical shifts referenced to 85% orthophosphoric acid. (*SP*: sugar-phosphates; P_i^{in} : intracellular phosphate; P_i^{ex} : extracellular phosphate; *PM*: phosphomannan; *UDPG*: uridine-diphospho-glucose; PP_1 : terminal phosphate resonances, PP_3 : penultimate phosphates, and, PP_4 : inner phosphate resonances from polyphosphate chains.)

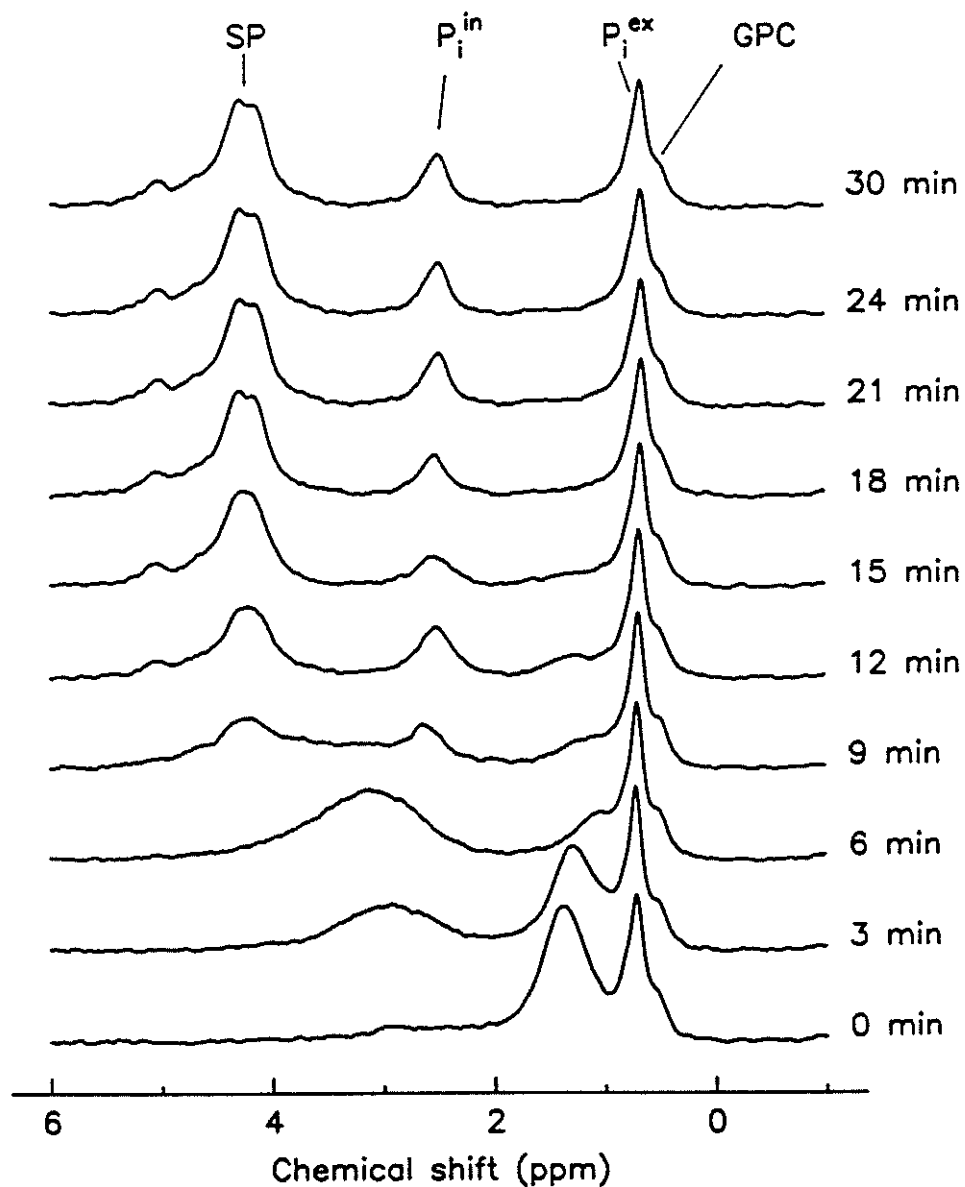


Figure 3: Transient ^{31}P NMR spectra for a step in glucose concentration for suspended cells.

Glucose was added at time zero to a final concentration of 300 mM. Times given for each spectrum represent the end of 3 min accumulation time. (*SP*: sugar-phosphates; P_i^{in} : intracellular phosphate; P_i^{ex} : extracellular phosphate; *GPC*: glycerol phosphorylcholine.)

The P_i^{in} and SP peaks of the immobilized cell spectrum appear at lower ppm than the corresponding peaks of the suspended cell spectrum. Because the position of the P_i^{in} resonance (its chemical shift) is pH dependent, it is possible to estimate the intracellular pH using *in vitro* calibration curves.^(12,16) Applying this calibration to these spectra indicate that the immobilized cell intracellular pH (6.80) is lower than the suspended cell intracellular pH (7.05) as shown in Table II.

Using ^{13}C NMR and ^{13}C -labelled glucose, differences in polysaccharide (trehalose and glycogen) storage between suspended and immobilized cells were detected. Figure 5 shows spectra of suspended and immobilized cells after 3 and 8 min of feeding 300 mM of labelled glucose. Trehalose production in immobilized cells is significantly greater than in suspended cells. Glycogen production is also different in immobilized cells; however the glycogen signal is not well resolved because relatively low mobility of the label of this polymer restricts its observation by ^{13}C NMR.

Analysis of quasi-steady state metabolite concentrations

The SP peak shape in Figure 3 is different in the two experiments, indicating that sugar-phosphate composition in immobilized cells is different from that of suspended cells. Applying a quantitative method developed in this laboratory, it is possible to deconvolute the *in vivo* sugar-phosphate region into its individual components.⁽¹⁶⁾ The SP resonance is a broad peak composed of overlapping resonances of different sugar phosphates that sum together to give the overall

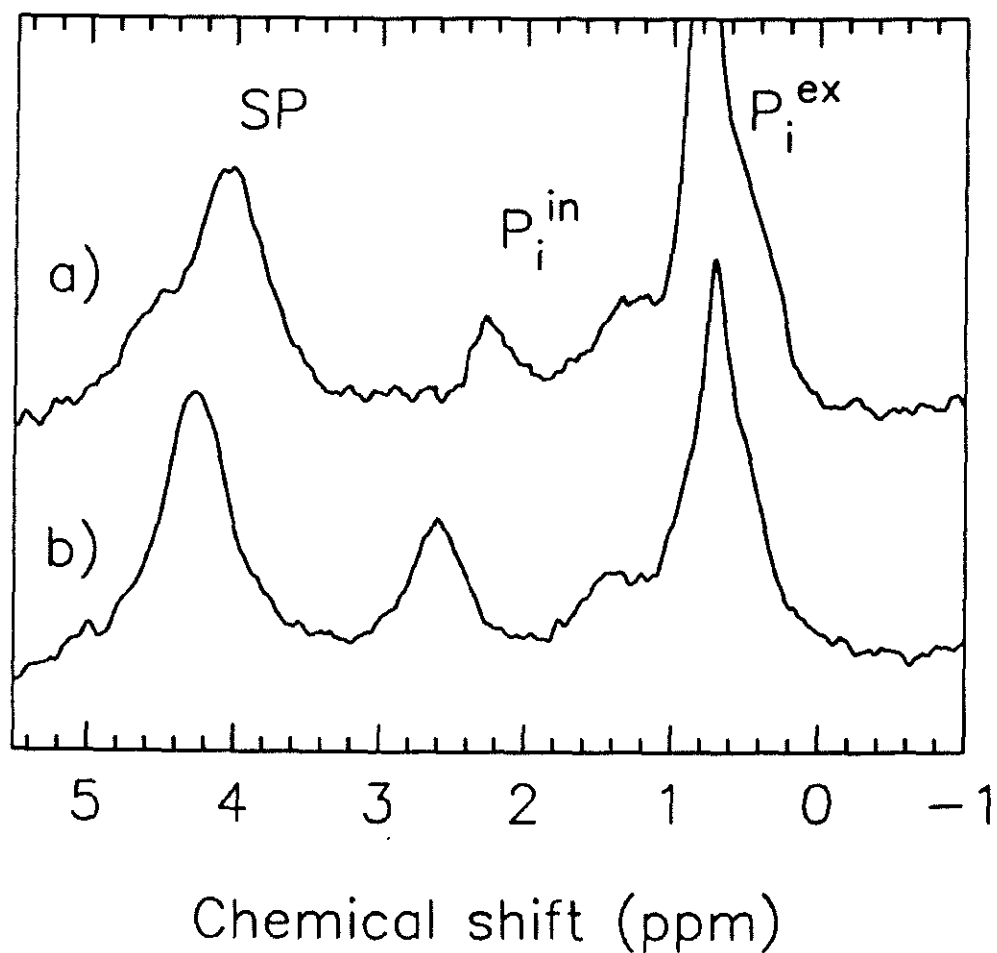


Figure 4: Comparison of the downfield region of ^{31}P NMR spectrum of suspended and immobilized cells.

Glucose was added to a final concentration of 300 mM to either (a) suspended or (b) entrapped cells in phosphate buffer (pH=5.5) at 20 °C. Note the different shape of the SP peaks. Other conditions as in Figure 2. (*SP*: sugar-phosphates; P_i^{in} : intracellular phosphate; P_i^{ex} : extracellular phosphate.)

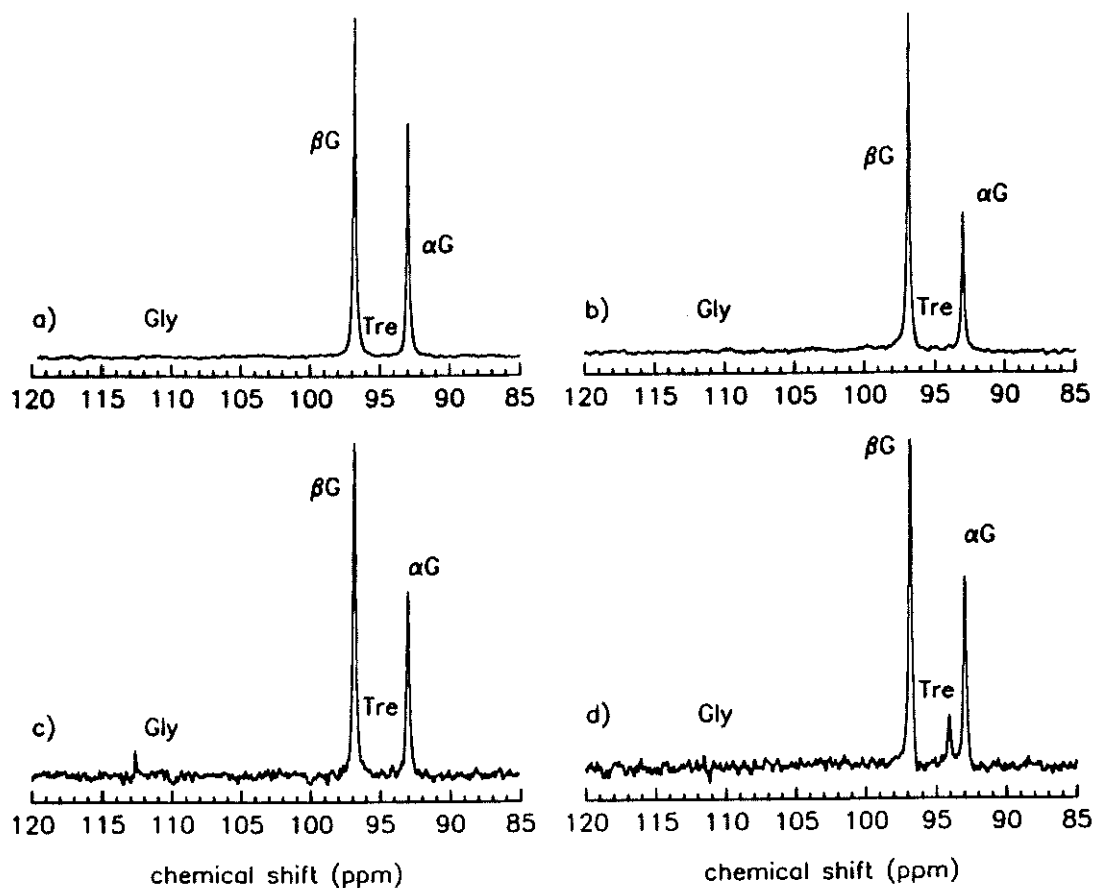


Figure 5: ^{13}C NMR spectra of suspended and immobilized cells.

^{13}C NMR spectra after 3 min of feeding 300 mM of $[^{13}\text{C}-1]$ glucose to (a) suspended cells or (b) immobilized cells, and ^{13}C NMR spectra after 8 min of feeding 300 mM of $[^{13}\text{C}-1]$ glucose to (c) suspended cells or (d) immobilized cells. ^{13}C NMR spectra were obtained at 125.76 MHz and were accumulated in 1.5 min blocks using 45° pulses and a repetition time of 0.34 sec. Gated decoupling of protons was employed to suppress nuclear Overhauser enhancement with a decoupling power during acquisition of 5 W. Chemical shifts were referred to tetramethylsilane through the use of the α - $[^{13}\text{C}-1]$ glucose resonance at 92.97 ppm as an internal reference. (α -G: α -glucose, β -G: β -glucose, Tre: trehalose, Gly: glycogen.)

SP signal. Using spectral analysis methods it is possible to deconvolute the SP peak into its components using a linear combination of the individual resonances. The deconvolution method consists of installing peaks in the SP main peak and then, using the NMR1 software,⁽¹⁸⁾ optimizing the correspondence between a linear combination of individual peaks and the experimental SP peak through a modified Levenberg-Marquardt algorithm. After convergence, several control criteria are employed to determine whether or not to accept the analysis:

- a) Agreement between predicted and *in vivo* chemical shifts: *in vivo* correlations relating intracellular inorganic phosphate chemical shift with chemical shifts of the α and β anomers of fructose-diphosphate and with fructose-6-phosphate and 3-phosphoglycerate have been established using extensive *in vitro* NMR data.⁽¹⁶⁾ The estimated individual sugar phosphate chemical shifts must be consistent with the expected values based on the *in vivo* correlations.
- b) The linewidths and intensities must be physically reasonable and consistent: For instance, β -fructose-diphosphate has two resonances corresponding to P-1 and P-6 phosphorous. These should have similar linewidths (± 3 Hz). Also, the concentration predicted from the P-1 peak cannot be greater than the concentration predicted from the P-6 peak because fructose-6-phosphate, if present, resonates at the same position as the P-6 peak of β -fructose-diphosphate.
- c) Changes in the phasing should not affect the results considerably; otherwise, the optimum solution has not been reached.

Therefore, the deconvolution method of the SP region is not a simple curve fitting of the experimental data because it has several consistency checks that provide a critical analysis.

The deconvolution method was tested by comparing the estimated *in vivo* concentration values with the values obtained from cell-extract as is explained in Appendix B. This was done for different strains and conditions. The agreement between the estimated and the cell-extract concentrations is very good.

Estimates of quasi-steady state intermediate concentrations obtained in this fashion for suspended and immobilized cells are shown in Table II. These intermediate concentrations for suspended cells are in good agreement with those reported in the literature.^(14,24) *ATP + ADP* and *UDPG* concentrations were determined from those separate resonances by direct integration of the corresponding peak. (The α resonance was employed to obtain *ATP + ADP* levels. Similar values were obtained in a few cases using the $\gamma + \beta$ resonance.)

There are substantial differences in glucose-6-phosphate, fructose-6-phosphate and 3-phosphoglycerate levels in suspended and immobilized cells. *ATP + ADP* and fructose-diphosphate concentrations are very similar in both configurations. *UDPG* concentration is larger in immobilized cells. This is consistent with the higher polysaccharide production in immobilized cells observed by ^{13}C NMR since *UDPG* is a key intermediate in polysaccharide biosynthesis.

TABLE II: Comparison of intermediate metabolite concentrations of cells grown in suspension.

Comparison of intermediate metabolite concentrations between suspended and immobilized cells measured by ^{31}P NMR. Units are in mmol per L of cell volume, assuming that 1.6 gr of wet cells contains 1.0 mL of cells.⁽¹⁷⁾ Sugar-phosphate concentrations were obtained using an *in vivo* deconvolution method.⁽¹⁶⁾ The $\text{ATP}_\alpha + \text{ADP}_\alpha$ peak was integrated to estimate $\text{ATP} + \text{ADP}$ levels, and the peak at -12.2 ppm was used to estimate UDPG concentration.

$\text{pH}^{\text{ex}} = 5.5$	Suspended cells	Immobilized cells
pH^{in}	7.05	6.80
	$\left(\frac{\text{mmol}}{\text{L}_{\text{cells}}}\right)$	$\left(\frac{\text{mmol}}{\text{L}_{\text{cells}}}\right)$
Glucose-6-P	1.4	4.4
Fructose-6-P	0.8	1.8
Fructose-1,6-P	6.6	5.4
3-P-Glycerate	0.1	4.5
ATP+ADP	2.7	2.7
UDPG	0.6	1.7

$\text{pH}^{\text{ex}} = 4.5$	Suspended cells	Immobilized cells
pH^{in}	6.94	6.76
	$\left(\frac{\text{mmol}}{\text{L}_{\text{cells}}}\right)$	$\left(\frac{\text{mmol}}{\text{L}_{\text{cells}}}\right)$
Glucose-6-P	0.7	3.1
Fructose-6-P	0.3	1.6
Fructose-1,6-P	10.1	5.8
3-P-Glycerate	0.1	1.4
ATP+ADP	2.2	2.3
UDPG	0.7	1.8

Influence of extracellular pH on fermentation kinetics and intracellular state

All the results presented so far have been obtained at an extracellular pH of 5.5. Decreasing the extracellular pH by one pH-unit affected fermentation kinetics and intracellular state of both suspended and immobilized cells as shown in Table I and Table II. However, the qualitative differences between suspended and immobilized cells remain mostly the same as observed at pH^{ex} 5.5. There is faster glucose uptake and ethanol and glycerol production in immobilized cells than in suspended cells, and the intracellular pH of immobilized cells is lower than the intracellular pH for suspended cells. Glucose-6-phosphate, fructose-6-phosphate, 3-phosphoglycerate and *UDPG* levels are also higher in immobilized cells. Lowering external pH alters the relative intracellular concentrations of fructose-diphosphate. At pH^{ex} 4.5, fructose-diphosphate concentration is considerably lower in immobilized cells (5.8 mM) than in suspended cells (10.1 mM).

DISCUSSION

In these experiments, *S. cerevisiae* was grown in suspension culture. After suspension in buffer, some of these cells were entrapped in alginate. Subsequently, samples of suspended cells and of immobilized cells were exposed to glucose. Accordingly, these experiments describe only the effects of alginate entrapment on the glucose uptake and carbon conversion reactions in the cell,

given cells with the same macromolecular composition and structure. These experiments do not reflect any further metabolic effects that might result from growth of cells in the matrix. In this case, interactions with the matrix could influence gene expression and cell structure, causing even more profound and complex alterations in metabolic kinetics.

These experiments show that immobilization enhances ethanol and glycerol production rates without affecting yields significantly. Therefore the increase in the rate of glucose utilization that accompanies immobilization must reflect a change in the upper part of the glucose pathway. Moreover, an increase in polysaccharyde production was also observed in immobilized cells. Since these steps precede all the branches to glycerol and ethanol, these data indicate that glucose transport and/or glucose phosphorylation are the steps most likely affected by immobilization.

At both extracellular pH values investigated, the immobilized cell intracellular pH was lower. Studies made *in vitro* investigating the effect of pH upon phosphofructokinase^(25,26) and hexokinase⁽²⁷⁾ concluded that pH is an important effector of those enzymes. A decrease in pH from values around 7.0 (characteristic of the suspended cell interior) produced an increase in the enzymatic rates *in vitro*. This observation is in qualitative agreement with the results presented here.

Comparing suspended cells at pH^{ex} 5.5 and 4.5, a decrease in extracellular pH resulted in a decrease in intracellular pH as well as an increase in fermentation rate. At lower extracellular pH it is expected that, in order to maintain similar intracellular pH, more proton pumping will be necessary and cell energy

maintenance requirements will be increased. The ATP production rate (*i.e.* fermentation rate) increased at pH^{ex} 4.5; however, $ATP + ADP$ concentration decreased instead of increasing. This suggests an increase of ATP consumption in agreement with the hypothesis of a larger maintenance at lower extracellular pH. Similar conclusions can be made comparing immobilized cell results at the two extracellular pHs.

There is a correlation between glucose-6-phosphate concentration and glucose uptake rate in all the experiments. The lower the glucose-6-phosphate concentration, the higher the glucose uptake. This result agrees with other studies for cells grown in similar conditions and with the hypothesis that there is feedback inhibition of glucose uptake by glucose-6-phosphate.^(26,28)

These experiments also show that the level of 3-phosphoglycerate is an order of magnitude higher in immobilized cells than in suspended cells, and this suggests that there is also a control point in the lower part of the pathway as has been postulated in other studies.^(24,29)

The most intriguing result of this work is that the effect of immobilization on cell metabolism is reflected in a very short period of time, and under conditions in which no significant DNA, RNA or protein synthesis occurs. Therefore, immobilization is directly affecting some rate-influencing step, possibly by changing its regulation or by altering the concentration of an effector of such a step. Most likely, glucose uptake and/or glucose phosphorylation are the steps affected by immobilization, since those steps are upstream of all the differences observed between suspended and immobilized cells. A detailed quantitative analysis of

these differences based upon a kinetic model for these pathways will be presented in a future publication.

Acknowledgements

This research was sponsored by the National Science Foundation. The nuclear magnetic resonance experiments were done at the Southern California Regional Nuclear Magnetic Resonance Center (NSF Grant No. CHE-84-40137). J. L. Galazzo has a fellowship from the National Research Council - CONICET, Argentina.

REFERENCES

1. Hahn-Hägerdal B., Larson M., and Mattiasson B., *Biotechnol. Bioeng. Symp.*, **12**, 199 (1982).
2. McGhee J., St. Julian G., Detroy R., and Bothast R., *Biotechnol. Bioeng.*, **24**, 1155 (1982).
3. Tyagi R., and Ghose T., *Biotechnol. Bioeng.*, **24**, 781 (1982).
4. Jirku V., Turkora J., and Krumphanzl V., *Biotechnol. Lett.*, **2**, 509 (1980).
5. Koshcheyenko K., Turkina M., and Skryabin G., *Enzyme Microb. Technol.*, **5**, 14 (1983).
6. Inloes D., Smith W., Taylor D., Cohen S., Michaels A., and Robertson C., *Biotechnol. Bioeng.*, **23**, 79 (1981).
7. Navarro J., and Durand G., *Eur. J. Appl. Microbiol.*, **4**, 243 (1977).
8. Larsson P., and Mosbach K., *Biotechnol. Lett.*, **1**, 501 (1979).
9. Brodelius P., Deus B., Mosbach K., and Zenk M., *FEBS Lett.*, **103**, 93 (1979).
10. Doran P., and Bailey J., *Biotechnol. Bioeng.*, **28**, 73 (1986).
11. Doran P., and Bailey J., *Biotechnol. Bioeng.*, **29**, 892 (1987).
12. Galazzo J., Shanks J., and Bailey J., *Biotechnol. Techniques*, **1**, 1 (1987).
13. Klein J., Stock J., and Vorlop K., *Eur. J. Appl. Microbiol. Biotechnol.*,

- 18, 86 (1983).
14. den Hollander J., Ugurbil K., Brown T., and Shulman R., *Biochemistry*, **20**, 5871 (1981).
 15. Navon G., Shulman R., Yamane T., Ecclesball T., Lam K., Baronotsky J., and Marmur J., *Biochemistry*, **18**, 4487 (1979).
 16. Shanks J., and Bailey J., *Biotechnol. Bioeng.*, **32**, 1138 (1988).
 17. Gancedo J., and Gancedo C., *Biochimie*, **55**, 205 (1973).
 18. LAB ONE™ NMR1 Spectroscopic Data Analysis Software System, Revision 2.70, Syracuse University, New Methods Research Inc., (1985).
 19. Weisz P., *Science*, **179**, 433 (1973).
 20. Bailey J., and Ollis D., In: "*Biochemical Engineering Fundamentals*", 2nd. Edition, McGraw-Hill, pp. 212-220, (1986).
 21. Kasche V., Kapune A., and Schwegler H., *Enzyme Microbiol. Technol.*, **1**, 41 (1979).
 22. Tanaka H., Matsumura M., and Veliky I., *Biotechnol. Bioeng.*, **26**, 53 (1984).
 23. Hannoum B., and Stephanopoulos G., *Biotechnol. Bioeng.*, **28**, 829 (1986).
 24. den Hollander J., Ugurbil K., and Shulman R., *Biochemistry*, **25**, 212 (1986).
 25. Bañuelos M., Gancedo C., and Gancedo J., *J. Biol. Chem.*, **252**, 6394 (1977).

26. Reibstein D., den Hollander J., Pilkis S., and Shulman R., *Biochemistry*, **25**, 219 (1986).
27. Wilkinson K., and Rose I., *J. Biol. Chem.*, **254**, 12567 (1979).
28. Becker J., and Betz A., *Biochim. Biophys. Acta*, **274**, 584 (1972).
29. Hess B., Boiteux A., and Kruger J., *Adv. Enzyme Regul.*, **7**, 149 (1969).

CHAPTER 3

**STUDY OF GLUCOSE METABOLIC KINETICS OF
SUSPENDED AND IMMOBILIZED *Saccharomyces cerevisiae*
CELLS GROWN IN CALCIUM-ALGINATE BEADS**

ABSTRACT

The effects of growing *Saccharomyces cerevisiae* cells within a Ca-alginate matrix were investigated using *in vivo* nuclear magnetic resonance (NMR) spectroscopy and macroscopic determinations of substrate uptake and product formation rates.

The growth rate of entrapped cells is 40% lower than the growth rate of cells cultivated in suspension under similar conditions. Ca-alginate grown cells were used to compare suspended and immobilized cell glucose metabolism. ^{31}P NMR shows differences in phosphorylated compound levels such as glucose-6-phosphate and polyphosphate. Glucose uptake and ethanol and glycerol production rates are higher in immobilized cells.

INTRODUCTION

A considerable number of processes using immobilized cells are now well established.^(1,2) Production of L-amino acids, antibiotics such as penicillins, and ethanol are products obtained using immobilized cell systems on an industrial scale.

Operational advantages of immobilized cell systems over more traditional suspended cell processes make these systems attractive for large-scale operation. The possibility of confining the cells within the bioreactor allows high-cell densities without the risk of washout. This improves productivity and also requires less downstream processing. However, cell immobilization may alter the cell metabolism. There are several reports showing that cell physiology and morphology sometimes change upon immobilization.⁽³⁻⁵⁾ Altered growth, substrate uptake and product formation rates are among the most common reported metabolic alterations observed in immobilized cells. It is important to understand the interactions between the cells and the immobilization process. This will allow the biocatalyst designer and formulator to conveniently manipulate the cell environment to optimize the output from immobilized cell systems.

When studying the effects of immobilization on cell metabolism, usually by contrasting suspended and immobilized cell behavior,⁽⁶⁻⁸⁾ it is essential to have a consistent and reproducible initial cell state. With this accomplished, any observed differences in metabolism can then be attributed to the immobilization

process and not to any other unknown or uncontrolled differences in the initial cell state.

Also, mass-transfer limitations need to be reduced to a minimum in order to observe true intrinsic effects, which may be hindered by transport limitations of nutrients and/or products in and out of the immobilization aggregate.

The results reported in Chapter 2 were obtained using suspended and immobilized cells grown in a rich-medium suspension. That study reflects the effect of immobilization upon glucose catabolism because the comparison was made under non-growing conditions. To accentuate the effect of immobilization on cell metabolism, *S. cerevisiae* cells were allowed to grow in a rich medium within the Ca-alginate matrix. A similar analysis as used in Chapter 2 was performed on these Ca-alginate grown cells. The results are reported in this chapter. They show the effect of immobilization on cell growth and on glucose catabolism.

MATERIALS AND METHODS

Organism

Saccharomyces cerevisiae ATCC 18790, a standard diploid strain, was obtained from the American Type Culture Collection. The stock culture was maintained on yeast extract, peptone and glucose agar plates at 4°C.

Culture and sample preparation

S. cerevisiae cells were grown as described previously⁽⁹⁾ in a rotary shaker at 30°C in a medium of the following composition: 1% yeast extract, 2% peptone, and 2% glucose, adjusted to pH 4.5 with citrate buffer (50 mM). A preculture (4 mL) was inoculated with one loop of cells and cultivated for 12-15 h. The preculture was used to inoculate the main culture (400 mL) in 1-L flasks. Mid-exponential phase cells (50% of growth saturation) were chilled in an ice bath to 4°C under manual shaking. The cells were harvested by low-speed centrifugation at 4°C and washed with 150 mL of wash medium per mL of cell pellet (0.85 g/L H₂KPO₄, 0.15 g/L HK₂PO₄, 0.5 g/L MgSO₄·7H₂O, 0.5 g/L NaCl in 50 mM MES buffer pH 5.5).

The cell pellet was resuspended in wash medium supplemented with 7.5 mM P_i at twice the desired cell concentration and mixed with an equal volume of 4% Na-alginate. The homogeneous mixture was filled into a cylindrical reservoir and compressed nitrogen gas was used to force the solution through a small tube (0.8 mm in diameter). A coaxial tube with a larger diameter (1.8 mm) was used to blow off the alginate droplets into 2% CaCl₂ solution at a controlled size by a compressed concentric air stream. ⁽¹⁰⁾

Beads that formed (*ca.* 1 mm in median diameter) were allowed to cure for 0.5 h, then, washed and stored in resuspension medium. All samples were kept on ice until they were used (always less than 1 hour).

Reactor system

The Ca-alginate beads with entrapped yeast cells were placed in a packed bed reactor to allow cell growth within the immobilization matrix.

A schematic of the system is shown in Figure 1. The fermentor used was a New Brunswick Bioflo with stirring, temperature and pH controls. Anaerobic conditions were maintained by sparging the fermentor liquid with nitrogen. Stirring speed was maintained at 300 rpm, temperature at 30°C and pH at 4.5. The column for the packed bed was a Pyrex column (35 mm ID, 160 mm height). The bead bed was supported between two stainless steel screens with openings approximately 0.6 mm wide. A recirculation loop connected the column with the fermentor vessel. Norprene tubing (Cole-Parmer Instrument Co.) was used in the recirculation loop in order to minimize oxygen diffusion into the recirculating medium. Recirculation flow rates were *ca.* 270 mL/min.

The medium used for cell growth consisted of glucose (50 g/L), yeast extract (5 g/L), H_2KPO_4 (0.85 g/L), HK_2PO_4 (0.15 g/L), $\text{MgSO}_4 \cdot 7\text{H}_2\text{O}$ (1 g/L), $\text{CaCl}_2 \cdot 2\text{H}_2\text{O}$ (1 g/L) and $(\text{NH}_4)_2\text{HPO}_4$ (2 g/L), pH was adjusted at 4.5.

Experimental procedure

Once the column was filled with the alginate beads containing the cell inoculum (*ca.* 4 $\text{mg}_{\text{dry wt.}}/\text{mL}_{\text{gel}}$), 300 mL of medium was used to wash the system. Then, the fermentor was filled with 450 mL of fresh medium and the growth phase began.

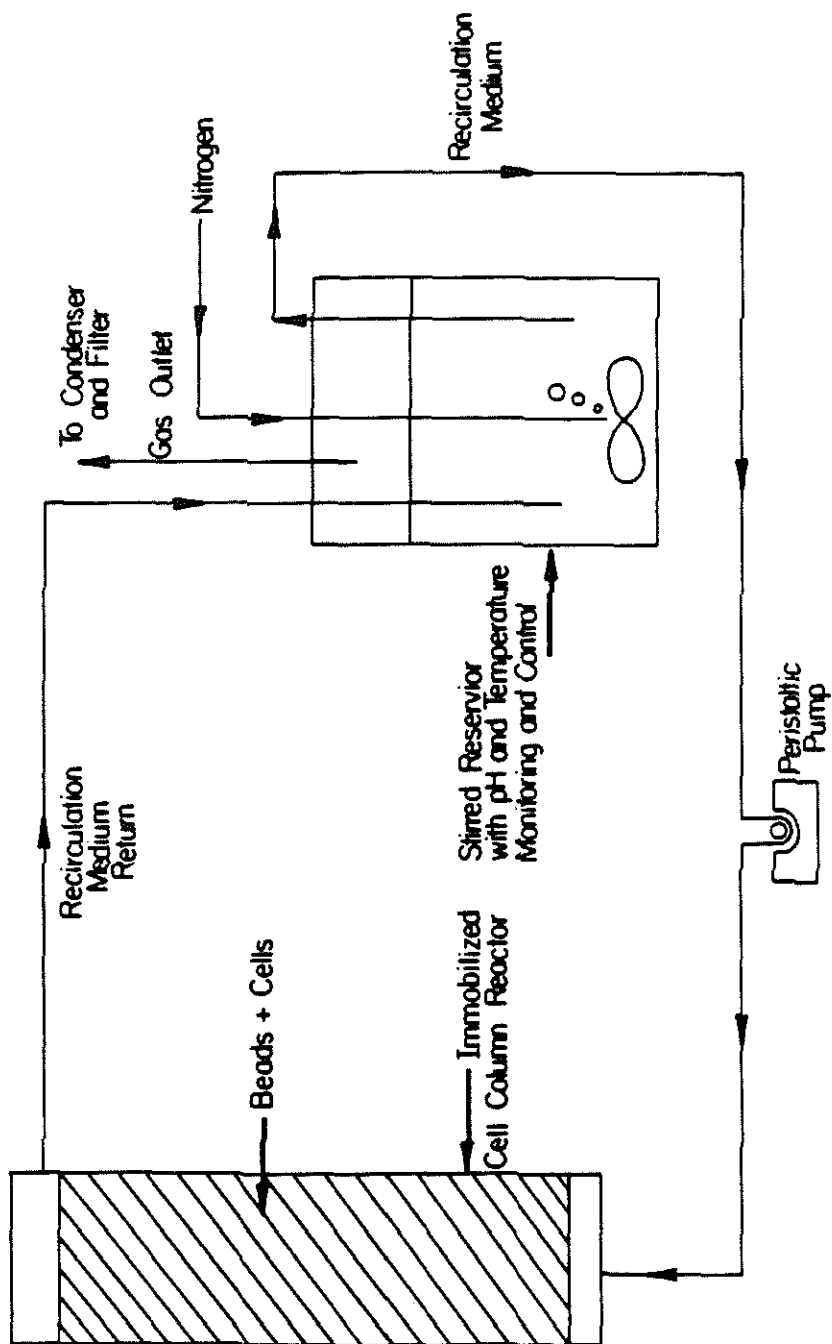


Figure 1: Immobilized cell recirculation reactor.

Liquid samples were taken from the fermentor vessel and bead samples were taken from the packed bed at different times. The liquid samples were analyzed for glucose and ethanol, and cell growth was determined from the beads according to the following procedure. 20-30 beads were placed in 50 mL of a phosphorus-citrate buffer (pH 5) to dissolve the Ca-alginate beads. The optical density of the suspensions obtained was measured at 590 nm on a Spectronic 21, and the dry weight per bead was obtained using a calibration curve that included a correction for the presence of alginate in suspension. At various times during the experiments, liquid samples were plated on YPD agar plates and incubated at 30°C to check for contamination. No contamination was observed in any of the experiments.

To study the glucose fermentation kinetics of alginate-grown cells, the medium was drained from the system after the desired growth interval, and replaced with 400 mL of cold wash buffer (0.85 g/L H_2KPO_4 , 0.15 g/L HK_2PO_4 , 0.5 g/L $\text{MgSO}_4 \cdot 7\text{H}_2\text{O}$, 0.5 g/L NaCl in 50 mM MES buffer pH 5.5). Then, the column was disconnected from the fermentation vessel, and the beads with the immobilized cells were aseptically transferred to a flask containing 200 mL of phosphate-citrate buffer at 4°C to allow bead dissolution. Complete dissolution took place in 15-20 min. The cells were then harvested by low-speed centrifugation at 4 °C and washed three times with 150 mL of wash medium per mL of cell pellet (0.85 g/L H_2KPO_4 , 0.15 g/L HK_2PO_4 , 0.5 g/L $\text{MgSO}_4 \cdot 7\text{H}_2\text{O}$, 0.5 g/L NaCl in 50 mM MES buffer pH 5.5).

Subsequently, the cell pellet was either resuspended in resuspension medium, or used further for immobilization following the same methodology

to entrap the cells in Ca-alginate as described above. This was done in order to have suspended and immobilized cells grown under similar conditions, so that a comparison between the two systems could be made, and also to have a diffusion-free immobilized cell configuration because colony formation within the alginate beads during the growth phase may impose mass-transfer limitations on the system. The final samples consisted of 2 mL of cell suspension (cell density *ca.* 0.5 gr_{wet}/mL) or Ca-alginate beads (cell density *ca.* 0.3 gr_{wet}/mL) in 10-mm o.d. NMR sample tubes. In the suspended cell experiments, N₂ gas was bubbled through the cell suspension using the two-bubbler scheme described by den Hollander *et al.*⁽¹¹⁾ (one bubbler at the bottom of the NMR tube generated small bubbles at a rate of 10 mL/min while a second bubbler generated bubbles above the level of the NMR detection coils at *ca.* 100 mL/min). In the immobilized cell experiments, a perfusion device allowed medium circulation through the NMR tube containing the Ca-alginate immobilized cells. The perfusion device consisted of a threaded 10-mm o.d. NMR tube (Wilmad Glass Co.) in which two capillary tubes were inserted, one in the bottom of the packed bed formed by the beads, and the other in the top of the packed bed. A peristaltic pump circulated the medium to and from a reservoir vessel outside the NMR magnet, in which N₂ gas was bubbled at *ca.* 300 mL/min. All experiments were conducted anaerobically.

Nuclear magnetic resonance (NMR) spectroscopy

NMR spectra were obtained in the Fourier-transform mode on a Bruker WM-300 spectrometer at 20°C. ³¹P NMR spectra were obtained at 121.49

MHz and were accumulated in 2 min blocks (240 scans) using 70° pulses and a repetition time of 0.5 sec. The chemical shifts were measured with glycerol phosphorylcholine (GPC) as internal standard which resonates at 0.49 ppm from 85% phosphoric acid (0 ppm) with upfield shifts given a negative sign. Peak resonance assignments were made from assignments reported in the literature.^(9,11-13) Intracellular pH was determined from the chemical shift of the intracellular P_i resonance using an NMR titration curve obtained at physiologic ionic strength.^(9,11,13)

For estimation of intracellular concentrations, saturation constants were obtained for each peak, comparing intensities in fully relaxed spectra with intensities in partially saturated spectra using the actual experimental pulsing conditions as described above. 50 μL of phosphate (1 M) was added at the end of each experiment to convert intensity to concentration. For estimation of intracellular concentrations it was assumed that 1.67 g wet cells contains 1 mL of intracellular volume.⁽¹⁴⁾

FIDs (free induction decays) were stored during the course of the experiments in 8K files in the Bruker Aspect 3000 computer hard disk and were transferred later to a VAX 11/780 computer where all subsequent processing was performed using the LAB ONE^(TM) NMR1 spectroscopic data analysis software system.⁽¹⁵⁾

Analyses

Samples taken from the reservoir vessel during the NMR immobilized cell experiments were filter sterilized and analyzed for glucose by Sigma Kit 510

using a Shimadzu UV-160 spectrophotometer. Ethanol was analyzed by gas chromatography utilizing a Shimadzu GC-9 chromatograph system equipped with a 2 m glass column packed with Chromosorb 101 (80/100) mesh: the helium carrier gas flow rate was 50 mL/min, the detector temperature was 200°C and the oven temperature was 130°C. Glycerol content was determined using an analytical kit for triglycerides (Sigma). Data processing of GC and HPLC chromatograms was made using a Shimadzu CR-3A integrator system. Also, suspended cell fermentations were done to mimic the conditions of the NMR experiments but used a lower cell density (*ca.* 0.1 gr_{wet wt.}/mL). Samples were taken at different times and analyzed for glucose, ethanol and glycerol as before.

RESULTS

Growth rate of immobilized cells

S. cerevisiae cells were immobilized at low cell density in Ca-alginate beads and placed in a packed-bed reactor as described in Materials and Methods. Subsequently, growth medium was circulated through the system, and cell growth was monitored as a function of time. Results are shown in Figure 2 for both immobilized and liquid phases. There is no lag in cell growth in the Ca-alginate beads. Cell growth in the liquid phase is evident 6 h after the start of the experiment. This indicates that cell release from the beads to the medium is not significant in the early stages and glucose uptake and ethanol production can be attributed to the cells growing within the immobilization matrix.

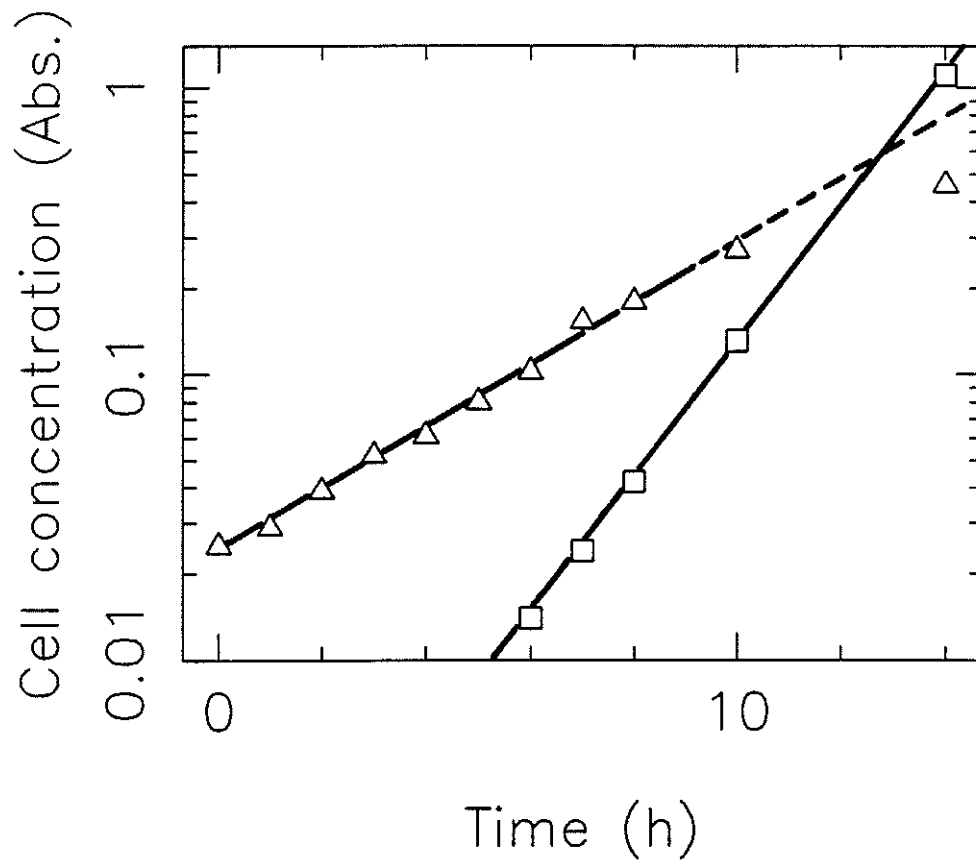


Figure 2: Cell concentration data for *Saccharomyces cerevisiae* growing in a recirculation reactor.

- (Δ) Immobilized cells (cell mass per bead).
- (\square) Suspended cells.

The average immobilized cell specific growth rate (μ) from two experiments is 0.25 h^{-1} . This result compares well with previous work done with *S. cerevisiae* entrapped in Ca-alginate. Hannoun⁽⁶⁾ and Simon⁽⁸⁾ obtained $\mu = 0.26 \text{ h}^{-1}$ in separate studies. The growth rate of immobilized cells corresponds to a doubling time of

$$d_t = \frac{\text{Ln } 2}{0.25} = 2.8 \text{ h}$$

The growth rate of immobilized cells is slower than the growth rate of suspended cells ($\mu = 0.41 \text{ h}^{-1}$), in agreement with several other studies.⁽⁶⁻⁸⁾

Glucose and ethanol concentrations were also monitored as functions of time in the fermentation vessel. Results of a typical experiment are shown in Figure 3.

Fermentation kinetics of immobilized-grown cells

In all the following experiments, *S. cerevisiae* cells were allowed to grow anaerobically for 7 h (ca. 3 generations) within the Ca-alginate beads. Then, the beads were dissolved and the cells harvested. These cells were used to compare suspended and immobilized cell glucose metabolism in a fashion similar to that described in Chapter 2. Resting cells in a buffer without any nutrients were suddenly exposed to glucose solution at time zero. No cell growth was detected either in the suspended cell or in the immobilized cell runs under these experimental conditions. Figure 4 shows ethanol production (per cell mass) as a function of time for suspended and immobilized Ca-alginate grown cells. Ethanol is produced faster in immobilized cells than in suspended cells with

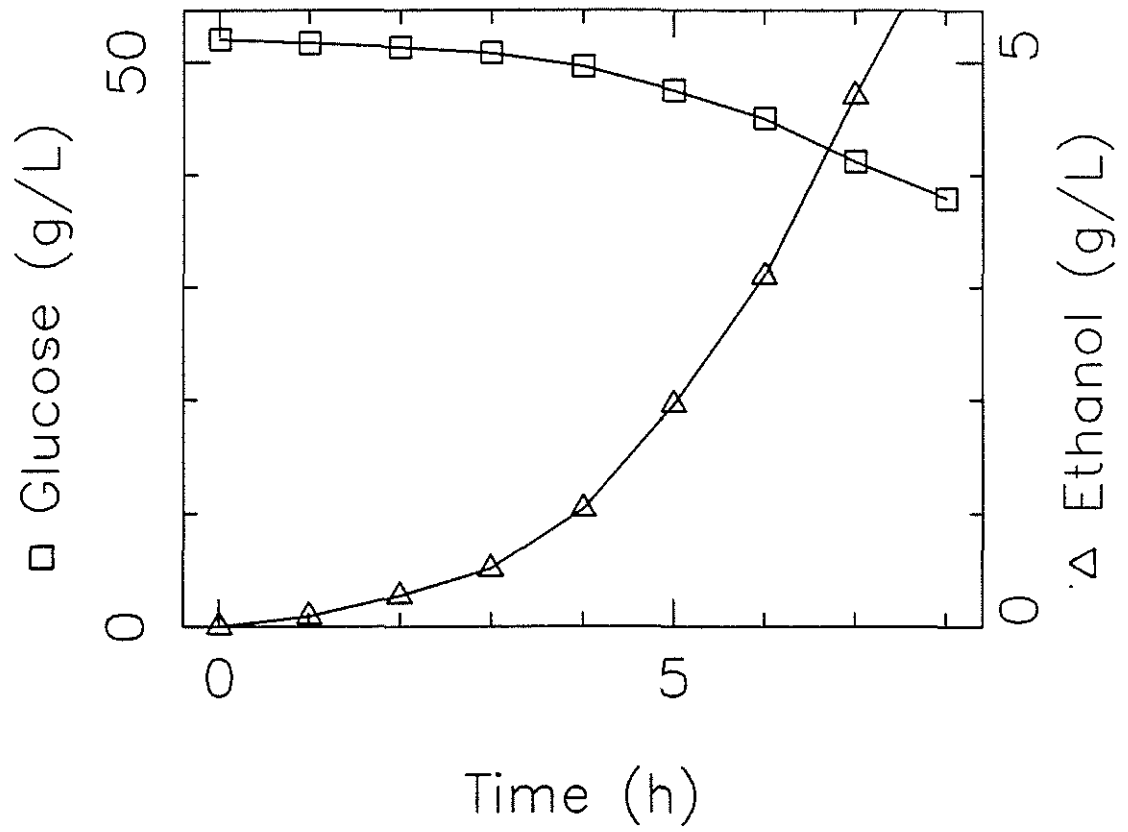


Figure 3: Glucose and ethanol concentrations in recirculation medium

approximately a 2:1 ratio, similar to the results of Chapter 2. Accordingly, glucose is consumed faster in immobilized cells. Glycerol production is about 10% of the ethanol production. The experimental values are listed in Table I. Observable Thiele modulus and Biot number calculations indicate that intra- and extraparticle diffusion limitations are negligible for this system.

TABLE I: Substrate uptake and product formation rates for cells grown within a Ca-alginate matrix.

Rates were estimated from the slope of concentration vs. time data and are expressed in mmol per L of cell volume per min, assuming that 1.6 gr of wet cells contains 1.0 mL of cells.⁽¹⁴⁾

	Suspended cells ($\frac{\text{mmol}}{\text{min L}_{\text{cells}}}$)	Immobilized cells ($\frac{\text{mmol}}{\text{min L}_{\text{cells}}}$)
Glucose uptake	21.1	42.7
Ethanol prod.	37.1	70.0
Glycerol prod.	3.5	6.9

Phosphorus-31 NMR measurements

Figure 5 shows a comparison between suspended and immobilized cell ^{31}P NMR spectra taken under resting conditions. The P_i^{zn} peak of the immobilized cell spectrum appears at lower ppm than the corresponding peak of the suspended cell spectrum. This indicates that the immobilized cell intracellular pH is lower initially, probably due to collapse of the transmembrane potential during the immobilization process. Another difference observed in Figure 5 is

in the polyphosphate content. Immobilized cells have a higher polyphosphate concentration (69 mM) than suspended cells (22 mM).

Figure 6 shows ^{31}P NMR spectra of immobilized *S. cerevisiae* cells over different time intervals after adding glucose to starved Ca-alginate grown cells. The qualitative features of these results are similar to the results described in Chapter 2. Prior to glucose addition the SP resonance is at its basal level and consists mostly of 3-phosphoglycerate. After glucose addition, SP rapidly increases and now is mainly composed of contributions from glucose-6-phosphate, fructose-6-phosphate and 3-phosphoglycerate. The $P_i^{i'n}$ peak decreases and shifts downfield. By 16-28 min a "steady-state" condition is established during which spectral components corresponding to intracellular species are relatively constant.

Figure 7 shows a comparison between suspended and immobilized cell spectra during the quasi-steady state after feeding glucose. The intracellular pH of immobilized cells (6.8) is slightly lower than the intracellular pH of suspended cells (6.9) as indicated by the position of the $P_i^{i'n}$ peak. Also, qualitative differences in the shape of the SP peak indicate a different SP composition between suspended and immobilized cells.

Quasi-steady state metabolite concentrations were estimated by deconvolution of the SP region into its individual components and by integration of the corresponding peaks as described in Chapter 2. Table II shows the values obtained. Suspended cells have lower levels of glucose-6-phosphate, fructose-6-phosphate, 3-phosphoglycerate and ATP+ADP than immobilized cells. Polyphosphate con-

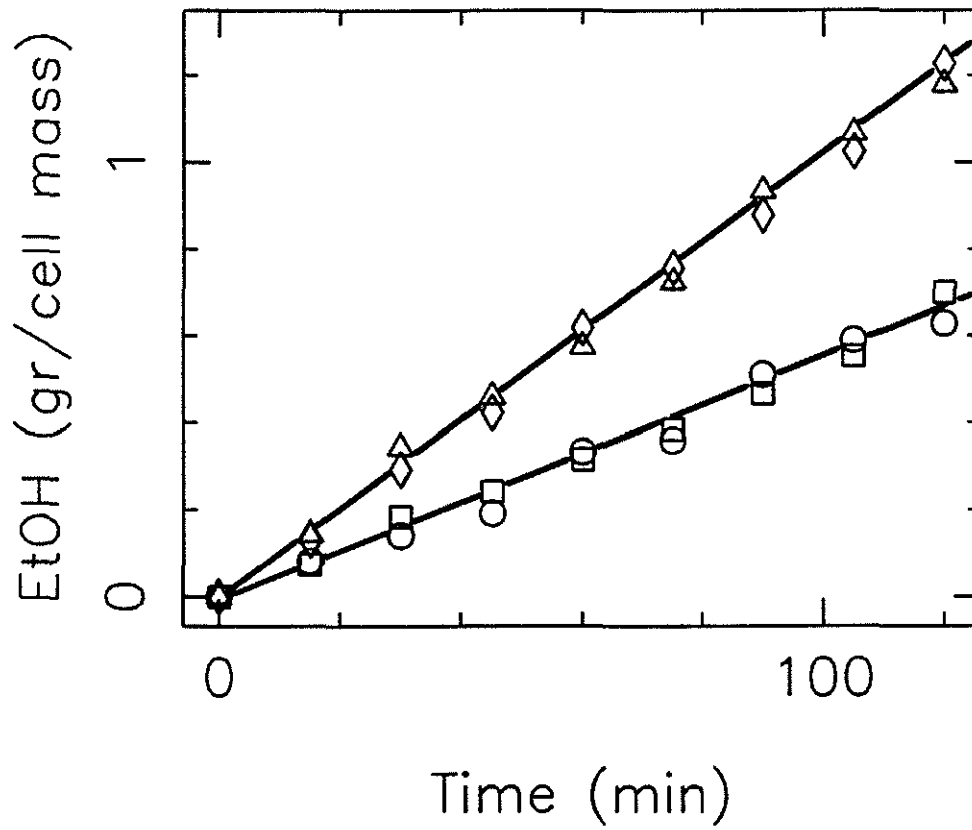


Figure 4: Ethanol production by *S. cerevisiae* cells.

(□,○) Suspended cells.
(△,◇) Immobilized cells.

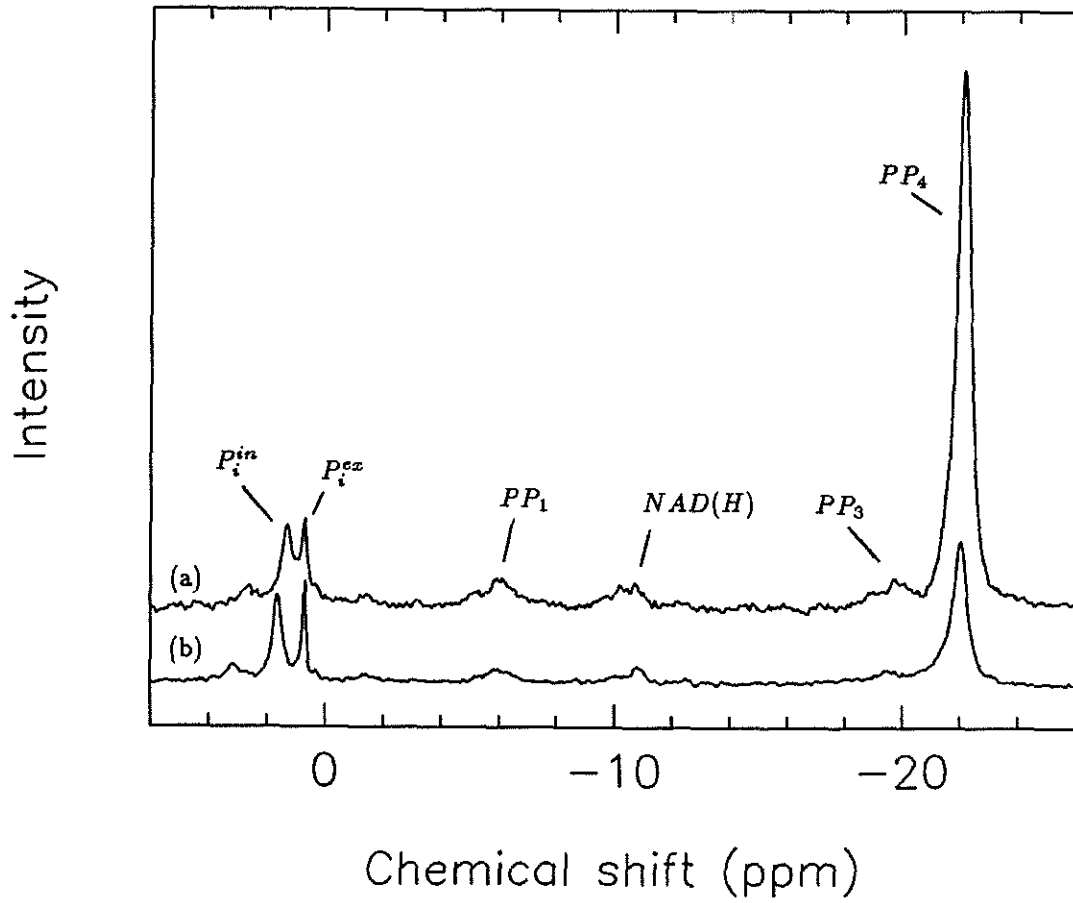


Figure 5: Comparison of ^{31}P spectra of cells resting in starvation buffer.

- (a) Suspended cells.
- (b) Immobilized cells.

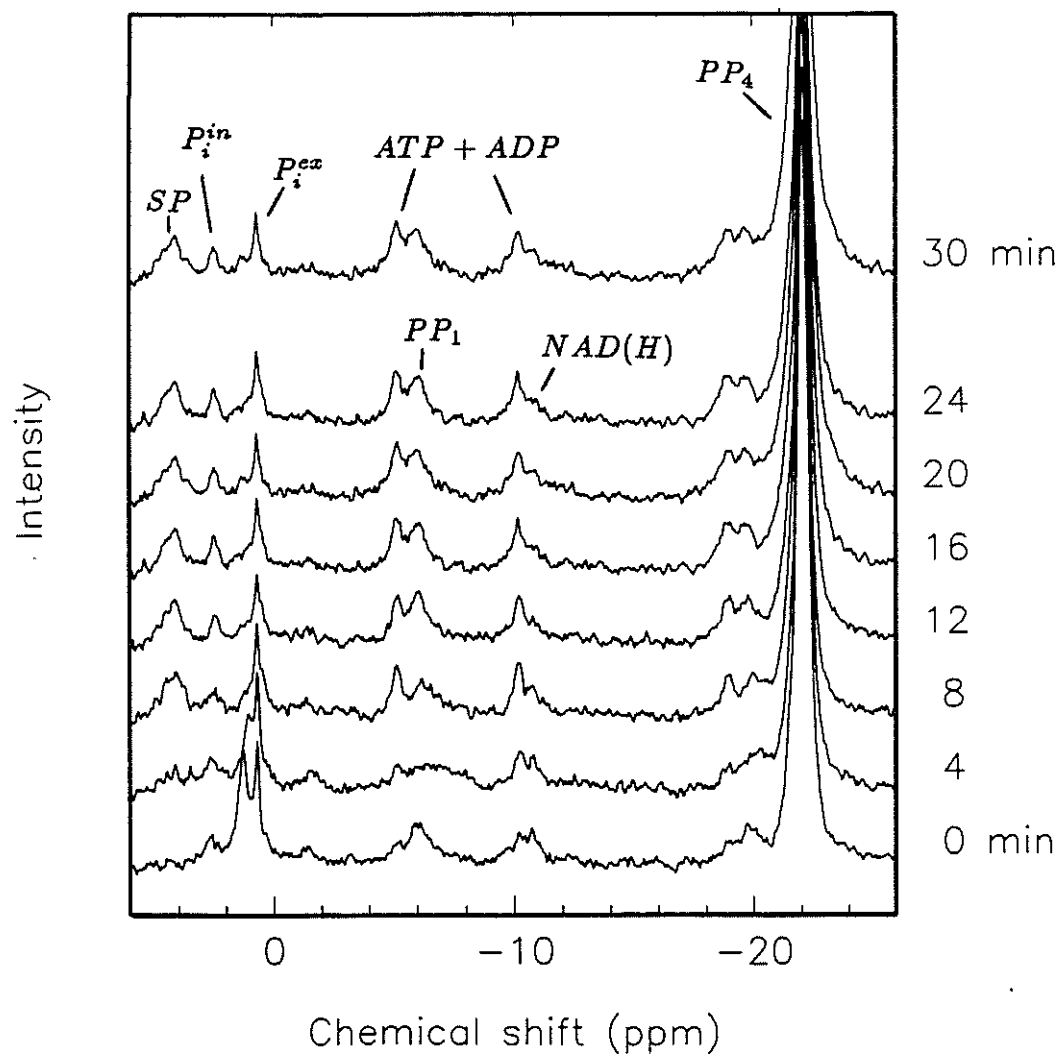


Figure 6: ^{31}P NMR spectra of *S. cerevisiae* cells entrapped in Ca-alginate.

Although the plotted spectra are on a 4 minute interval, a spectrum was accumulated every 2 minutes.

TABLE II: Comparison of intermediate metabolite concentrations of cells grown in a Ca-alginate matrix.

Units are in mmol per L of cell volume, assuming that 1.6 gr of wet cells contains 1.0 mL of cells.⁽¹⁴⁾ Sugar-phosphate concentrations were obtained using an *in vivo* deconvolution method.⁽¹³⁾ The $ATP_{\alpha} + ADP_{\alpha}$ peak was integrated to estimate $ATP + ADP$ levels.

	Suspended cells	Immobilized cells
pH ⁱⁿ	6.9	6.8
	($\frac{\text{mmol}}{\text{L}_{\text{cells}}}$)	($\frac{\text{mmol}}{\text{L}_{\text{cells}}}$)
Glucose-6-P	0.6	1.5
Fructose-6-P	0.2	0.7
Fructose-1,6-P	3.9	2.3
3-P-Glycerate	0.1	1.0
ATP+ADP	2.2	3.1
UDPG	0.8	0.8
PP ₄	21.	75.

centration (PP₄) is substantially lower in suspended cells while UDPG levels are similar in both configurations.

DISCUSSION

Metabolic changes due to cell immobilization are evident in several investigations. However, interpretation of the results is sometimes difficult because experimental complexities complicate conclusions about the observed differences.

In the experiments described in this chapter, *S. cerevisiae* cells were grown

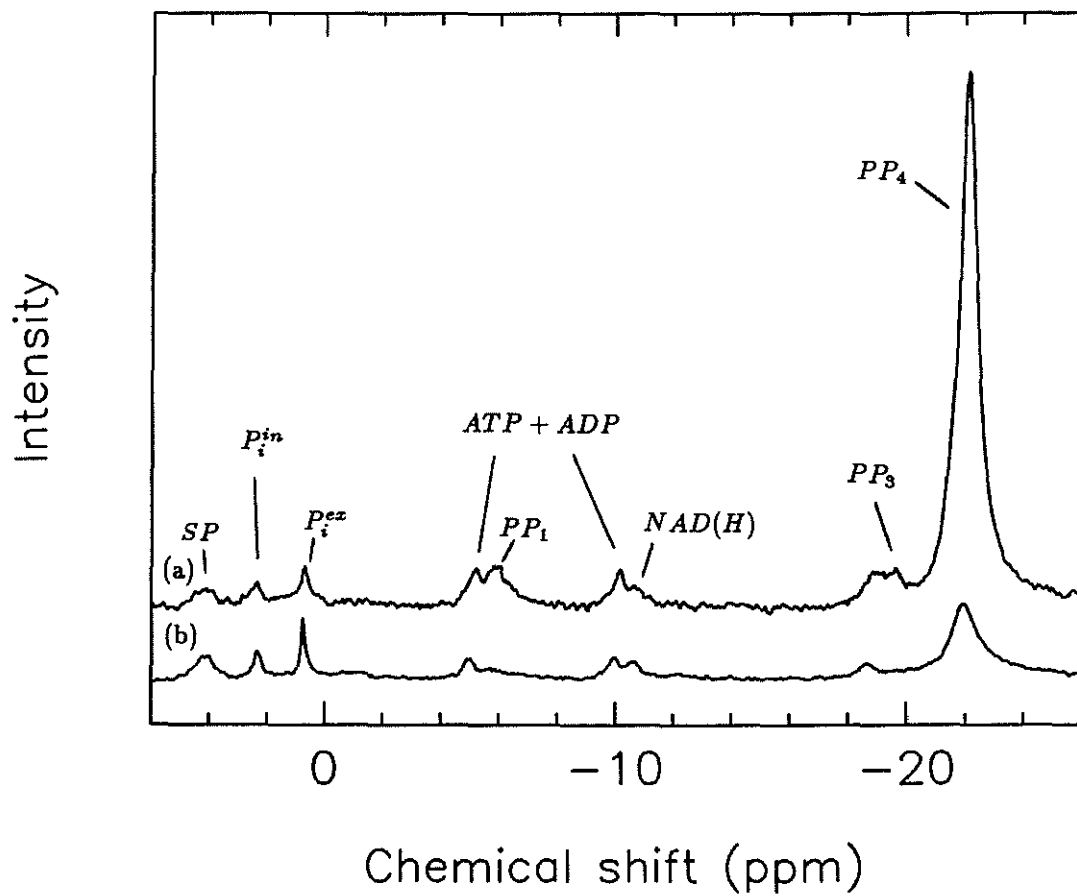


Figure 7: ^{31}P spectra of *S. cerevisiae* cells grown in Ca-alginate beads at steady-state glucose metabolism.

- (a) Suspended cells.
- (b) Immobilized cells.

within Ca-alginate beads in a well defined system and under the same controlled conditions in order to provide a consistent biomass sample for each of the kinetic studies.

The growth rate of yeast *S. cerevisiae* is lower when the cells are grown entrapped in Ca-alginate ($\mu = 0.25 \text{ h}^{-1}$) than when they are grown in suspension ($\mu = 0.41 \text{ h}^{-1}$) under similar conditions. This has been observed for similar cells entrapped in alginate,^(6,7) and in cells on the surface of beads coated with cross-linked gelatin.⁽⁸⁾ In the case of cell entrapment, the reduction in growth rate may be partly due to the physical constraint imposed by the alginate matrix. In situations where cells are confined to regions of fixed volume, cell growth can generate pressures of many atmospheres, possibly altering normal metabolic regulation in the cells.⁽¹⁶⁾

In order to study the effects of growing the cells within the alginate matrix on glucose catabolism, the beads were dissolved and the cells harvested. Some of these cells were entrapped again in alginate. This was done for two reasons: to have a diffusion-free system because cell colony formation within the beads during the growth phase may impose a mass-transfer limitation in the system;⁽¹⁷⁾ and, to have suspended cells grown similarly to be able to compare with the immobilized cell behavior. Subsequently, samples of suspended cells and immobilized cells were exposed to glucose. Therefore, in contrast to the experiments in Chapter 2, these experiments reflect alterations in metabolic kinetics from growth of cells within the immobilization matrix.

The qualitative differences between suspended and immobilized cells grown in a Ca-alginate matrix catabolizing glucose are similar to the differences ob-

served in Chapter 2 for cells grown in suspension. Immobilized cells have higher ethanol and glycerol production. Also the intracellular pH in immobilized cells is slightly lower than in suspended cells. This may indicate that cell membrane permeability is affected. Several researchers have suggested that immobilization leads to permeabilization of the cell membrane.⁽¹⁸⁻²⁰⁾ An increase in cell membrane permeability has been proposed to explain observed increases in glucose uptake and ethanol production rates. However, glucose transport in yeast *S. cerevisiae* is accomplished by facilitated diffusion through a carrier protein,^(21,22) and increasing the membrane permeability should have no direct effect on the rate of glucose uptake. Cell immobilization may increase the leakiness of the cell membrane, making it more permeable to protons. This would affect ATP requirements because the cell would have to consume more ATP to keep a constant intracellular pH. This is consistent with the higher fermentation rate observed in immobilized cells.

Another striking difference between suspended and immobilized cells is in the polyphosphate content. (This difference was not observed for the suspension-grown cells discussed in Chapter 2.) Immobilized resting-cells have three times more polyphosphate than suspended resting-cells. A different distribution of polyphosphates was also observed in *S. cerevisiae* during dehydration.⁽²³⁾ Polyphosphates are mainly localized in the vacuolar space,⁽²⁴⁾ although there is experimental evidence that some fraction of polyphosphate is localized outside the plasma membrane.^(25,26) It has been suggested that vacuolar polyphosphate provides maintenance energy by hydrolysis of their high-

TABLE III: Ethanol production ratios as functions of growth and biocatalyst state.

All ratios are referred to ethanol production rate of suspended suspension-grown cells (26.7 mM/min) at pH^{ex} 5.5.

	Suspended cells	Entrapped cells
Suspension-grown cells	1	1.8
Alginate-grown cells	1.4	2.7

energy phosphates.^(27,28) Also, polyphosphates function as a cation trap reducing the osmotic pressure by binding to cationic substances.⁽²⁹⁾

At steady-state glucose metabolism, the concentration of polyphosphates slightly decreased in suspended cells from 22 to 21 mM as observed elsewhere for cells in similar conditions.^(27,30,31) On the other hand, polyphosphate concentration increased from 69 mM to 75 mM for the entrapped cells. The synthesis of polyphosphate in immobilized cells may be in response to a decrease in water activity in the cell environment. Ca-alginate entrapped cells are in an environment with molecules capable of organizing water and thereby decreasing the amount of water available to the cells. A similar increase in polyphosphate synthesis was observed in *Saccharomyces mellis* grown in different salt levels,⁽³²⁾ in agreement with the reduced water activity hypothesis. These results suggest that polyphosphate exhibits compartmentalization not only regarding cellular localization, but also with respect to metabolic behavior.

Cells grown within a Ca-alginate matrix have a different glucose catabolism kinetics than similar cells grown in suspension. Table III summarizes ethanol production ratios of suspension-grown cells (Chapter 2) and of alginate-grown cells (this chapter). The ethanol production rate of suspended suspension-grown cells at pH^{ex} 5.5 is taken as reference (26.7 mM/min). If biocatalyst states (suspended or immobilized cells) are compared in Table III, ethanol production rate is a factor of two higher in immobilized cells, independent of the cell growth conditions. If growth conditions (in suspension or entrapped) are compared, ethanol is produced 1.5 times faster in alginate-grown cells than in suspension-grown cells, independent of the biocatalyst configuration. The highest increment in ethanol production rate is observed in immobilized alginate-grown cells. Ethanol is produced 2.7 times faster in these cells than in suspended suspension-grown cells. Intracellular metabolite concentrations in suspension-grown cells differ from those in entrapped-grown cells (Table II, Chapter 2; and Table II, this chapter). Total sugar phosphate levels are higher in suspension-grown cells than in alginate-grown cells (12 mM and 5 mM respectively), but the composition of the sugar phosphates is similar in both systems. Intracellular pH has similar values in all cases.

These results suggest that cell immobilization is affecting cell metabolism at different levels. The differences in glucose catabolism observed in suspension-grown cells entrapped in Ca-alginate are manifested in a very short period of time and under non-growing conditions. This reflects changes in the regulation of some rate-influencing step in the yeast glucose catabolism pathway. On the other hand, when cells are allowed to grow within the alginate matrix, the

biosynthetic pathways respond differently than when similar cells are grown in suspension, as indicated by the lower specific growth rate observed in these entrapped cells. Glucose catabolism is also altered as indicated by the increase in fermentation rates and by different levels of intracellular components.

Major shifts in metabolism and in fermentation kinetics due to cell entrapment in Ca-alginate are evident from the result of this work. An understanding of the interactions between cells and environment is essential when designing and applying immobilized cell biocatalysts.

Acknowledgements

This research was sponsored by the National Science Foundation.

REFERENCES

1. Linko P., and Linko Y., *CRC Critical Reviews in Biotechnology*, **1**, 289-338 (1983).
2. Margaritis A., and Merchant F., *CRC Critical Reviews in Biotechnology*, **1**, 339 (1983).
3. Jirku V., Turkora T., and Krumphanzl V., *Biotechnol. Lett.*, **2**, 509 (1980).
4. Koshcheyenko K., Turkina M., and Skryabin G., *Enzyme Microb. Technol.*, **5**, 14 (1983).
5. Inloes D., Smith W., Taylor D., Cohen S., Michaels A., and Robertson C., *Biotechnol. Bioeng.*, **23**, 79 (1981).
6. Hannoun B., "Ethanol Production by *Saccharomyces cerevisiae* Immobilized in Calcium Alginate", Ph. D. Thesis, California Institute of Technology, Pasadena, CA, (1988).
7. Simon J., Dubois E., and Messenguy F., *Arch. Int. Physiol. Biochim.*, **94**, B45 (1986).
8. Doran P., and Bailey J., *Biotechnol. Bioeng.*, **28**, 73 (1986).
9. Galazzo J., Shanks J., and Bailey J., *Biotechnol. Techniques*, **1**, 1 (1987).
10. Klein J., Stock J., and Vorlop K., *Eur. J. Appl. Microbiol. Biotechnol.*, **18**, 86 (1983).

11. den Hollander J., Ugurbil K., Brown T., and Shulman R., *Biochemistry*, **20**, 5871 (1981).
12. Navon G., Shulman R., Yamane T., Ecclesball T., Lam K., Baronotsky J., and Marmur J., *Biochemistry*, **18**, 4487 (1979).
13. Shanks J., and Bailey J., *Biotechnol. Bioeng.*, **32**, 1138 (1988).
14. Gancedo J., and Gancedo C., *Biochimie*, **55**, 205 (1973).
15. LAB ONE™ NMR1 Spectroscopic Data Analysis Software System, Revision 2.70, Syracuse University, New Methods Research Inc., (1985).
16. Fowler J., and Robertson C., *Nutrient Transport and Cellular Morphology in Immobilized Cell Aggregates.* Engineering Foundation Conference. Biochemical Engineering VI, Santa Barbara, CA,(1988).
17. Karel S, Libicki S., and Robertson C., *Chem. Eng. Sci.*, **40**, 1321 (1985).
18. Mattiason B., "Immobilized Viable Cells." In CRC Handbook of Immobilized Cells and Organelles, **2**, 23 (1983).
19. Marcipar A., Cochet T., Brankerridge L., and Lebeault A., *Biotechnol. Lett.*, **1**, 65 (1979).
20. Vijayalakshmi M., Marcipar A., Segard E., and Brown G., *Ann. N.Y. Acad. Sci.*, **326**, 249 (1979).
21. Lang J., and Cirillo V., *J. Bacteriol.*, **169**, 2932 (1987).
22. Kotyk A., *Fol. Microbiol.*, **12**, 121 (1967).
23. Kulaev I., Laivenieks M., Bobyk M., and Beker M., *Prikl. Biokhim. Mikrobiol.*, **13**, 893 (1977).

24. Cooper T., "Transport in *Saccharomyces cerevisiae*" In: The Molecular Biology of the Yeast, Metabolism and Gene Expression", p. 399, Cold Spring Harbor, New York, (1982).
25. Urech K, Durr M, Boller T., and Wiemken A., *Arch. Microbiol.*, **116**, 275 (1978).
26. Tijssen J., and Van Steveninck J., *Biochem. Biophys. Res. Comm.*, **119**, 447 (1984).
27. Gillies R., Ugurbil K., den Hollander J., and Shulman R., *Proc. Natl. Acad. Sci.*, **78**, 2125 (1981).
28. Nicolay K., Scheffers W., Bruinenberg P., and Kaptein R., *Arch. Microbiol.*, **134**, 270 (1983).
29. Tijssen J., Dubbelman T., and Van Steveninck J., *Biochim. Biophys. Acta*, **721**, 394 (1983).
30. den Hollander J. A., Ugurbil K., Brown T., and Shulman R. G., *Biochemistry*, **20**, 5871 (1981).
31. Shanks J., "Metabolic Engineering Applications of In Vivo ^{31}P and ^{13}C NMR Studies of *Saccharomyces cerevisiae*", Ph. D. Thesis, California Institute of Technology, Pasadena, CA, (1988).
32. Weinber R., *J. Bacteriol.*, **121**, 1122 (1975).

CHAPTER 4

**FERMENTATION PATHWAY KINETICS AND METABOLIC
FLUX CONTROL IN SUSPENDED AND IMMOBILIZED
*SACCHAROMYCES CEREVISIAE***

ABSTRACT

Measurements of rates of glucose uptake and of glycerol and ethanol formation combined with knowledge of the metabolic pathways involved in *S. cerevisiae* were employed to obtain *in vivo* rates of reactions catalyzed by pathway enzymes for suspended and alginate-entrapped cells at pH 4.5 and 5.5. Intracellular concentrations of substrates and effectors for most key pathway enzymes were estimated from *in vivo* phosphorus-31 nuclear magnetic resonance measurements. These data show the validity, *in vivo*, of kinetic models previously proposed for phosphofructokinase and pyruvate kinase based on *in vitro* studies. Kinetic representations of hexokinase, glycogen synthase, and glyceraldehyde 3-phosphate dehydrogenase, which incorporate major regulatory properties of these enzymes, are all consistent with the *in vivo* data. This detailed model of pathway kinetics and these data on intracellular metabolite concentrations allow evaluation of flux-control coefficients for all key enzymes involved in glucose catabolism under the four different cell environments examined. This analysis indicates that alginate entrapment increases the glucose uptake rate and shifts the step most influencing ethanol production from glucose uptake to phosphofructokinase. The rate of ATP utilization in these nongrowing cells strongly limits ethanol production at pH 5.5, but is relatively insignificant at pH 4.5.

INTRODUCTION

Many differences between suspended and immobilized cell metabolism have been determined experimentally by several independent investigations. Altered cellular composition,^(1,2) unusual cell morphology⁽²⁻⁵⁾ and productivity and substrate uptake enhancement^(2,6,7) are among the differences most often reported. However, all the studies provide only a qualitative explanation about the possible causes of such alterations. A more quantitative description of immobilization effects upon cell metabolism is needed in order to manipulate the output of immobilized cell systems, either to optimize a particular process or to intensify the production of any product of interest.

Application of the principles of the metabolic control theory (MCT) developed in the 1970s by Kacser and Burns⁽⁸⁾ and by Heinrich and Rapoport⁽⁹⁾ provides a quantitative method to identify the effects of cell immobilization on cell metabolism. The MCT is related to another approach called Biochemical System Theory (BST) developed in the late 1960s by Savageau.⁽¹⁰⁻¹²⁾ MCT assumes that the rate law of each step is independent of any other step and a linear function of enzyme concentrations. In BST those assumptions are not needed. BST provides a general approach to deal with cases when overall enzymatic reactions depend on gene dose, enzyme concentration or molecular activity in a non-linear fashion. [See references (11) and (12) for a detailed discussion.]

MCT requires the calculation of control coefficients for each step in the

pathway being studied. The magnitudes of such coefficients give the extent of control exerted by each step on the overall flux throughout the pathway. Therefore, a quantitative measure of immobilization effects will be provided by comparing the control coefficients of suspended cells with the control coefficients of immobilized cells. The calculation of control coefficients requires a detailed knowledge of the intracellular state as well as *in vivo* values of system parameters such as intracellular pH and allosteric effector levels.

In Chapter 2 a comparison of glucose metabolism between suspended and alginate-entrapped *Saccharomyces cerevisiae* cells previously grown in suspension, is reported. Nuclear magnetic resonance (NMR) spectroscopy, a non-invasive technique, was used to monitor the intracellular state of both suspended and immobilized cells during anaerobic conversion of glucose to ethanol. Phosphorus-31 NMR of fermenting immobilized and suspended cells shows differences in intermediate metabolite levels such as fructose-1,6-diphosphate, glucose-6-phosphate and 3-phosphoglycerate and in intracellular pH. Carbon-13 NMR shows an increase in polysaccharide production. Glucose uptake and ethanol and glycerol production are approximately two times faster in immobilized cells than in suspended cells.

The experimental results⁽¹³⁾ are summarized in Table I. In this paper, these results are used together with *in vitro* information from the literature to obtain *in vivo* kinetic representations for each key step in the pathway from glucose to ethanol and the associated branches going to glycerol and polysaccharide storage. Then, the calculation of control coefficients is done by applying

TABLE I: Experimental data summary for suspension-grown cells.

Experimental data summary for suspended and immobilized cell experiments at steady-state glucose fermentation for suspension-grown cells.⁽¹³⁾ Intracellular pH (pH^{in}) and intermediate metabolite concentration were estimated using ^{31}P NMR. Substrate uptake and ethanol and glycerol production rates were estimated from the slope of concentration vs. time data.⁽¹³⁾ Concentrations are expressed in mmol per L of cell volume (mM) and velocities in mM per min.

	Suspended cells pH^{ex} 5.5	Suspended cells pH^{ex} 4.5	Immobilized cells pH^{ex} 5.5	Immobilized cells pH^{ex} 4.5
pH^{in}	7.05	6.94	6.80	6.76
Glucose-6-P	1.4	0.7	4.4	3.1
Fructose-6-P	0.8	0.3	1.8	1.6
Fructose-1,6-P	6.6	10.1	5.4	5.8
3-P-Glycerate	0.1	0.1	4.5	1.4
ATP+ADP	2.7	2.2	2.7	2.3
UDPG	0.6	0.7	1.7	1.8
Glucose uptake	14.5	17.3	35.1	38.2
Ethanol prod.	26.7	32.2	49.0	55.0
Glycerol prod.	1.8	1.9	3.7	3.8

MCT principles, allowing a quantitative comparison between suspended and immobilized cell metabolism.

MODEL DESCRIPTION

The metabolic pathway from glucose to ethanol, glycerol and polysaccha-

rides is shown in Figure 1. The enzymes of the intermediate steps not shown are assumed to catalyze very fast reactions so that equilibria are maintained at all times.

Glucose enters the cell by facilitated diffusion^(14,15) and then enters the cell enzymatic network. The rate of this step is denoted by V_{In} . Glucose is then phosphorylated by hexokinase, producing glucose-6-phosphate at rate V_{HK} . The flow of glucose-6-phosphate into the oxidative and non-oxidative pentose pathways is not included in the model because experimental evidence^(16,17) under the same conditions as used in the experiments reported in Table I shows that the flow through those pathways is not significant. Trehalose and glycogen production are considered important because an increase in polysaccharide storage is one of the observed differences between suspended and immobilized cells.^(2,13) V_{Tre} and V_{Gly} are the rates of trehalose and glycogen production, respectively. Glucose-6-phosphate is considered to be at equilibrium with fructose-6-phosphate. Fructose-6-phosphate is then phosphorylated by phosphofructokinase at rate V_{PFK} . A futile cycle between fructose-6-phosphate and fructose-1,6-diphosphate is possible if the enzyme fructose-1,6-diphosphatase is active. However, this enzyme is mostly inactive under the experimental conditions used in this study.⁽¹⁷⁾ Glycerol production is also included as a branch at the fructose-1,6-diphosphate level with rate V_{Gol} . Glyceraldehyde 3-phosphate dehydrogenase has some degree of control in the pathway⁽¹⁸⁾ and is included in the model to connect the phosphofructokinase and pyruvate kinase steps. The rate of this step is denoted by V_{GAPD} . Finally, pyruvate kinase produces ethanol at rate V_{PK} . (V_{Eth} is the ethanol production rate measured experimentally.)

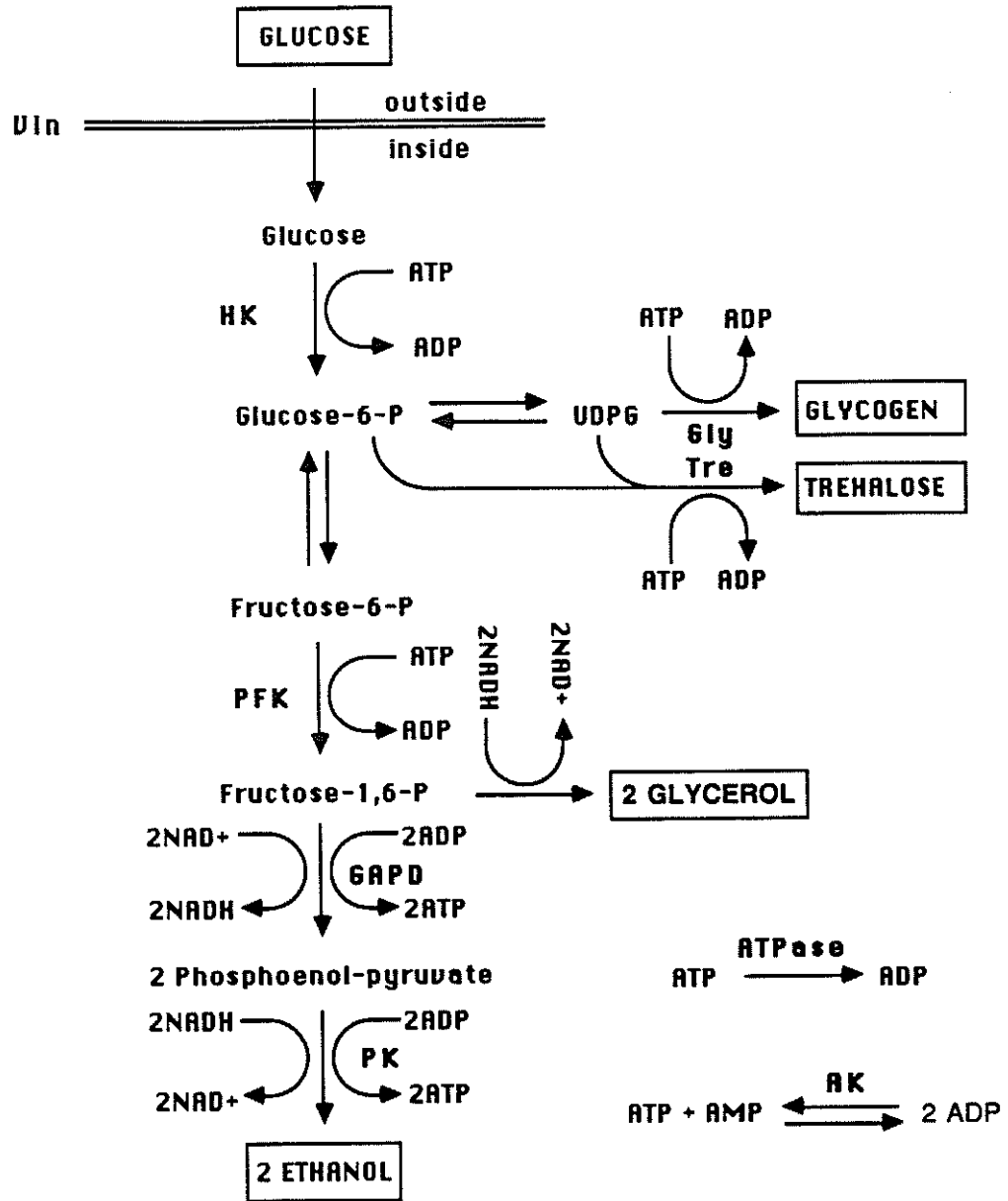


Figure 1: Anaerobic fermentation pathway of yeast *S. cerevisiae*.

The enzymes of the intermediate steps not shown are assumed to catalyse very fast reactions so that equilibria is maintained at all times.

Other important reactions taking place in glucose metabolism are adenylate kinase, which exchanges ATP, ADP and AMP levels, and a generalized ATPase functioning as an ATP-sink reaction with rate V_{ATPase} , which represents ATP consumption due to any maintenance requirements by the cell.

Quasi-steady state flux relationships

The comparison between suspended and immobilized cells has been done at steady-state conditions of intermediate metabolite concentrations. After 10-15 min of feeding glucose to either suspended or immobilized cells, a quasi-steady state is observed during which intermediate metabolite concentrations are relatively constant.⁽¹³⁾ This is confirmed by observing in a ^{31}P NMR experiment an approximate time-invariant shape of the peak corresponding to the sugar-phosphates.

At this steady state the rates through each step are related through the following relationships:

$$V_{In} = V_{HK} = V_{Tre} + V_{Gly} + V_{PFK}$$

$$V_{PFK} = \frac{1}{2} \cdot (V_{EtOH} + V_{Gol}) \quad (1)$$

$$V_{Pol} = V_{Tre} + V_{Gly} = V_{In} - \frac{1}{2} \cdot (V_{EtOH} + V_{Gol})$$

$$V_{ATPase} = 2 \cdot (V_{EtOH} - V_{In})$$

Thus, measurement of glucose uptake (V_{In}), glycerol production (V_{Gcl}) and ethanol production (V_{EtOH}) rates provides most of the internal reaction rates at the steady-state conditions.

Estimation of *in vivo* rate parameters for key pathway reactions

Estimation of *in vivo* parameters for the reactions in the model pathway is done using the results of the suspension-grown cell experiments (Table I).

Processes that change the total amount of adenine nucleotides are considered negligible in the time span of the experiments and are not included in the model. Therefore, the sum of adenine nucleotides (AN) is assumed to be constant:

$$AN = ATP + ADP + AMP \quad (2)$$

AN is a free parameter of the model, but the same value is used for both suspended and immobilized cells in all the experimental conditions shown in Table I because the cells are at the same initial state. A lower bound for AN is known from the information available from NMR:

$$AN > ATP + ADP \quad (3)$$

and since AMP concentration is lower than the ATP and ADP concentrations in glucose metabolizing cells,^(19,20,33) the upper bound is conservatively assumed to be:

$$AN < \left(\frac{1}{2}\right) \cdot (ATP + ADP) \quad (4)$$

ATP+ADP intracellular levels are between 2.7 mM and 2.2 mM (Table I), thus, the bounds of AN are:

$$2.7 \text{ mM} < AN < 3.3 \text{ mM} \quad (5)$$

A value of 3 mM was assumed for the total adenine nucleotide concentration in all the experiments.

At steady state the adenylate kinase reaction provides the following relationship:

$$K_{eq} = \frac{ADP^2}{ATP \cdot AMP} \quad ; \quad K_{eq} = 1 \quad \text{from reference (21)} \quad (6)$$

The values of ATP, ADP and AMP shown in Table II are obtained using equations (2) and (6) together with the NMR information of Table I regarding ATP+ADP concentration.

TABLE II: ATP, ADP and AMP concentrations.

ATP, ADP and AMP concentrations ($mmol/L_{cells}$) calculated using NMR information from Table I and equations (2) and (6) from the text (AN = 3 mM).

(mM)	Suspended cells pH ^{ex} 5.5	Suspended cells pH ^{ex} 4.5	Immobilized cells pH ^{ex} 5.5	Immobilized cells pH ^{ex} 4.5
ATP	2.02	1.19	1.94	1.35
ADP	0.72	0.99	0.76	0.96
AMP	0.26	0.82	0.30	0.69

Regulation of sugar transport in *S. cerevisiae* involves changes in the apparent affinity of the transport carrier controlled by glucose-6-phosphate

concentration.⁽²²⁻²⁴⁾ Glucose-6-phosphate appears to be bound to a part of the monosaccharide transport system that is not accessible from the cell exterior, impairing both the transport capacity of the system as well as its affinity.⁽²²⁾ Therefore, the glucose uptake step (V_{In}) is assumed to have a feed-back mechanism regulated by the intracellular glucose-6-phosphate level. A linear functionality is assumed between V_{In} and glucose-6-phosphate concentration as suggested experimentally in the literature⁽²³⁾ and by the data of Table I

$$V_{In} = V_{In}^0 + K_{G6P} \cdot G6P \quad (7)$$

The parameter values obtained from the data of Table I are:

$K_{G6P} = -2.1 \text{ mmol}/L_{cells}$, $V_{In}^0 = 19.7 \text{ mmol}/(L_{cells} \cdot \text{min})$ for suspended cells and $V_{In}^0 = 45.7 \text{ mmol}/(L_{cells} \cdot \text{min})$ for immobilized cells.

Hexokinase (HK) catalyzes a two substrate reaction with ordered single-displacement mechanism.⁽²⁵⁾ ATP and intracellular glucose are the two enzyme substrates. The analytical expression for this enzyme is shown in Table III. The binding constants of glucose and ATP were estimated by curve-fitting *in vitro* experiments from the literature.⁽²⁸⁾ The least-squares fitting shown in Figure 2 produced the parameter values listed in Table III.

There is evidence that hexokinase activity is affected by changes in pH, but this influence is negligible in the presence of ATP in the range of pHs observed experimentally.⁽²⁶⁾ Therefore no pH dependence is included in this model. The maximal velocity of HK is taken from reference (27) : $V_{HK}^{max} = 68.5 \text{ mM}/\text{min}$. This value was obtained for the same yeast strain used in this work and under

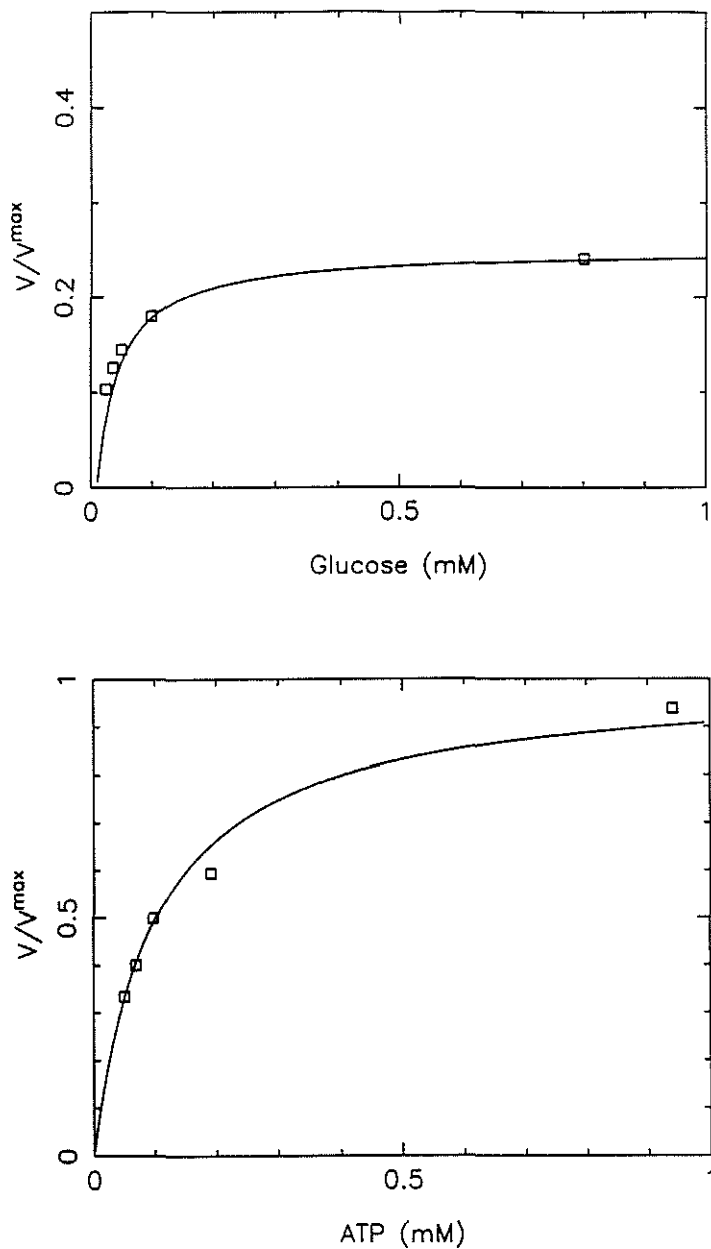


Figure 2: Least-squares fitting for estimation of hexokinase kinetic parameters.

In vitro experiments were taken from reference (28). The values obtained for glucose and ATP binding constants are listed in Table III. (\square) experimental values, (—) model fit.

TABLE III: Hexokinase kinetic expression.

Two-substrate reaction with an ordered single-displacement mechanism.⁽²⁵⁾ Concentration units are in ($mmol/L_{cells}$), rate units are in ($mmol/L_{cells}/min$) and binding-constant units are in ($mmol/L_{cells}$). V_{HK}^{max} from reference (27) and K_G^m , K_G^s and K_{ATP}^m were estimated by curve-fitting experimental data of reference (28) G^{in} is the intracellular glucose concentration (adjustable parameter).

$$V_{HK} = V_{HK}^{max} \cdot \left(\frac{1}{\frac{K_G^s \cdot K_{ATP}^m}{G^{in} \cdot ATP} + \frac{K_G^m}{G^{in}} + \frac{K_{ATP}^m}{ATP} + 1} \right)$$

parameter values:

$$\begin{array}{ll} V_{HK}^{max} = 68.5 & K_G^s = 0.0062 \\ K_G^m = 0.11 & K_{ATP}^m = 0.1 \end{array}$$

similar growth conditions. V_{HK}^{max} is assumed to be the same for both suspended and immobilized cells.

Trehalose is generally produced at 10-20% of the glycogen production rate.⁽²⁹⁾ In this model it is assumed that $V_{Tre} = 0.1 \cdot V_{Gly}$.

Glycogen synthetase (Gly) is represented by Michaelis-Menten kinetics with respect to the concentration of the substrate UDPG. Glucose-6-phosphate, a precursor in glycogen production, is an allosteric effector of Gly. Enzyme activity has been observed to be stimulated more than 20 times in the presence of glucose-6-phosphate.⁽³⁰⁾ Glucose-6-phosphate modifies both the UDPG binding affinity and the enzyme maximum velocity.^(30,31) The expression used to represent Gly is shown in Table IV.

The Hill model is used to describe the allosteric effect of glucose-6-

TABLE IV: Glycogen synthetase kinetic expression.

Glycogen synthetase is represented by Michaelis-Menten kinetics with Glucose-6-P as effector of the UDPG binding constant and of the enzyme maximum velocity.^(30,31) V_{Gly}^{max} and N estimated from experimental data of Table I. K_o^m , K^m and K_{gly} from reference (30) and (31). Units as in Table III. *UDPG*: uridine diphospho-glucose concentration.

$$V_{Gly} = \frac{V_{Gly}^{max} \cdot G6P^N}{(K_{Gly})^N + G6P^N} \cdot \left(\frac{1}{\frac{K_o^m}{UDPG} \left(1 + \frac{K^m}{G6P}\right) + 1} \right)$$

parameter values:

$$\begin{array}{ll} K_o^m = 1 & V_{Gly}^{max} = 14.31 \\ K^m = 1.1 & N = 8.26 \\ K_{Gly} = 2 & \end{array}$$

phosphate upon the maximum velocity:

$$V_{Gly}^{app} = \frac{V_{Gly}^{max} \cdot G6P^N}{K_{Gly}^N + G6P^N} \quad (8)$$

Changes in glucose-6-phosphate concentration above 5 mM cause no effect on enzyme activation.^(31,32) Therefore, V_{Gly}^{max} was calculated using the experimental data obtained for immobilized cells pH^{ex} 4.5 assuming that in this condition $V_{Gly}^{app} = V_{Gly}^{max}$. Also, half-maximum activation by glucose-6-phosphate is 2 mM.⁽³²⁾ Then, the only adjustable parameter in this expression is the Hill coefficient (N). Figure 3 shows the best fit to the V_{Gly}^{app} data calculated from the experimental values of Table I and the Gly kinetic expression of Table IV, with $N=8.25$. The number of sites in Gly to which glucose-6-phosphate may interact with (given by the Hill coefficient N) are not exactly known. A model of the enzyme has been proposed, which includes a single site for substrate binding

and several sites (at least six) for glucose-6-phosphate activation.⁽³¹⁾

Phosphofructokinase (PFK) is an allosteric enzyme with several effectors. AMP, P_i , fructose-2,6-diphosphate and pH are among the most important ones. P_i is not included in the kinetic expression because its concentration is about the same in all the experiments of Table I (ca. 10 mM). Fructose-2,6-diphosphate has been shown to be the missing effector in the discrepancy between measured *in vivo* and *in vitro* PFK rates.⁽³³⁾ However, in anaerobic conditions fructose-2,6-diphosphate has little effect on the glycolytic rate even when its concentration changes over the range from 3.2 mM to 0.6 mM.⁽³³⁾ Thus, this effector is not included in the kinetic expression of PFK.

The model of Monod, Wyman and Changeux⁽³⁴⁾ has been used extensively to describe the PFK reaction. The concerted transition model for allosteric enzymes described by Hess and Plesser⁽³⁵⁾ is used to represent this enzyme (Table V) with AMP as the allosteric effector. Typically, no pH dependence is considered in the kinetic expression.^(35,36) However, *in vitro* kinetic data show that pH strongly affects PFK activity, primarily by altering the allosteric constant L_0 .^(33,37) The influence of pH upon PFK was obtained from *in vitro* data^(33,37) and by calculating how the allosteric constant L_0 varies with pH using the kinetic expression of Table V.

Figure 4 shows the functionality of L_0 with pH so estimated. Therefore, knowing the intracellular pH, an estimation of the allosteric constant for the *in vivo* conditions can be made. An evaluation of how well the PFK kinetic expression represents the experimental data can be made using all the available data from Table I.

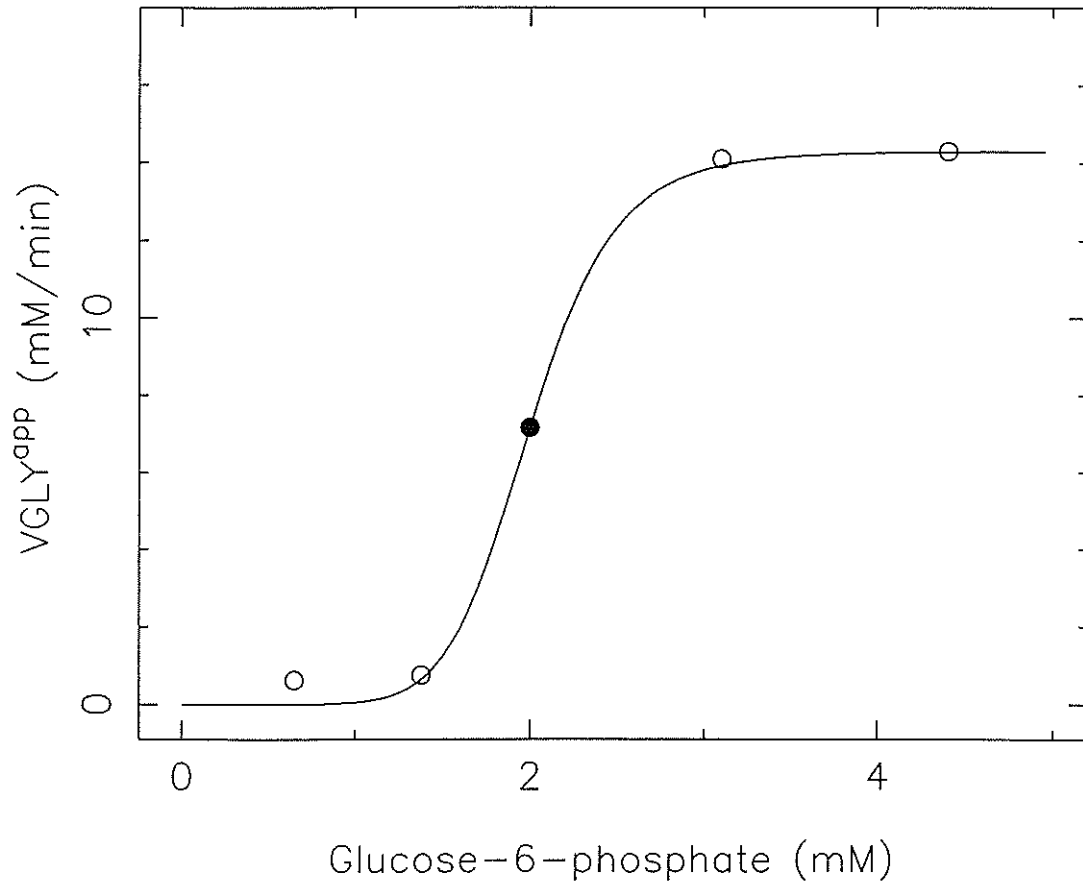


Figure 3: Glycogen synthetase maximum velocity as a function of glucose-6-phosphate *in vivo* concentration.

Glycogen synthetase maximum velocity (V_{Gly}^{app}). (○) calculated from the experimental data of Table I and kinetic expression of Table IV, (—) least-squares fit with $N = 8.25$ in Equation (8). Point (●) from reference (32).

TABLE V: Phosphofructokinase kinetic expression.^(33,34)

Parameter values from reference (34). L_0 value as a function of pH taken from the *in vitro* relationship shown in Figure 4. V_{PFK}^{max} estimated from experimental data of Table I. Units as in Table III.

$$V_{PFK} = V_{PFK}^{max} \cdot v_{PFK}(\lambda_1, \lambda_2, \gamma)$$

$$v_{PFK} = \frac{g_R \lambda_1 \lambda_2 R^{n-1} + q L g_T c_1 \lambda_1 c_2 \lambda_2 T^{n-1}}{R^n + L T^n}$$

where:

$$\lambda_1 = F6P / K_{R,F6P}$$

$$\lambda_2 = ATP / K_{R,ATP}$$

$$\gamma = AMP / K_{R,AMP}$$

$$c_j = K_{R,j} / K_{T,j}$$

$$q = V_{T,max} / V_{R,max}$$

$$L = L_0 \cdot \left(\frac{1 + c_\gamma \gamma}{1 + \gamma} \right)^n$$

$$R = 1 + \lambda_1 + \lambda_2 + g_R \lambda_1 \lambda_2$$

$$T = 1 + c_1 \lambda_1 + c_2 \lambda_2 + g_T c_1 \lambda_1 c_2 \lambda_2$$

$$L_0 \text{ is pH dependent}$$

parameter values:

$$K_{R,F6P} = 1.$$

$$K_{R,ATP} = 0.06$$

$$K_{R,AMP} = 0.025$$

$$c_{F6P} = 0.0005$$

$$c_{ATP} = 1.$$

$$c_{AMP} = 0.019$$

$$q = 0.$$

$$g_R = 10.$$

$$g_T = 1.$$

$$V_{PFK}^{max} = 31.7$$

At steady state:

$$V_{PFK} = V_{PFK}^{max} \cdot v_{PFK} = \frac{1}{2} (V_{EtOH} + V_{Gol}) \quad (9)$$

V_{PFK}^{max} is not known, but it can be calculated using one data set from Table I

(suspended cells at pH^{ex} 5.5) and equation (10):

$$V_{PFK}^{max} = \frac{\left(\frac{1}{2}\right) \cdot (V_{EtOH} + V_{Gol})^{exp.}}{v_{PFK}(F6P, ATP, AMP, pH^{in})_{exp.}} \quad (10)$$

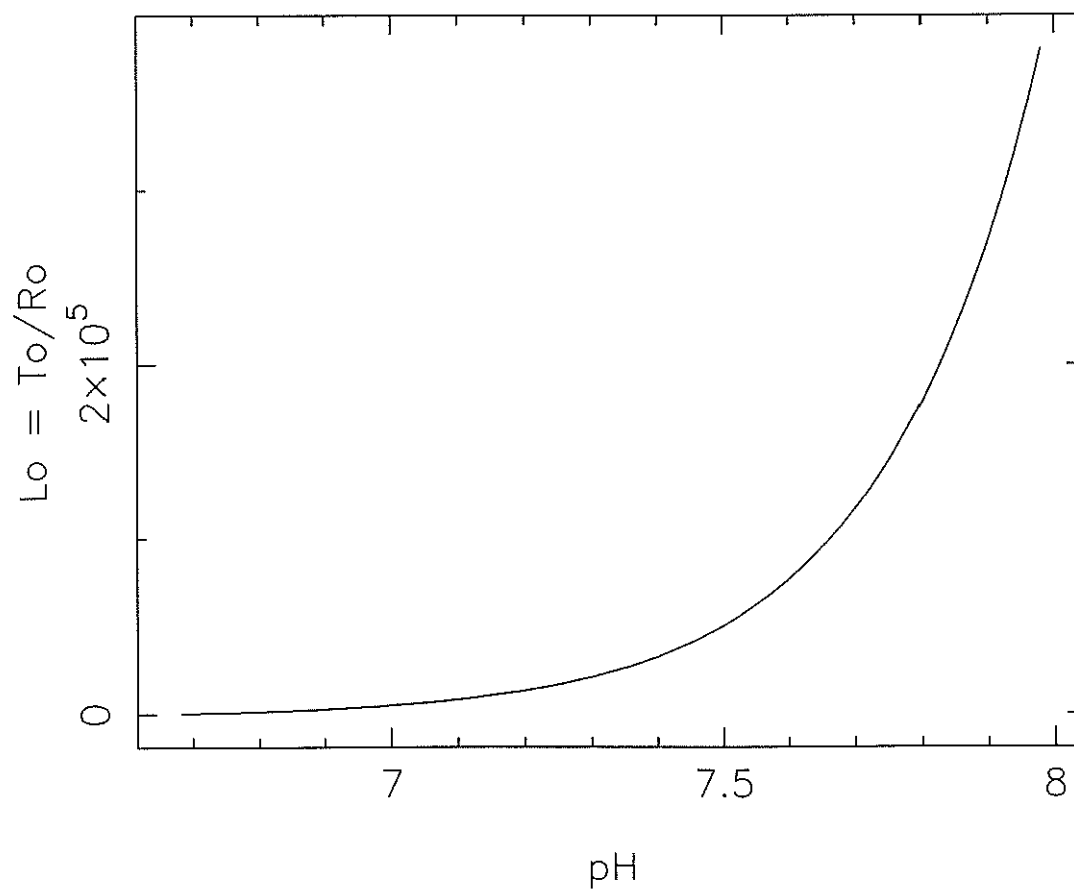


Figure 4: pH model dependence of phosphofructokinase allosteric constant.

Model for dependence of phosphofructokinase allosteric constant L_0 on pH obtained using the kinetic expression of Table V and *in vitro* data from references (33) and (37).

which gives $V_{PFK}^{max} = 31.7 \text{ mmol}/(L_{cells} \cdot \text{min})$. Assuming that V_{PFK}^{max} is the same for all the other experiments because the initial cell state is the same, this value can be used together with the PFK kinetic expression and the other experimental data to calculate:

$$V_{PFK}^{calc.} = V_{PFK}^{max} \cdot v_{PFK}(F6P, ATP, AMP, pH^{in})_{exp.} \quad (11)$$

and to compare this value with the experimental value of PFK activity obtained from the quasi-steady state rates of ethanol and glycerol production:

$$V_{PFK}^{exp.} = \left(\frac{1}{2}\right) \cdot (V_{EtOH} + V_{Gol})^{exp.} \quad (12)$$

Figure 5 shows a plot of V_{PFK} calculated vs. V_{PFK} experimental. The kinetic model represents the *in vivo* experimental data in the experimental range tested, even without including the effects of P_i and fructose-2,6-diphosphate, which can be considered lumped in the parameter V_{PFK}^{max} .

The glyceraldehyde 3-phosphate-dehydrogenase (GAPD) kinetic expression is shown in Table VI. The concentration of two substrates, glyceraldehyde 3-phosphate and NAD^+ , are involved in the rate equation. Product inhibition by $NADH$ is also included, as are the inhibitory effects of AMP, ADP, and ATP.^(38,39) The maximal velocity (V_{GAPD}^{max}) of this enzyme is assumed to be the same for both suspended and immobilized cells. The ratio $NADH/NAD^+$ is an adjustable parameter of the model, as no experimental data on this ratio was obtained.

Pyruvate kinase (PK) is also an allosteric enzyme whose kinetics are described by an expression similar to the one used to describe PFK^(34,35) (Table V). In this case, the two substrates are phosphoenolpyruvate and ADP.

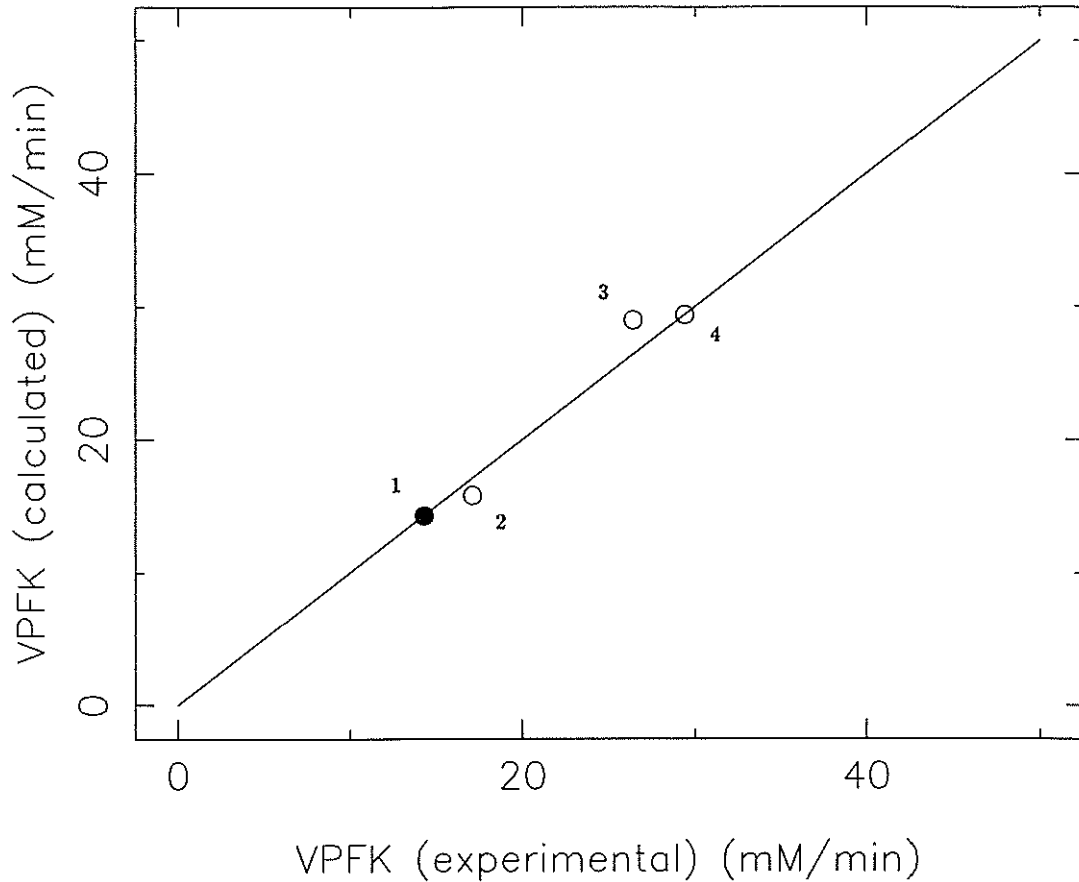


Figure 5: Comparison of experimental and calculated phosphofructokinase reaction rates.

Experimental ethanol and glycerol production rates were used to obtain V_{PFK}^{exp} , and the kinetic expression in Table V and *in vivo* NMR pH and metabolite concentration data were used to obtain V_{PFK}^{calc} . Point (●) was used to calculate V_{PFK}^{max} which was assumed to be the same for all of the other experiments.

- (1) suspended cells, $pH^{ex}=5.5$
- (2) suspended cells, $pH^{ex}=4.5$
- (3) immobilized cells, $pH^{ex}=5.5$
- (4) immobilized cells, $pH^{ex}=4.5$

TABLE VI: Glyceraldehyde 3-phosphate dehydrogenase kinetic expression.

Glyceraldehyde 3-phosphate dehydrogenase kinetic expression taking into account crossed product inhibition and competitive inhibition from other effectors (ATP, ADP and AMP).^(38,39) Units as in Table III. $\zeta_1 = AMP$, $\zeta_2 = ADP$, $\zeta_3 = ATP$. Parameter values from references (38) and (39). V_{GAPD}^{max} was obtained by multiplying the maximum specific enzyme activity (1248 min^{-1}) by the *in vivo* concentration of GAPD in yeast (0.04 mM).⁽³⁷⁾

$$V_{GAPD} = V_{GAPD}^{max} \left[1 + \frac{K_{G3P}}{G3P} + \frac{K_{NAD^+}}{NAD^+} \left(1 + \sum_{i=1}^3 \frac{\zeta_i}{K_i} \right) + \frac{K_{G3P} K_{NAD^+}}{G3P NAD^+} \left(1 + \frac{NADH}{K_{I,NADH}} \right) \left(1 + \sum_{i=1}^3 \frac{\zeta_i}{K_i} \right) \right]^{-1}$$

parameter values:

$$\begin{array}{ll} V_{GAPD}^{max} = 49.9 & K_1 = 1.1 \\ K_{G3P} = 0.0025 & K_2 = 1.5 \\ K_{NAD^+} = 0.18 & K_3 = 2.5 \\ K_{I,NADH} = 0.0003 & \end{array}$$

Fructose-1,6-diphosphate is the allosteric activator. Pyruvate kinase activity is also affected by pH through changes in the maximum velocity (through L_0) and in the binding affinity ($K_{R,PEP}$) of phosphoenolpyruvate.^(40,41) The functionality of PK on pH was obtained from *in vitro* data⁽⁴¹⁾ using the kinetic expression of Table VII. Figure 6 shows L_0 and $K_{R,PEP}$ as a function of pH.

Following a similar analysis as the one used for PFK, an evaluation of how well the PK kinetic expression represents the *in vivo* experimental data can be made at steady state:

TABLE VII: Pyruvate kinase kinetic expression.

Similar model as phosphofructokinase (Table V) with fructose-1,6-diphosphate as allosteric activator.^(34,35) Parameter values from references (35) and (40). The pH dependencies of L_0 and $K_{R,PEP}$ were determined from *in vitro* data⁽⁴¹⁾ and are shown in Figure 6. V_{PK}^{max} estimated from experimental data of Table I. Units as in Table III.

$$V_{PK} = \left(\frac{V_{PK}^{max}}{1 + K_{pH}/H^+} \right) \cdot v_{PK}(\lambda_1, \lambda_2, \gamma)$$

$$v_{PK} = \frac{g_R \lambda_1 \lambda_2 R^{n-1} + q L g_T c_1 \lambda_1 c_2 \lambda_2 T^{n-1}}{R^n + L T^n}$$

where:

$$\begin{aligned} \lambda_1 &= PEP/K_{R,PEP} & L &= L_0 \cdot \left(\frac{1 + c_\gamma \gamma}{1 + \gamma} \right)^n \\ \lambda_2 &= ADP/K_{R,ADP} & R &= 1 + \lambda_1 + \lambda_2 + g_R \lambda_1 \lambda_2 \\ \gamma &= FDP/K_{R,FDP} & T &= 1 + c_1 \lambda_1 + c_2 \lambda_2 + g_T c_1 \lambda_1 c_2 \lambda_2 \\ c_j &= K_{R,j}/K_{T,j} & L_0 & \text{pH dependent} \\ q &= V_{T,max}/V_{R,max} \end{aligned}$$

parameter values:

$$\begin{array}{lll} K_{R,PEP} & \text{pH dependent} & c_{PEP} = K_{R,PEP}/50. & g_R = 0.1 \\ K_{R,ADP} = & 5. & c_{ADP} = 1. & g_T = 1. \\ K_{R,FDP} = & 0.2 & c_{FDP} = 0.01 & K_{pH} = 8.02 \\ & & q = 1. & V_{PK}^{max} = 3440. \end{array}$$

$$V_{PK} = \left(\frac{V_{PK}^{max}}{1 + K_{pH}/H^+} \right) \cdot v_{PK}(PEP, ADP, FDP, pH^{in}) \quad (13)$$

Again, V_{PK}^{max} is not known, but it can be calculated using the data set for suspended cells at pH^{ex} 5.5 and equation (14):

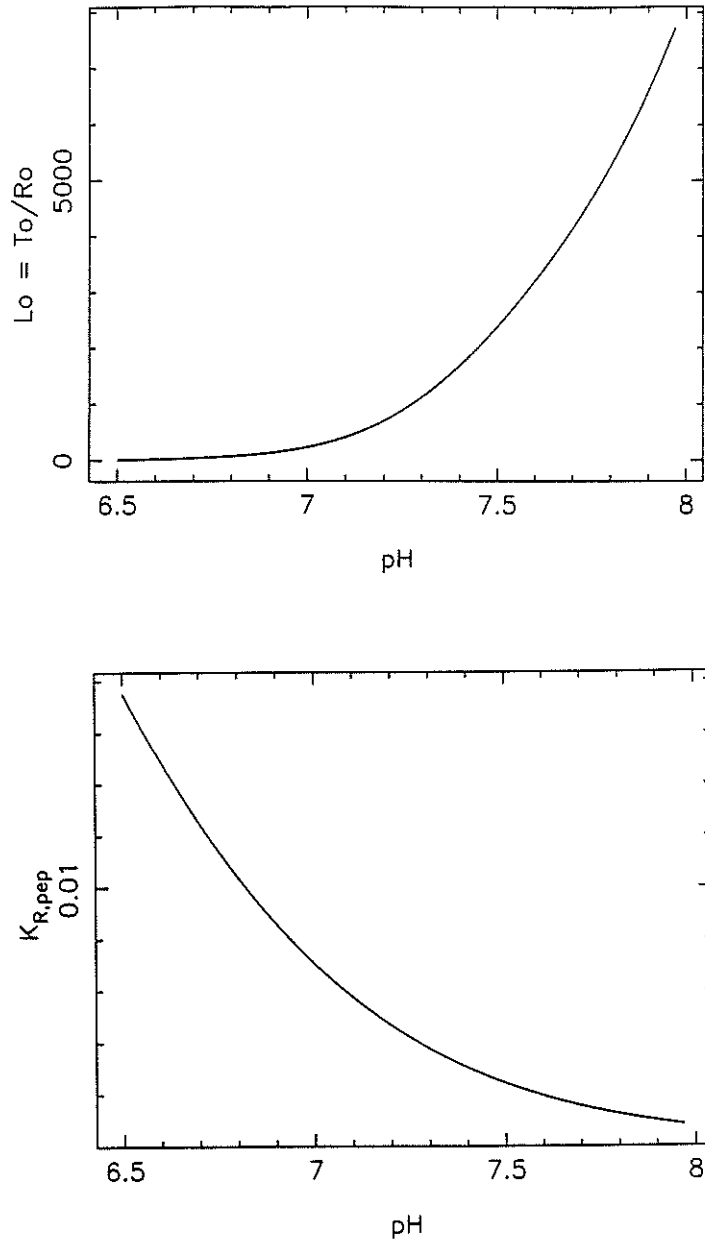


Figure 6: pH model dependence of pyruvate kinase allosteric constant and phosphoenolpyruvate binding constant.

Model for dependence of pyruvate kinase allosteric constant L_0 and phosphoenolpyruvate binding constant on pH obtained using the kinetic expression of Table VII and *in vitro* data from reference (41).

$$V_{PK}^{max} = \frac{V_{PK}^{exp.} \cdot (1 + K_{pH}/H^+)_{exp.}}{v_{PK}(PEP, ADP, FdP, pH^{in})_{exp.}} \quad (14)$$

where $V_{PK}^{exp.} = V_{EtOH}$. This gives $V_{PK}^{max} = 3,440 \text{ mmol}/(L_{cells} \cdot \text{min})$.

Assuming that V_{PK}^{max} is the same for all the other experiments because the initial cell state is the same, it can be used together with the PK kinetic expression and the other experimental data to calculate:

$$V_{PK}^{calc.} = \left(\frac{V_{PK}^{max.}}{1 + K_{pH}/H^+} \right) \cdot v_{PK}(PEP, ADP, FdP, pH^{in})_{exp.} \quad (15)$$

and compare this value with the experimental value of the rate of PK reaction obtained from measurement of the rate of ethanol production. Figure 7 shows a plot of the calculated V_{PK} vs. the experimental V_{PK} . The kinetic model represents the *in vivo* experimental data in the range tested.

Consumption of ATP by ATPase and other enzymes is assumed to depend linearly on ATP concentration. Therefore, the generalized ATPase in this model is represented by first order kinetics:

$$V_{ATPase} = k_{ATPase} \cdot ATP \quad (16)$$

The overall rate constant k_{ATPase} is an adjustable parameter of the model.

In summary, the only adjustable parameters of the model are the intracellular glucose concentration (G^{in}), the ratio between reduced and oxidized NAD ($NADH/NAD^+$) and the overall rate constant of ATP consumption (k_{ATPase}). The values for these parameters are shown in Table VIII. All the other model

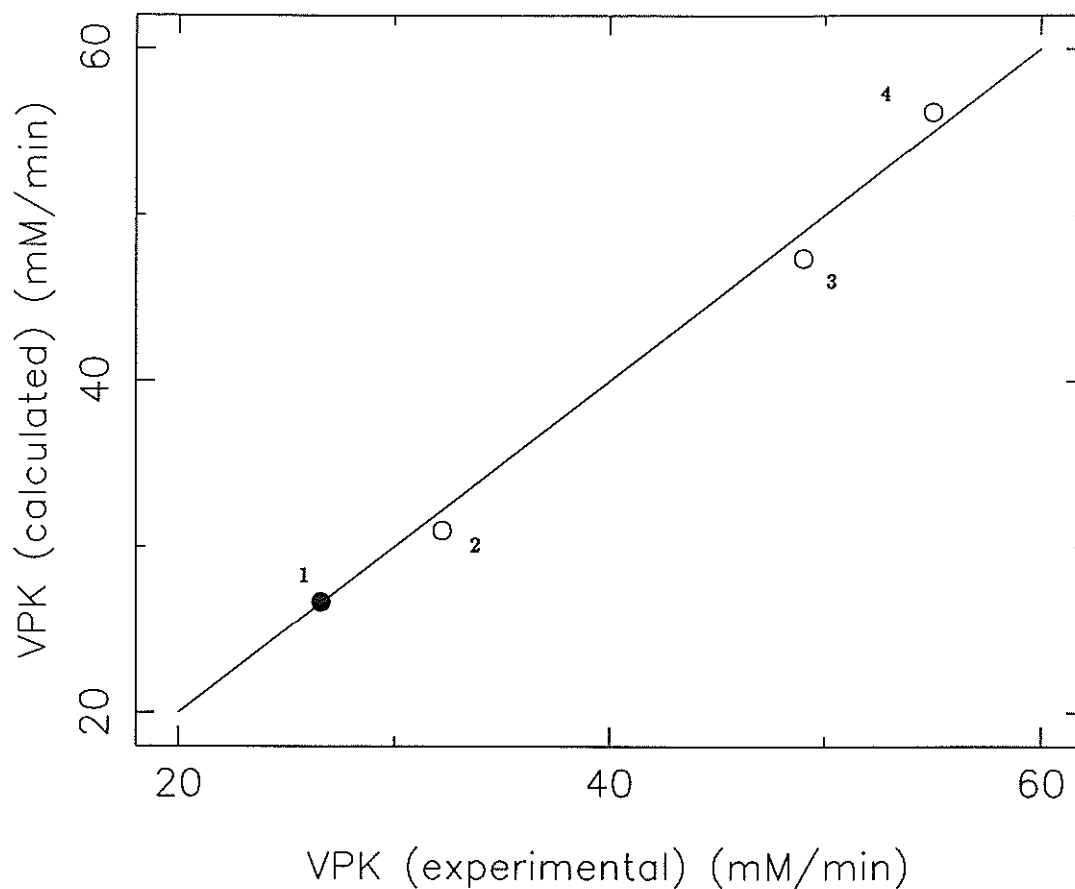


Figure 7: Comparison of experimental and calculated pyruvate kinase reaction rates.

Experimental ethanol production rate was used to obtain V_{PK}^{exp} , and the kinetic expression in Table VII and *in vivo* NMR pH and metabolite concentration data were used to obtain V_{PK}^{calc} . Point (●) was used to calculate V_{PK}^{max} which was assumed to be the same for all of the other experiments.

- (1) suspended cells, $\text{pH}^{ex}=5.5$
- (2) suspended cells, $\text{pH}^{ex}=4.5$
- (3) immobilized cells, $\text{pH}^{ex}=5.5$
- (4) immobilized cells, $\text{pH}^{ex}=4.5$

parameters are assumed to have the same values in all the experiments. Intracellular glucose in wild-type yeast at steady-state glucose fermentation was nondetectable (less than 0.5 mM) in some cases,⁽⁴²⁾ or it was found at very low concentrations (*ca.* 0.2 mM) in others.⁽⁴³⁾ Therefore, the G^{in} values predicted by the model in these wild-type cells are physically reasonable. Also, the values of NADH/NAD⁺ are in agreement with other studies^(44,45) where NADH was found to be much less than NAD⁺ concentration (1:100 ratio). Moreover, fluorescence measurements of suspended and immobilized cells under similar conditions as the ones discussed here (results not shown), indicate that the ratio of initial to steady-state fluorescence in suspended cells is higher than in immobilized cells, in qualitative agreement with the values of Table VIII.

TABLE VIII: Model parameter values.

	G^{in} (mM)	NADH/NAD ⁺	k_{ATPase} (min ⁻¹)
Suspended cells pH ^{ex} 5.5	0.03	0.042	12.1
Suspended cells pH ^{ex} 4.5	0.04	0.042	25.1
Immobilized cells pH ^{ex} 5.5	0.12	0.011	14.3
Immobilized cells pH ^{ex} 4.5	0.15	0.007	25.0

METABOLIC CONTROL THEORY

The extent to which a step k in a pathway controls the steady-state flux (J) through that pathway is given by the flux-control coefficient

$$C_{V_k}^J \stackrel{\text{def}}{=} \frac{\delta J/J}{\delta V_k/V_k} \quad (17)$$

$C_{V_k}^J$ has a value of zero for a completely non-controlling step and unity for a totally-controlling step. Values between these extremes are expected for most steps in practice. Thus, the effect of cell immobilization on steady-state fluxes can be quantitatively established comparing flux-control coefficients between suspended and immobilized cells.

The steady-state concentrations of metabolic intermediates are also dependent on the enzymatic activity of each step. MCT defines the concentration-control coefficient as

$$C_{V_k}^{X_i} \stackrel{\text{def}}{=} \frac{\delta X_i/X_i}{\delta V_k/V_k} \quad (18)$$

$C_{V_k}^{X_i}$ represents the extent to which a given step k in a pathway controls the steady-state concentration of metabolite i (X_i). The flux- and concentration-control coefficients can be obtained knowing the elasticity coefficients.^(46,47) Elasticity coefficients represent the fractional response of the rate of a given step k (V_k) to a fractional change in concentration of a metabolite or effector (X_i):

$$\epsilon_{X_i}^{V_k} = \frac{\delta V_k/V_k}{\delta X_i/X_i} \quad (19)$$

where δX_i represents metabolite i concentration change (cause), and δV_k represents the change in the rate of step k (effect). In the limit as $\delta X_i \rightarrow 0$:

$$\epsilon_{X_i}^{V_k} = \frac{X_i}{V_k} \left(\frac{\partial V_k}{\partial X_i} \right) \quad (20)$$

It is interesting to note that MCT considers only relative changes in fluxes. The magnitude of the fluxes themselves are not relevant. This is important in cases where there is uncertainty in the absolute magnitude of some parameters of a kinetic expression, such as in the case of glucose uptake. Even approximate values for the elasticity coefficients will provide quantitative information regarding flux-control coefficients. In all the calculations that follow, parameters such as V_{In}^0 and K_{G6P} of equation 6 were varied from the *in vivo* estimation by $\pm 10\%$. No considerable qualitative difference regarding flux-control coefficients were obtained with such variations.

Using the enzyme kinetics described previously with the indicated parameter values and the measured intracellular levels of substrates, products and effectors, it is possible to calculate the elasticity coefficients, and subsequently, to calculate the flux-control coefficients, applying connectivity and summation theorems for the case of a branched pathway.^(46,47)

The enzymes in the model pathway have been classified into enzymes catalyzing irreversible reactions and those catalyzing equilibrium reactions. The steps that are very fast and close to equilibrium can be treated regarding the input and output substances as "joint" metabolites.⁽⁴⁷⁾ Obviously, the flux-control coefficients of the equilibrium enzymes are zero, and only the flux-control coefficients of the non-equilibrium steps (*In*, *HK*, *PFK*, *GAPD*, *PK*, *Pol*, *Gol*,

ATPase) are important. Here *Pol* refers to total polysaccharide production ($V_{Pol} = V_{Tre} + V_{Gly}$).

The elasticity coefficients for each step are calculated according to equation (19) using its respective kinetic expression. The flux- and concentration-coefficients are calculated using equation (21)⁽⁴⁶⁾

$$\mathbf{C} = \mathbf{E}^{-1} \quad (21)$$

assuming \mathbf{E} to be non-singular. \mathbf{C} is the matrix of control coefficients (fluxes and concentrations) and \mathbf{E} is the elasticity matrix which has 1s in the first row, the elasticity coefficients in the following rows, and the branch relationships in the last two rows.^(46,47)

RESULTS AND DISCUSSION

MCT allows the identification of rate-controlling steps. It is important to identify those steps because they are the points of pathway kinetic control inside the cell. Any difference observed in cell metabolism upon cell immobilization would imply a change at any of those control points. Table IX shows the flux-control coefficients for suspended and immobilized cells calculated using the kinetic expressions described above and the *in vivo* conditions determined experimentally using NMR.

In suspended cells most flux control lies in the glucose uptake step for both extracellular pHs (83% for pH^{ex} 4.5 and 65% for pH^{ex} 5.5) This result is in

TABLE IX: Flux-control coefficients of suspension-grown cells.

Flux-control coefficients calculated using equation (21) of the text.

	Suspended cells pH ^{ex} 5.5	Suspended cells pH ^{ex} 4.5	Immobilized cells pH ^{ex} 5.5	Immobilized cells pH ^{ex} 4.5
<i>In</i>	0.646	0.831	0.297	0.316
<i>HK</i>	0.008	0.011	0.007	0.007
<i>PFK</i>	0.098	0.115	0.336	0.497
<i>GAPD</i>	0.002	0.002	0.009	0.016
<i>PK</i>	0.001	0.001	0.003	0.003
<i>Pol</i>	0.006	0.000	0.109	0.157
<i>Gol</i>	0.001	0.001	0.001	0.002
<i>ATPase</i>	0.238	0.039	0.237	0.002

agreement with experimental results obtained previously^(23,24,33,48,49) in which glucose uptake step has been found to be limiting the rate of glucose metabolism. PFK also has a relatively important role in controlling the flux throughout the pathway (12% for pH^{ex} 4.5 and 10% for pH^{ex} 5.5).

In the case of pH^{ex} 5.5, ATPase also exerts significant control over the pathway (24%). This indicates that the cell has decreased the fermentation rate (ATP-producing process) because ATP is not consumed rapidly. Yeast plasma membrane ATPase is an ion pump involved in the maintenance of a relatively constant intracellular pH for a wide range of extracellular pHs.⁽⁵⁰⁾ In order to maintain the intracellular pH at lower extracellular pH, more proton pumping will be necessary and cell energy requirements will be increased. This reduces ATP inhibition of the glucose fermentation rate as shown in Table I. Now, at

pH^{ex} 4.5, ATPase has little influence in controlling the pathway flux (4%) in suspended cells.

It follows from these results that metabolic control is shared by several steps and is not confined to one "key" step. This phenomenon has been observed previously⁽⁵¹⁻⁵⁵⁾ in several pathways, and it explains why so many rounds of mutations and selections are generally required to produce a "productive" strain by conventional methods.^(56,57)

In immobilized cells, flux control is exerted mainly at the PFK step (50% for pH^{ex} 4.5 and 34% for pH^{ex} 5.5). Glucose uptake still exerts significant flux control (32% and 30% for pH^{ex} 4.5 and 5.5 respectively). The shift in the control point from glucose uptake in suspended cells to PFK in immobilized cells indicates that immobilization is affecting the glucose uptake step. This result has been suggested as a possible cause in explaining differences between suspended and immobilized cell glucose metabolism.^(58,59)

Similarly to the situation in suspended cells, ATPase is important in controlling the pathway in immobilized cells at pH^{ex} 5.5 (24%) but not at pH^{ex} 4.5 (0.2%). In immobilized cells, polysaccharide storage has become an important step in controlling the flow throughout the pathway at both extracellular pHs. It has 16% and 11% of the pathway control for pH^{ex} 4.5 and 5.5 respectively.

The increase in polysaccharide storage in immobilized cells is mainly due to the increase in glucose uptake. The flux-control coefficients of the branch going to polysaccharide are shown in Table X. In suspended cells the flux of this branch is strongly controlled by glucose uptake, phosphofructokinase and

TABLE X: Flux-control coefficients for the branches going to polysaccharide and glycerol.

POLYSACCHARIDE STORAGE BRANCH ($V_{Tre} + V_{Gly}$)

	Suspended cells pH ^{ex} 5.5	Suspended cells pH ^{ex} 4.5	Immobilized cells pH ^{ex} 5.5	Immobilized cells pH ^{ex} 4.5
<i>In</i>	10.4	14.2	-0.03	0.27
<i>HK</i>	0.14	0.20	-0.01	0.01
<i>PFK</i>	-3.3	-11.3	-0.62	-1.2
<i>GAPD</i>	-0.05	-0.19	-0.02	-0.04
<i>PK</i>	0.01	-0.04	0.02	0.02
<i>Pol</i>	0.82	0.95	1.1	0.93
<i>Gol</i>	-0.01	-0.06	-0.01	-0.01
<i>ATPase</i>	-8.16	-3.8	-0.44	-0.01

GLYCEROL PRODUCTION BRANCH (V_{Gol})

	Suspended cells pH ^{ex} 5.5	Suspended cells pH ^{ex} 4.5	Immobilized cells pH ^{ex} 5.5	Immobilized cells pH ^{ex} 4.5
<i>In</i>	-1.84	-2.10	0.12	-0.09
<i>HK</i>	-0.02	-0.03	0.01	-0.01
<i>PFK</i>	0.57	1.27	0.34	0.29
<i>GAPD</i>	0.02	0.02	0.01	0.01
<i>PK</i>	-0.89	-0.58	-1.10	-0.78
<i>Pol</i>	-0.14	-0.11	-0.34	-0.25
<i>Gol</i>	0.95	1.11	0.72	0.82
<i>ATPase</i>	1.38	0.44	0.24	0.01

ATPase. An increase in glucose uptake will increase polysaccharide production while an increase in PFK or ATPase will reduce its production. Glucose uptake and PFK have opposite effects on polysaccharide production because they are

upstream and downstream, respectively, of the branch to polysaccharide synthesis. The net effect of increasing glucose uptake is to increase polysaccharide production because glucose uptake has a higher control coefficient than PFK. On the other hand, in immobilized cells the flux to polysaccharide is controlled mainly by the enzymes producing glycogen and trehalose, and polysaccharide production is limited in this case by the activity of those enzymes.

The flux-control coefficients of glycerol production are also shown in Table X. In this case, all the pathway steps have a certain degree of control over glycerol production.

Glucose-6-phosphate concentration in suspended and immobilized cells is mainly determined by glucose uptake, PFK and ATPase as shown in Table XI. An increase in glucose uptake will increase glucose-6-phosphate concentration while an increase in PFK or ATPase will reduce its concentration. The difference in glucose-6-phosphate levels between suspended and immobilized cells is mainly due to the high concentration-control coefficient of glucose uptake upon glucose-6-phosphate and the suggested effect of immobilization on V_{I_n} .

In the intracellular conditions of suspended cells, fructose-1,6-diphosphate concentration is mainly controlled by ATPase and by PFK (Table XI). Increasing the rates of any of these steps will increase the fructose-1,6-diphosphate concentration. This explains the increase from 6.6 mM to 10.1 mM of fructose-1,6-diphosphate on the changing extracellular pH (from 5.5 to 4.5) in suspended cells.

The experimental results of Table I show that the level of 3-phosphoglycerate is higher in immobilized cells. This observation suggests that there

TABLE XI: Concentration-control coefficients of suspension-grown cells.

Glucose-6-phosphate concentration-control coefficients

	Suspended cells pH ^{ex} 5.5	Suspended cells pH ^{ex} 4.5	Immobilized cells pH ^{ex} 5.5	Immobilized cells pH ^{ex} 4.5
<i>In</i>	1.6	1.7	2.8	3.5
<i>HK</i>	0.02	0.02	0.06	0.09
<i>PFK</i>	-0.46	-1.3	-1.4	-2.6
<i>GAPD</i>	-0.01	-0.02	-0.04	-0.09
<i>PK</i>	0.01	-0.01	0.01	0.01
<i>Pol</i>	-0.03	-0.01	-0.45	-0.85
<i>Gol</i>	-0.01	-0.01	-0.01	-0.03
<i>ATPase</i>	-1.1	-0.41	-0.98	-0.02

Fructose-1,6-diphosphate concentration control coefficients

	Suspended cells pH ^{ex} 5.5	Suspended cells pH ^{ex} 4.5	Immobilized cells pH ^{ex} 5.5	Immobilized cells pH ^{ex} 4.5
<i>In</i>	-1.8	-3.7	1.5	0.87
<i>HK</i>	-0.02	-0.05	0.03	0.02
<i>PFK</i>	0.96	4.8	2.2	2.8
<i>GAPD</i>	-1.5	-1.6	-2.8	-3.1
<i>PK</i>	0.23	-0.31	0.20	0.52
<i>Pol</i>	-0.20	-0.38	-0.37	-0.29
<i>Gol</i>	-0.28	-0.48	-0.87	-0.99
<i>ATPase</i>	2.6	1.7	0.07	0.19

is also a control point in the triose part of the pathway that has been changed by cell immobilization. This is reflected in the flux-control coefficients of Table X. The flux-control coefficient of GAPD increases 5 times (from 0.2% to 1%)

and the flux-control coefficient of PK increases 10 times (from 0.03% to 0.3%) upon cell immobilization.

Overall, the results of this work show that the observed differences between suspended and immobilized cell glucose metabolism can be quantitatively explained using MCT. In suspension-grown cells, immobilization changes the glucose uptake step regulation. An increase in this step produces an overflow in the first stage of glycolysis. The cell tries to overcome this overflow by increasing the flux in all the branches down the pathway (ethanol, glycerol and polysaccharide production) up to a point when PFK becomes the main limiting step. This causes the concentration of glucose-6-phosphate to increase well beyond the normal suspended cell levels.

The methodology used here to compare suspended and immobilized cell metabolism can also be used in other contexts. For instance, one can find the best strategy to “design” a pathway, originally present in the cell (and optimized) to fulfill a given task, by changing those controlling steps identified by MCT using metabolic engineering, aiming to maximize the production of a product or the intracellular concentration of any intermediate.

Acknowledgements

This research was sponsored by the National Science Foundation.

REFERENCES

1. Siess M., and Divies C., *Eur. J. Appl. Microbiol. Biotechnol.*, **12**, 10 (1981).
2. Doran P., and Bailey J., *Biotechnol. Bioeng.*, **28**, 73 (1986).
3. Inloes D., Smith W., Taylor D., Cohen S., Michaels A., and Robertson C., *Biotechnol. Bioeng.*, **23**, 79 (1981).
4. Jirku V., Turkora J., and Krumphanzl V., *Biotechnol. Lett.*, **2**, 509 (1980).
5. Koshcheyenko K., Turkina M., and Skryabin G., *Enzyme Microb. Technol.*, **5**, 14 (1983).
6. Brodelius P., Deus B., Mosbach K., and Zenk M., *FEBS Lett.*, **103**, 93 (1979).
7. Larsson P., and Mosbach K., *Biotechnol. Lett.*, **1**, 501 (1979).
8. Kacser H., and Burns J., *Symp. Soc. Exp. Biol.*, **27**, 65 (1973).
9. Heinrich R., and Rapoport T., *Eur. J. Biochem.*, **42**, 89 (1974).
10. Savageau M., *J. Theoret. Biol.*, **25**, 365 (1969).
11. Savageau M., Voit E., and Irvine D., *Math. Biosciences*, **86**, 127 (1987).
12. Savageau M., Voit E., and Irvine D., *Math. Biosciences*, **86**, 147 (1987).
13. Galazzo J., and Bailey J., *Biotechnol. Bioeng.*, in press, (1988).
14. Lang J., and Cirillo V., *J. Bacteriol.*, **169** 2932 (1987).

15. Kotyk A., *Fol. Microbiol.*, **12**, 121 (1967).
16. Campbell-Burk S., den Hollander J., Alger J., and Shulman R., *Biochemistry*, **26**, 7493 (1987).
17. den Hollander J., Ugurbil K., Brown T., Bednar M. and Shulman R., *Biochemistry*, **25**, 203 (1986).
18. Hess B., Boiteux A., and Kruger J., *Adv. Enzyme Regul.*, **7**, 149 (1969).
19. Betz A., and Moore C., *Arch. Biochem. Biophys.*, **120**, 268 (1967).
20. Betz A., and Becker J., *Physiol. Plant.*, **33**, 285 (1975).
21. Su S., and Russel P., *J. Biol. Chem.*, **243**, 3826 (1968).
22. Becker J., and Betz A., *Biochim. Biophys. Acta*, **274**, 584 (1972).
23. Azam F., and Kotyk A., *FEBS Lett.*, **2**, 333 (1969).
24. Serrano R., and DeLaFuente G., *Mol. Cell. Biochem.*, **5**, 161 (1974).
25. Wilkinson K., and Rose I., *J. Biol. Chem.*, **254**, 12567 (1979).
26. Kosov D. and Rose I., *J. Biol. Chem.*, **246**, 2618 (1971).
27. Groz R., In: "*Biochemical and Mathematical Modelling of Microaerobic Continuous Ethanol Production by Saccharomyces cerevisiae*", Ph. D. Dissertation, California Institute of Technology, Pasadena, California, (1987).
28. Danenberg K., and Cleland W., *Biochemistry*, **14**, 28 (1975).
29. Kuenzi M., and Fiechter A., *Arch. Microbiol.*, **84**, 254 (1972).
30. Rothman L., and Cabib E., *Biochemistry*, **6**, 2098 (1967).
31. Rothman L., and Cabib E., *Biochemistry*, **6**, 2107 (1967).

32. Becker J., *Arch. Microbiol.*, **115**, 181 (1977).
33. Reibstein D., den Hollander J., Pilgis S., and Shulman R., *Biochemistry*, **25**, 219 (1986).
34. Monod J., Wyman J., and Changeux J., *J. Mol. Biol.*, **12**, 88 (1965).
35. Hess B., and Plesser T., *Ann. N. Y. Acad. Sci.*, **316**, 203 (1978).
36. Eschrich K., Schellenberger W., and Hofman E., *Arch. Biochem. Biophys.*, **205**, 114 (1980).
37. Bañuelos M., Gancedo C., and Gancedo J., *J. Biol. Chem.*, **252**, 6394 (1977).
38. Doran P., In: *"The Effects of Immobilization on the Metabolism of Yeast"*, Ph. D. Dissertation, California Institute of Technology, Pasadena, CA, (1985).
39. Yang S., and Deal W., *Biochemistry*, **8**, 2806 (1969).
40. Brown C., Taylor J., and Chan L., *Biochim. Biophys. Acta*, **829**, 342 (1985).
41. Wieker H., and Hess B., *Biochemistry*, **10**, 1243 (1971).
42. Hofer M., and Nassar F., *J. Gen. Microbiol.*, **133**, 2163 (1987).
43. Becker J., and Betz A., *Biochym. Biophys. Acta*, **274**, 584 (1972).
44. Hess B., Kleinhans H., and Kuschmitz D., in *"Biological and Biochemical Oscillations"*, B. Chance, E. Pye, A. Ghosh and B. Hess (eds.), Academic Press, New York, pp 229-241, (1973).

45. Heinrich R., Rapoport S., and Rapoport T., *Prog. Biophys. Molec. Biol.*, **32**, 1 (1977).
46. Westerhoff H., and Kell D., *Biotechnol. Bioeng.*, **30**, 101 (1987).
47. Fell D., and Sauro H., *Eur. J. Biochem.*, **148**, 555 (1985).
48. Kotyk A., and Kleinzeller A., *Biochim. Biophys. Acta*, **135**, 106 (1967).
49. Becker J., and Betz A., *Biochim. Biophys. Acta*, **274**, 584 (1972).
50. Willsky G., *J. Biol. Chem.*, **254**, 3326 (1979).
51. Rapoport T., Heinrich R., Jacobash G., and Rapoport S., *Eur. J. Biochem.*, **42** 107 (1974).
52. Ottaway J., and McMinn C., In: *Enzyme Regulation and Mechanism of Action*, (Midler and Hess Eds.), pp. 69-82, Pergamon Press NY, (1980).
53. Flint H., Tateson R., Barthelmess I., Porteous D., Donachie W., and Kacser H., *Biochem. J.*, **200**, 231 (1981).
54. Bohnensack R., Kuster U., and Letko G., *Biochim. Biophys. Acta*, **680**, 271 (1982).
55. Westerhoff H., Groen A., and Wanders R., *Biochem. Soc. Trans.*, **11**, 90 (1983).
56. Westerhoff H., Groen A., and Wanders R., *Bioscience Rep.*, **4**, 1 (1984).
57. Kell D., and Westerhoff H., *FEMS Microbiol. Rev.*, **39**, 305 (1986).
58. Suzuki S., and Karube I., *Amer. Chem. Soc. Symp. Ser.*, **106**, 59 (1979).
59. D'Sousa S., and Nadkarni G., *Biotechnol. Bioeng.*, **22**, 2191 (1980).

CHAPTER 5

ANALYSIS OF THE POTENTIAL FOR IMPROVING YEAST *Saccharomyces cerevisiae* FERMENTATION ACTIVITY BY METABOLIC ENGINEERING

ABSTRACT

An analysis of the anticipated effects of genetic manipulation to improve the ethanol production rate in yeast *S. cerevisiae* is presented using the framework of the metabolic control theory. The main control points in the pathway from glucose to ethanol in yeast are the glucose uptake step, phosphofructokinase and ATP consumption.

In suspended suspension-grown cells, the highest improvement in ethanol production is achieved by increasing the activity of glucose transport, and in immobilized suspension-grown cells, the greatest fermentation rate enhancement is obtained by increasing the maximum activity of phosphofructokinase. This indicates that the metabolic engineering strategy used to enhance any properties in the cell will depend not only on the specific microorganism but also on the environmental conditions in which it is placed.

In conditions where several steps share the flux control in a pathway, a substantial enhancement in pathway rate will be possible only if the activities of all those steps are increased simultaneously.

INTRODUCTION

Metabolic engineering⁽¹⁾ provides the means to introduce virtually any new protein into the living cell. This opens the door to a whole new set of engineering variables that have to be taken into account in designing and optimizing any given process.

Organisms have been designed by evolutionary processes of mutation and selection. This involved numerous trials of variants and selection of the traits that best served the organism and its survival. Obviously, the strategy to be applied when trying to modify an organism in order to accomplish a desired task must to be quite different from the traditional trial and error method. It would be impractical to test experimentally all the possible combinations. In order to identify effective strategies efficiently, a quantitative description of the pathway of interest, including its interactions and regulations, should be available to the engineer. Only then is it possible to properly narrow all the alternatives to a few ones worthy of trial.

The answers to the following two questions provide guidelines for the genetic manipulation of microorganisms to enhance metabolite production:

- (1) Which enzymes should be amplified, and to what degree, to increase the production of a given product in the pathway? and,
- (2) How should enzyme activities be modified to increase the intracellular concentration of a given intermediate in the pathway.?

A quantitative answer to the above questions is provided by elements of the metabolic control theory.^(2,3) The extent to which a given step in a pathway controls the steady-state flux through that pathway is given by the flux-control coefficient.^(4,5) Values for these coefficients are most often zero for a non-controlling step and unity for an absolutely-controlling step. Therefore, if the goal is to increase the production rate of any product in a pathway, metabolic engineering should focus on altering the activities of those steps that have the largest flux-control coefficients.

A methodology to analyze *in vivo* cellular metabolism has been presented in previous chapters. This allowed to develop a detailed description of glucose consumption in anaerobic yeast *S. cerevisiae*. That model is used in this chapter to study which enzymes (steps) in the pathway should be modified in order to improve ethanol production.

TABLE I: Flux-control coefficient summary.

Flux-control coefficients obtained in Chapter 4 for *in vivo* conditions.

Step	Suspended cells pH ^{ex} = 5.5	Suspended cells pH ^{ex} = 4.5	Immobilized cells pH ^{ex} = 5.5	Immobilized cells pH ^{ex} = 4.5
<i>In</i>	0.646	0.831	0.297	0.316
<i>HK</i>	0.008	0.011	0.007	0.007
<i>PFK</i>	0.098	0.115	0.336	0.497
<i>GAPD</i>	0.002	0.002	0.009	0.016
<i>PK</i>	0.001	0.001	0.003	0.003
<i>Pol</i>	0.006	0.000	0.109	0.157
<i>Gol</i>	0.001	0.001	0.001	0.002
<i>ATPase</i>	0.238	0.039	0.237	0.002

In Table I are listed the flux-control coefficients obtained in Chapter 4 for suspension-grown *S. cerevisiae* cells. As discussed previously, the main control point in suspended cells is at the glucose uptake step. Phosphofructokinase has about 10% of the flux control. At extracellular pH 5.5, ATP consumption seems to be important in controlling the flux throughout the pathway.

In immobilized cells, phosphofructokinase has the biggest flux-control coefficient. Glucose uptake exerts a significant flux control (30%). Polysaccharide storage has become important in limiting ethanol production. ATPase is playing a significant role in the pathway flux control at extracellular pH 5.5. As observed in Table I, the distribution of control among steps in the pathway depends on the experimental conditions at which the cells are exposed, in agreement with several other studies.⁽⁶⁻⁸⁾

From the results of Table I, the obvious steps to modify in order to increase ethanol production are glucose uptake, phosphofructokinase and ATP consumption. This chapter presents an analysis of how the flux-control coefficients and ethanol production would change if the activity of any of the above mentioned steps is altered. This will be done using the model and parameters described in Chapter 4.

RESULTS

In all the following results, the effect of altering the activity of any given step is obtained by changing the parameter of interest from the *in vivo* value

obtained in Chapter 4 to a new fixed value. Subsequently, a new steady-state for that value is calculated, keeping all other parameters constant. The flux-control coefficients are then obtained as described in Chapter 4.

Effects of altering the glucose uptake step

An increase in glucose uptake rate (V_{In}^0) would decrease the control coefficient (c_{In}) of that step, improving ethanol production. It is reasonable to predict from the flux-control coefficients of Table I that the improvement in ethanol production rate will be more pronounced for suspended cells at extracellular pH 4.5, because c_{In} has a value close to unity in those conditions, thus indicating that glucose uptake is almost completely limiting the flux throughout the pathway.

Figure 1 shows the control coefficients of suspended and immobilized cells at different extracellular pHs as a function of V_{In}^0 . In suspended cells at pH^{ex} 5.5, a change in V_{In}^0 from 20 to 26 mM/min produces minor changes in the flux-control coefficients. This is a 30% increase from the *in vivo* conditions. Glucose uptake dominates the flux control up to V_{In}^0 of *ca.* 30 mM/min. For values larger than that, ATPase becomes the main control point in ethanol production as indicated by the c_{ATPase} values. c_{PFK} is not altered by changes in V_{In}^0 under these experimental conditions. Similar changes in c_{In} are observed in suspended cells at pH^{ex} 4.5. Under these conditions, c_{PFK} increases and PFK assumes the greatest control of the pathway flux for V_{In}^0 larger than 40 mM/min.

For immobilized cells, the *in vivo* value determined in Chapter 4 is $V_{In}^0 = 47$ mM/min. A 30% increase at the pH^{ex} 5.5 conditions increments c_{ATPase}

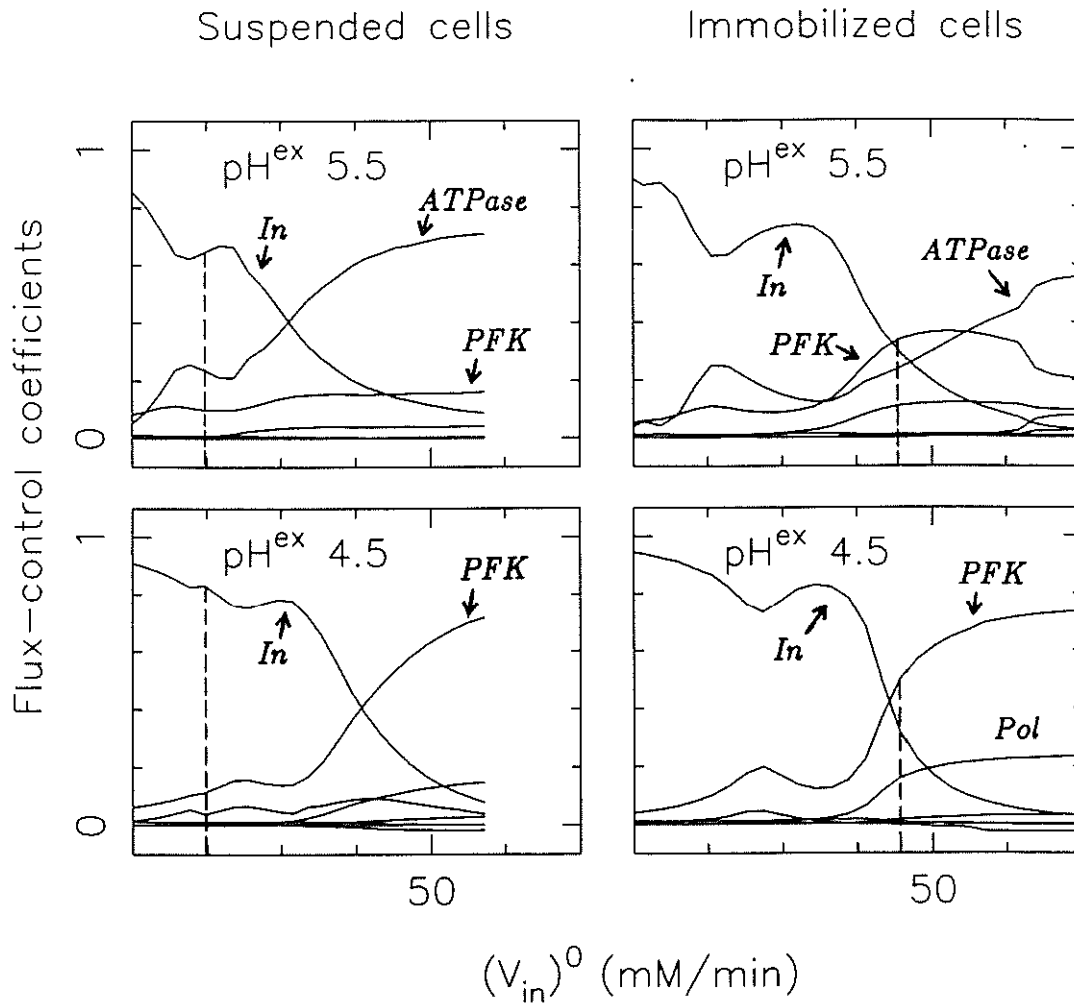


Figure 1: Flux-control coefficients as a function of glucose uptake velocity.

Flux-control coefficients for suspended and immobilized cells at different extracellular pH, as a function of glucose uptake velocity. Dashed line represents the *in vivo* values of Table I.

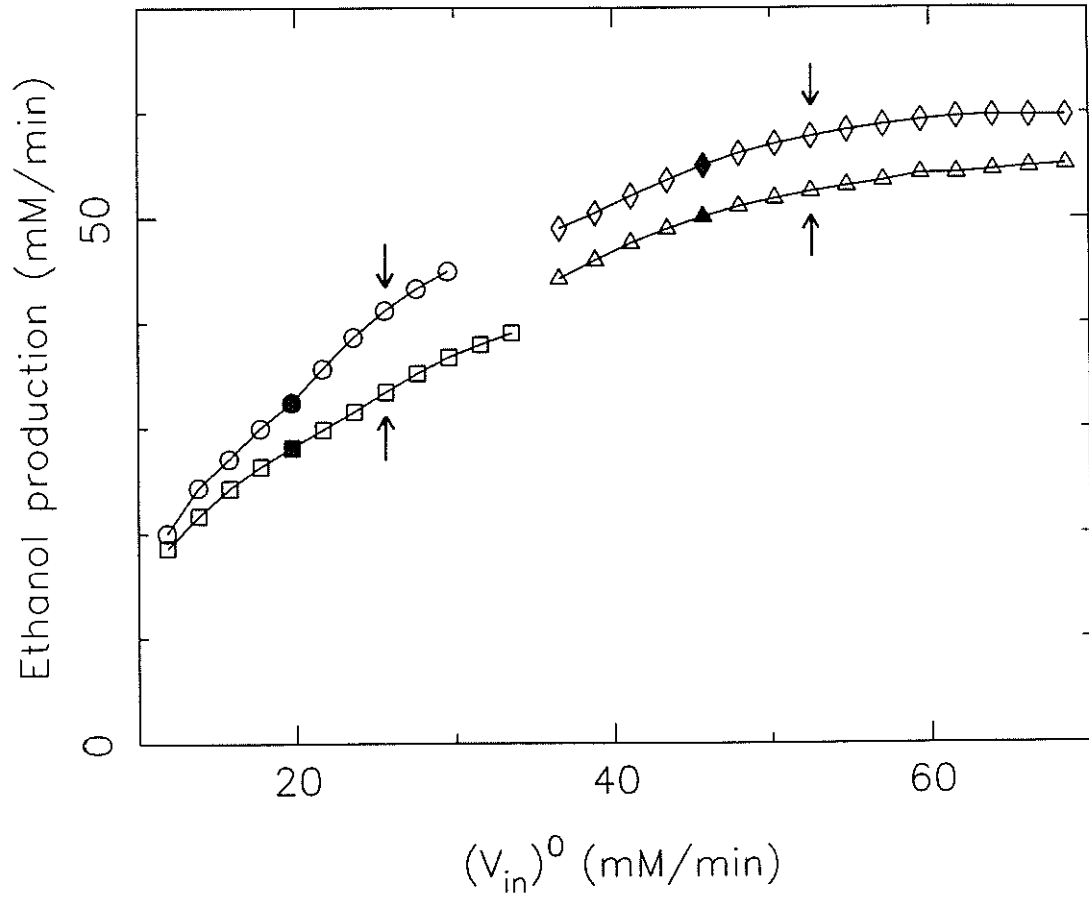


Figure 2: Ethanol production rate as a function of glucose uptake velocity.

Ethanol production rate for suspended and immobilized cells of Figure 1. Full symbols are for *in vivo* conditions (Chapter 4.) Arrows indicate a 30% increase in glucose uptake velocity from the *in vivo* value.

- (□) suspended cells pH^{ex} 5.5
- (○) suspended cells pH^{ex} 4.5
- (△) immobilized cells pH^{ex} 5.5
- (◇) immobilized cells pH^{ex} 4.5

and ATPase becomes the most controlling step in the pathway. While c_{PFK} is not affected by increasing V_{In}^0 , c_{In} decreases as expected. At pH^{ex} 4.5, c_{PFK} increases and c_{In} decreases. In this condition ATPase is not as important as at pH^{ex} 5.5 in controlling ethanol production, as seen before with the suspended cells.

The effect of changing V_{In}^0 on ethanol production is shown in Figure 2. A 30% increase in V_{In}^0 produces a 22% increase in ethanol production in suspended cells at pH^{ex} 5.5 and a 28% increase in suspended cells at pH^{ex} 4.5. A similar percentage increase in V_{In}^0 in immobilized cells increments ethanol production by 7% at pH^{ex} 5.5 and by 10% at pH^{ex} 4.5.

As expected from Table I, the improvement in ethanol production altering the glucose uptake rate is more important for suspended cells than for immobilized cells.

Effects of altering phosphofructokinase maximum activity

Figure 3 shows how flux-control coefficients vary as a function of phosphofructokinase maximum activity (V_{PFK}^{max}). There are no significant changes for suspended cells at both pH^{ex} 5.5 and 4.5. Glucose uptake is the predominant flux-controlling step in the V_{PFK}^{max} range tested.

Increasing V_{PFK}^{max} from the *in vivo* value in immobilized cells at pH^{ex} 5.5 causes c_{PFK} to decrease and c_{ATPase} to increase. ATP hydrolysis becomes the most controlling step for V_{PFK}^{max} values larger than 33 mM/min. c_{In} does not change significantly with increases in V_{PFK}^{max} , and remains almost constant, as

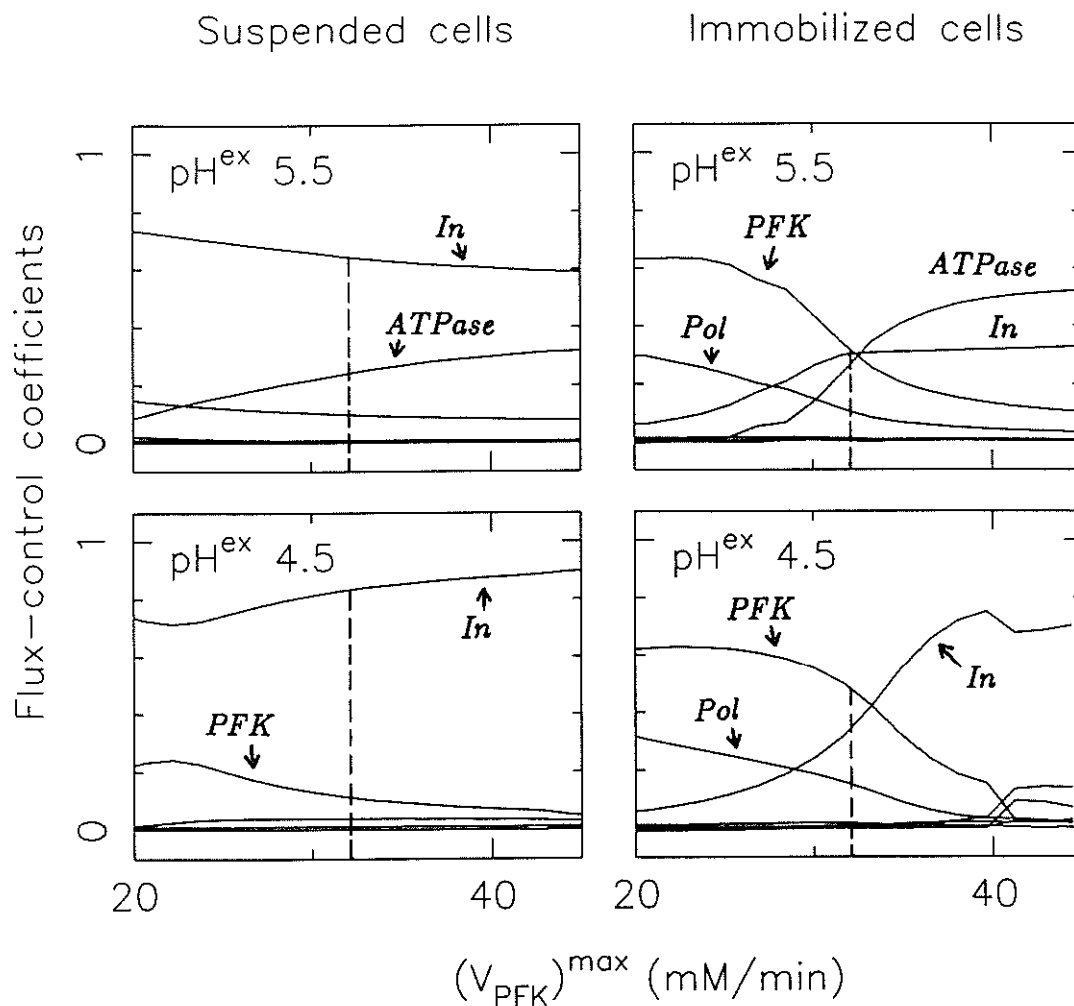


Figure 3: Flux-control coefficients as a function of phosphofructokinase maximum activity.

Flux-control coefficients for suspended and immobilized cells at different extracellular pH, as a function of phosphofructokinase maximum activity. Dashed line represents the *in vivo* values of Table I.

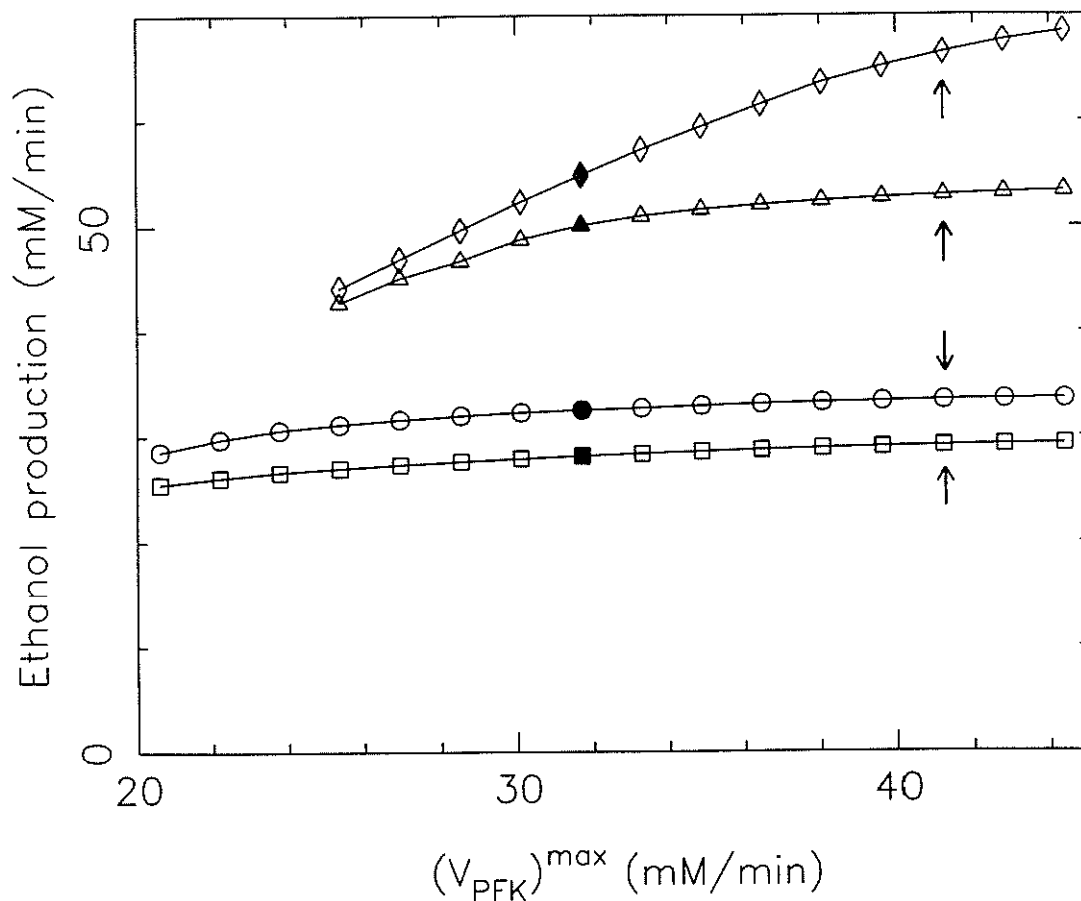


Figure 4: Ethanol production rate as a function of phosphofruktokinase maximum activity.

Ethanol production rate for suspended and immobilized cells of Figure 3. Full symbols are for *in vivo* conditions (Chapter 4.) Arrows indicate a 30% increase in glucose uptake velocity from the *in vivo* value.

- (□) suspended cells pH^{ex} 5.5
- (○) suspended cells pH^{ex} 4.5
- (△) immobilized cells pH^{ex} 5.5
- (◇) immobilized cells pH^{ex} 4.5

can be observed in Figure 3. At pH^{ex} 4.5, ATPase activity does not contribute to the pathway flux control. The two most important steps are glucose uptake and phosphofructokinase (Table I.) An increase in V_{PFK}^{max} from the *in vivo* value produces an increase in c_{In} and a decrease in c_{PFK} in these conditions.

It may be anticipated from these results that an increase in V_{PFK}^{max} from the *in vivo* value would have no significant effect on ethanol production in suspended cells, whereas the effect would be more pronounced in immobilized cells. This is more clearly observed in Figure 4 where the ethanol production rate is plotted as a function of PFK maximum activity. There is almost no variation in ethanol production with PFK activity for suspended cells. On the other hand, increasing V_{PFK}^{max} by 30% from the *in vivo* value in immobilized cells produces an increase of 6% in ethanol production at pH^{ex} 5.5 and an increase of 22% at pH^{ex} 4.5.

Effects of altering ATP consumption rate

ATP consumption is included in the pathway model as a generalized ATPase reaction represented by first order kinetics. Figure 5 shows the effect of altering the ATPase kinetic constant (k_{ATPase}) on the flux-control coefficients of the more important steps of the pathway.

Similar functionalities are observed between the flux-control coefficients of suspended cells at pH^{ex} 5.5 and those at pH^{ex} 4.5. An increase in k_{ATPase} produces a decrease in c_{ATPase} and an increase in c_{In} , the other controlling step. c_{PFK} is not affected by changes in k_{ATPase} .

Flux-control coefficients of immobilized cells at pH^{ex} 5.5 and at pH^{ex} 4.5 also behave similarly as a function of k_{ATPase} . Increasing k_{ATPase} produces

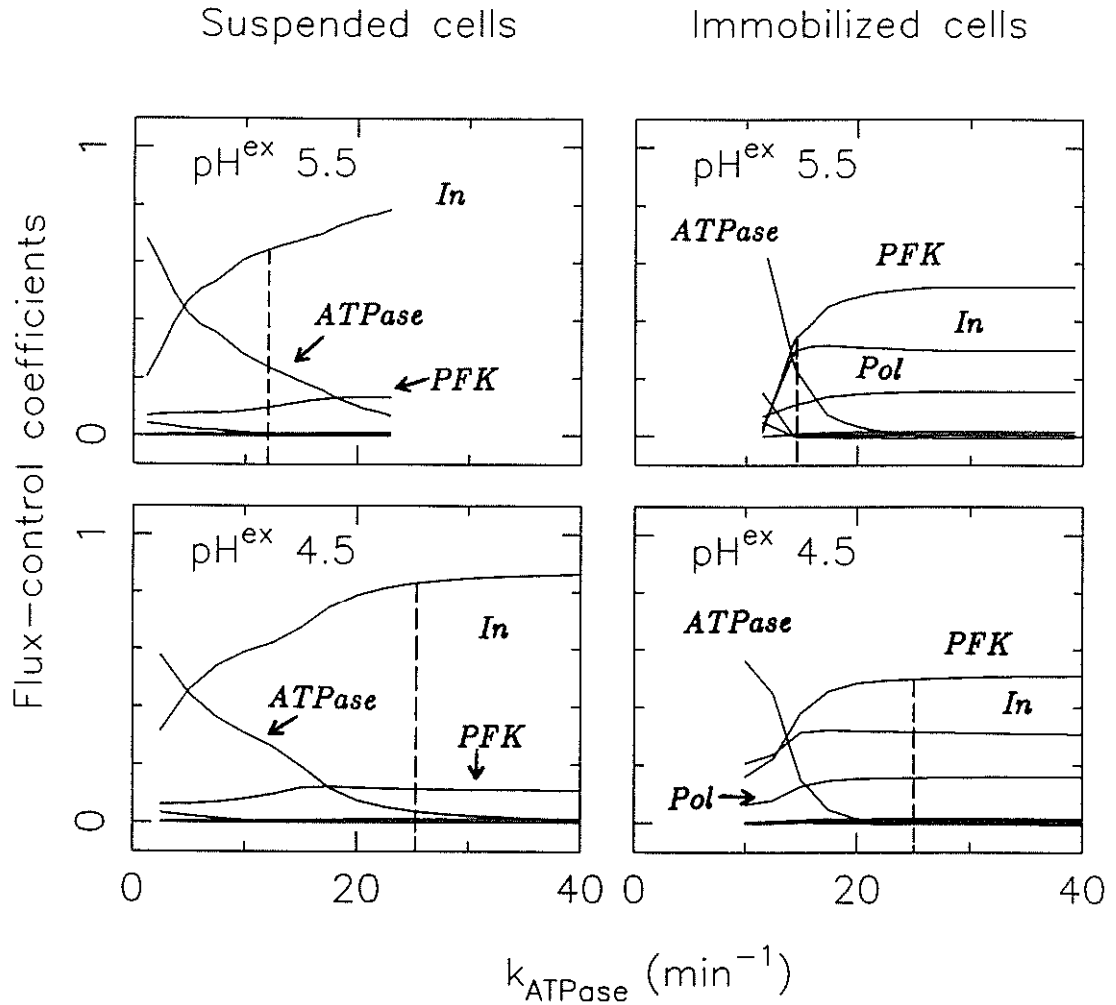


Figure 5: Flux-control coefficients as a function of ATPase kinetic constant.

Flux-control coefficients for suspended and immobilized cells at different extracellular pH, as a function of ATPase kinetic constant. Dashed line represents the *in vivo* values of Table I.

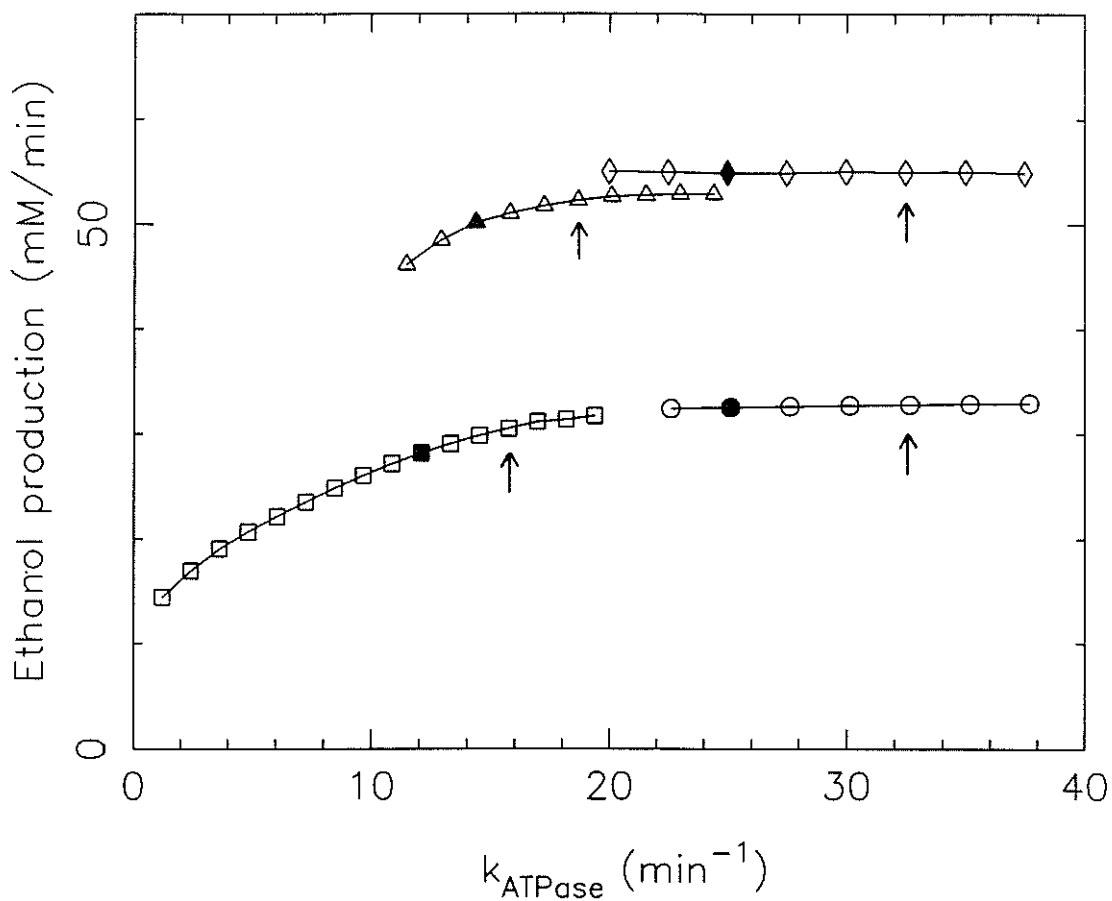


Figure 6: Ethanol production rate as a function of ATPase kinetic constant.

Ethanol production rate for suspended and immobilized cells of Figure 5. Full symbols are for *in vivo* conditions (Chapter 4.) Arrows indicate a 30% increase in glucose uptake velocity from the *in vivo* value.

- (□) suspended cells pH^{ex} 5.5
- (○) suspended cells pH^{ex} 4.5
- (△) immobilized cells pH^{ex} 5.5
- (◇) immobilized cells pH^{ex} 4.5

a decrease in c_{ATPase} and an increase in c_{PFK} at both extracellular pHs. c_{In} remains almost unaffected by changes in k_{ATPase} .

At pH^{ex} 4.5, there are no significant changes in the flux-control coefficients of both suspended and immobilized cells upon increasing k_{ATPase} from the *in vivo* values. This is because ATPase does not contribute to the flux control of the pathway at this extracellular pH (Table I.) Therefore, there is no effect on the ethanol production rate by increasing k_{ATPase} at pH^{ex} 4.5 as observed in Figure 6.

On the other hand, at pH^{ex} 5.5, ethanol production increases 11% in suspended cells and 7% in immobilized cells by increasing k_{ATPase} 30% over the *in vivo* values reported in Chapter 4.

DISCUSSION

Traditionally, the concept of pathway kinetic control is that a metabolic pathway has a single rate-limiting step, usually at the beginning. However, this is not always the case as can be seen not only in this work but also in several other studies.^(6,8,9) The identification of the main kinetic control points in a pathway is of great importance when trying to modify the pathway rate in a microorganism by means of metabolic engineering.

The flux-control points in ethanol production in *S. cerevisiae* are differently distributed in suspended cells than in immobilized cells. Thus, the highest improvement in ethanol production in suspended cells is achieved by increasing

the glucose uptake rate, and in immobilized cells by increasing phosphofructokinase maximum activity. A corollary of this is that optimization of any given process will depend not only on the specific microorganism used, but also on the environmental conditions in which it is placed.

Some general trends are observed in the results. The increase in the activity of a limiting step under any given condition will substantially improve the flux throughout the pathway if the control coefficient of that step is close to unity and there are no other steps with control coefficients as important as the one modified. For instance, the relative increase in ethanol production due to incrementing V_{In}^0 is larger in suspended cells than in immobilized cells because glucose uptake is the main control point in suspended cells while several steps share the flux control in immobilized cells.

In conditions where several steps are sharing the flux control in a pathway, the way to increase product formation rate is by simultaneously increasing the activities of all those steps. There are four steps sharing the control of ethanol production in immobilized cells at $\text{pH}^{ex} 5.5$: glucose uptake, phosphofructokinase, polysaccharide storage and ATP consumption. Only increasing the activities of all these steps at the same time will substantially increase ethanol production.

Ethanol production rate increased from 50 mM/min in immobilized cells at $\text{pH}^{ex} 5.5$ to 70 mM/min in immobilized cells, which had been previously grown in Ca-alginate (Chapter 3). According to the argument presented here, such an increment would only be possible if the activities of all the controlling steps were incremented. This is what the kinetic model described in Chapter 4 indicates

from the experimental results obtained for the alginate-grown cells. Phosphofructokinase maximum activity and the ATPase kinetic constant increased by a factor of two (from 32 to 63 mM/min and from 14 to 24 min⁻¹, respectively). In addition, the polysaccharide storage maximum activity increased ten times (from 14 to 137 mM/min) in agreement with the above statement. The calculation of flux-control coefficients in the alginate-grown cells indicates that glucose uptake is limiting the ethanol production rate in both suspended and immobilized cells. The flux-control coefficients of the glucose uptake step are 0.92 in suspended cells and 0.87 in immobilized cells. This 5% reduction in c_{In} is enough to produce an increase in ethanol production from 21 to 70 mM/min as it is observed in Figure 7, where ethanol production is plotted as a function of V_{In}^0 .

The combination of *in vivo* measurements with mathematical modelling provides a powerful tool for understanding and quantifying the effects of altering different steps in a pathway. This in turn will help in devising strategies for the genetic manipulation of microorganisms towards improvement of productivity or any other desirable property of interest.

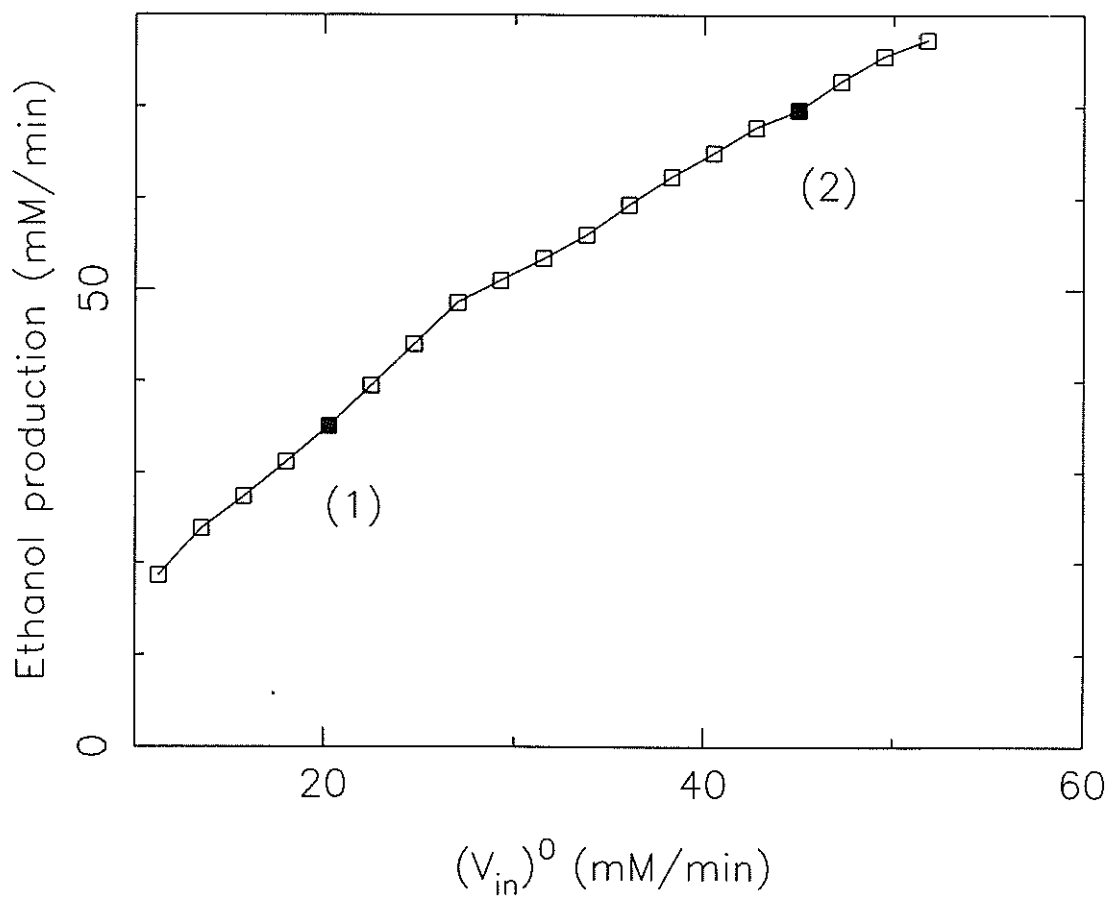


Figure 7: Ethanol production rate for alginate-grown cells as a function of glucose uptake velocity.

Full symbols are for *in vivo* conditions.

- (1) Suspended cells
- (2) Immobilized cells

REFERENCES

1. Bailey J., and Ollis D., In: "*Biochemical Engineering Fundamentals*", 2nd. Ed. pp.353-355, Mc Graw-Hill, (1986).
2. Kacser H., and Burns H., *Sump. Soc. Exp. Biol.*, **27**, 65 (1979).
3. Heinrich R., and Rapoport T., *Eur. J. Biochem.*, **42**, 89 (1974).
4. Westerhoff H., and Kell D., *Biotechnol. Bioeng.*, **30**, 101 (1987).
5. Fell D., and Sauro H., *Eur. J. Biochem.*, **148**, 555 (1985).
6. Westerhoff H., Groen A., and Wanders R., *Bios. Rep.*, **4**, 1 (1984).
7. Rapoport T., Heinrich R., and Rapoport S., *Biochem. J.*, **154**, 449 (1976).
8. Rapoport T., Heinrich R., Jacobash G., and Rapoport S., *Eur. J. Biochem.*, **42**, 107 (1974).
9. Holzhutter H., Jacobash G., and Bisdorff A., *Eur. J. Biochem.*, **149**, 101 (1985).

CHAPTER 6

CONCLUSIONS

Saccharomyces cerevisiae cells have different metabolic behavior in suspension, than when entrapped within a calcium-alginate matrix. The results obtained in this work suggest that immobilization alters cell metabolism at different levels. Glucose catabolism of suspension-grown cells is faster in immobilized cells than in suspended cells. These changes are reflected in a very short period of time and under conditions in which no significant biosynthesis of macromolecules such as DNA, RNA or protein occurs. The results indicate that glucose uptake is the step altered by cell entrapment.

When cells are allowed to grow within the Ca-alginate matrix in order to accentuate the effect of immobilization on cell metabolism, biosynthetic pathways respond differently as reflected by the slower growth rate observed in these cells. Also, glucose catabolism is faster in these alginate-grown cells studied under nongrowing conditions.

Using knowledge of the metabolic pathway involved in *S. cerevisiae* with the experimental determinations of intracellular intermediates *in vivo* and rates of glucose uptake and glycerol and ethanol production allows to provide a quantitative description of glucose catabolism in yeast. The validity of kinetic models previously proposed for phosphofructokinase and pyruvate kinase based on *in vitro* studies have been shown for the *in vivo* cell conditions. Also, kinetic representations of other important steps in glucose catabolism are consistent with *in vivo* data. The detailed pathway description makes possible the evaluation of flux-control coefficients for all key enzymes involved. This analysis indicates

that alginate entrapment reduces the flux control of the glucose uptake step by increasing the glucose uptake rate. Phosphofructokinase becomes the most influencing step in ethanol production in immobilized suspension-grown cells. Glucose uptake is still limiting the pathway flux in immobilized alginate-grown cells.

The specific mechanism by which the alteration of the glucose uptake step takes place is not evident from the results of this work. Glucose is transported inside the cells in *S. cerevisiae* by facilitated diffusion. Hence, a carrier protein is involved in the process. Limited information is available on the characteristics of the yeast glucose transporter. These carrier proteins are usually asymmetric and exit in two conformations with binding sites available first at one, and then at the other, side of the membrane in which they are embedded. Regulation effects take place at either side. Data on the yeast glucose carrier show that the interconversion between the two forms of the carrier is the most likely rate-limiting step in the transport. Thus, one may speculate that cell entrapment is interacting with the carrier conformational step, accelerating the interconversion between the two protein states, and hence, glucose uptake.

A key element in this study has been the application of nuclear magnetic resonance (NMR) as a noninvasive analytic technique. The determination of intracellular components has been made under the actual conditions of ionic strength and pH in the cell, and in the presence of any unknown effector or inhibitor of the cell metabolism. This is crucial in metabolic regulation studies as the one presented here. Also, the additional complication of cell release from the immobilization matrix, which is necessary when using cell extraction

methods for intracellular component determinations, has been avoided by using NMR techniques.

The methodology used in this work to compare suspended and immobilized cell metabolism can also be used in other contexts. The combination of *in vivo* determinations with mathematical modelling provides a powerful tool for understanding and quantifying the effects of altering different steps in a pathway. This provides a rationale for designing metabolic engineering strategies when trying to improve any properties of interest in a microorganism by means of genetic manipulation.

APPENDIX A

APPLICATION OF LINEAR PREDICTION
SINGULAR VALUE DECOMPOSITION FOR PROCESSING *IN VIVO*
NMR DATA WITH LOW SIGNAL-TO-NOISE RATIO

ABSTRACT

Low sensitivity of nuclear magnetic resonance (NMR) measurements of living cell composition by conventional methods requires samples with high cell density compared to that in growing cultures. Reasonably accurate intracellular concentration estimates from lower cell density samples can be obtained by treating the time-domain NMR data by linear prediction singular value decomposition (LPSVD) prior to Fourier transformation. Alternatively, application of LPSVD enables intracellular concentration estimates in less NMR acquisition time, improving time resolution in NMR measurements of intracellular transients.

INTRODUCTION

Nuclear Magnetic Resonance (NMR) spectroscopy has become a powerful method to study cell metabolism *in vivo*.⁽¹⁻³⁾ NMR provides quantitative information about several intracellular components allowing noninvasive study of cell metabolic functions. Contrary to cell-extract methods, NMR is a nondestructive technique that makes possible the study of transient phenomena using the same cell sample.

A disadvantage of NMR is its inherent lack of sensitivity.^(2,3) A minimum concentration of test material is required to produce a detectable signal above the level of the noise. The signal-to-noise ratio depends upon a wide range of factors.⁽⁴⁾ The two most commonly and easily manipulated are the cell sample concentration and the time during which free-induction decays (the NMR signals in the time domain) are accumulated. Typical experiments for yeast are carried out using cell concentrations of 40-50%, expressed as volume of wet cell pellet per volume of total sample (percent), and scanning intervals of 2-5 min.⁽⁵⁻⁸⁾ This high cell density, *ca.* 80-100 g cell dry weight/L, is much greater than those obtained in laboratory growth studies and in most bioreactor operations. Also, in the case of mammalian cells, obtaining a sample of high cell density may be very difficult without producing considerable cell damage.⁽⁹⁾ Therefore, study of cell metabolism in these situations requires some change in the NMR experiment in order to increase the signal or decrease the contributions from

noise. Increasing the acquisition time is one possible approach to obtain a good signal-to-noise ratio, but this reduces time resolution in transient experiments, and may also introduce problems in maintaining the cell sample in a constant state during measurement.

In conventional Fourier transform NMR data processing, the accumulated free induction decay (FID) is transformed to the final, frequency domain spectrum using a fast Fourier transform (FFT) algorithm. This algorithm is computationally very efficient but has poor resolution when the signal-to-noise ratio in the FID is low.⁽¹⁰⁾ Thus, standard methods provide spectra that are difficult to interpret and quantify at the low signal-to-noise conditions characteristic of short FID acquisition or low sample densities.

Recently, two alternative methods for processing FIDs have been proposed: linear prediction singular value decomposition (LPSVD) and the maximum entropy method (MEM).^(11,12) After assuming a reasonable functional model for the FID (typically a linear combination of noninteracting decaying oscillators), the LPSVD method systematically estimates parameters in that functional representation and performs an error analysis to discard insignificant components. LPSVD has proven useful in extracting information from several types of signals with low signal-to-noise ratios.^(13,14) In NMR applications, the parameter values obtained from LPSVD are used to reconstruct a FID less contaminated by noise, which is subsequently converted to the final processed spectrum using FFT.

MEM is a spectral method that does not require any assumption for the data processing. MEM starts with a trial spectrum and, using backward Fourier

transform, compares the trial FID with the experimental FID. The obtained residual is converted to the frequency domain using forward Fourier transform. Then the trial spectrum is changed to try to minimize the residual spectrum. From all possible spectra giving a minimum residue, the one with maximum entropy is chosen as the final result.⁽¹²⁾ MEM is useful for recovering signal frequencies in very noisy FIDs but it does not provide accurate quantitative information such as line widths and peak intensities, on the recovered line positions.⁽¹⁵⁾

In this work, LPSVD is applied to obtain intracellular concentrations in a dilute cell suspension, resembling more closely reactor-like conditions, and in experiments using short-time acquisitions that allow observation of rapidly changing processes in the cell. For economy of terminology, the use of LPSVD to fit and reconstruct the FID, followed by calculation of the spectrum using FFT, will be called the "LPSVD method". Calculation of the spectrum from FFT of the original FID will be denoted the "FFT method".

MATERIALS AND METHODS

Saccharomyces cerevisiae ATCC 18790, a standard diploid yeast strain, was used in all the experiments. Cell sample preparation was carried out as described previously.⁽¹⁶⁾

For the low cell density experiments, ³¹P NMR spectra were obtained at 121.49 MHz on a Bruker AM-300 wide bore spectrometer, using a 20-mm-

diameter broad-band probe. For the short-term acquisition experiments, ^{31}P NMR spectra were obtained at 202.46 MHz on a Bruker AM-500 spectrometer, using a 10-mm-diameter broad-band probe. All experiments were done at 20° , using pulse intervals and pulse width angle of 0.5 sec and 70° , respectively. Sample spinning and ^1H decoupling were not employed. Nitrogen gas was bubbled continuously through the cell suspension as reported elsewhere.⁽¹⁶⁾

The 8K FID files taken by the Bruker Aspect-3000 computer were transferred to a VAX 11/780 computer for analysis using the LAB ONE NMR1 Spectroscopic Data Analysis Software System⁽¹⁷⁾ and to a SUN 3/160 computer to perform the LPSVD analysis.⁽¹¹⁾ In the FFT method, the experimental FIDs were baseline corrected, multiplied by an exponential apodization function corresponding to a line broadening of 10 Hz, Fourier transformed, phased, and baseline flattened (4th degree polynomial) using the NMR1 software. In order to properly apply the LPSVD method to the quadrature FID data of the Bruker spectrometers, which sample the real and imaginary channels sequentially,⁽¹⁸⁾ the sign of alternate complex pairs of the experimental FID were first inverted and the data were then considered as reals without any further treatment. The processing of each FID using the LPSVD analysis required 1.5 h of CPU time.

The signal-to-noise defined as: $S/N = 2.5$ (peak height)/(peak-to-peak value of noise) refers to the largest peak of any given spectrum.

For estimation of intracellular concentrations, saturation constants were obtained for each resonance, comparing intensities in fully relaxed spectra with intensities in saturated spectra using the actual experimental pulsing conditions as described above. 50 μL of phosphate (1 M) was added at the end of each

experiment to convert intensity to concentration. For estimation of intracellular concentration, it was assumed that 1.67 g wet cells contains 1 mL of intracellular volume.⁽¹⁹⁾

Linear prediction singular value decomposition method

The mathematical description of the model is described in detail in the literature.⁽¹¹⁾ The method is based on fitting a model function to a discretely sampled magnetic resonance time-domain signal. The model function is a sum of exponentially damped sinusoids. The four parameters describing each harmonic component are frequency, decay rate, amplitude and phase. In order to avoid nonlinear fitting, the problem is first linearized by means of the method of Linear Prediction (LP). This LP yields an under-determined matrix equation, which is solved by Singular Value Decomposition (SVD) of the data matrix. The elements of the solution vector are used as coefficients in an Lth degree polynomial, the roots of which yield the frequency and decay rate parameters.⁽¹⁰⁾ The frequencies and decay rates obtained in this way are substituted in the equations for the data points, yielding a linear algebraic equation that is solved by a linear least squares method for the remaining amplitude and phase parameters.

An error analysis was performed on the results provided by LPSVD. The minimum variance bound method provides a lower bound on the standard deviations of the model parameters.⁽²⁰⁾ Signals with amplitude smaller than the corresponding standard deviation were removed. The time-domain signal was reconstructed using the parameters obtained by the LPSVD procedure. Performing a Fourier transform of this reconstructed FID signal allows comparison

with the original spectrum obtained using the FFT method. In the case of proper fitting, the difference between the original FID and the reconstructed time domain signal should contain only noise.

RESULTS

Low cell density experiments

In the low cell density experiments, 15 mL of a sample with 5% (v/v) cell concentration (*ca.* 10 g/L) were placed in a 20-mm-diameter NMR tube. At time zero, glucose was added to a final concentration of 200 mM. Phosphorus-31 metabolism was monitored on the spectrometer computer. A pseudo-steady state was reached after 15-16 min as indicated by invariant intracellular component resonances in the ^{31}P spectra. Subsequently, FIDs were stored in 1-min blocks (120 scans).

A reference FID was obtained by adding accumulated scans from 15 1-min acquisitions. The signal-to-noise ratio of the FFT spectrum of this reference signal was 162. The information provided by this spectrum was used as the reference for analysis of low cell density data. Figure 1 shows the reference data. The estimated metabolite concentrations obtained by integration of both the FFT and the LPSVD-reconstructed spectra are listed in Table I. The agreement is very good. The ratio of concentrations estimated by LPSVD to those estimated by FFT has a mean value of 0.983 and a standard deviation of 0.071.

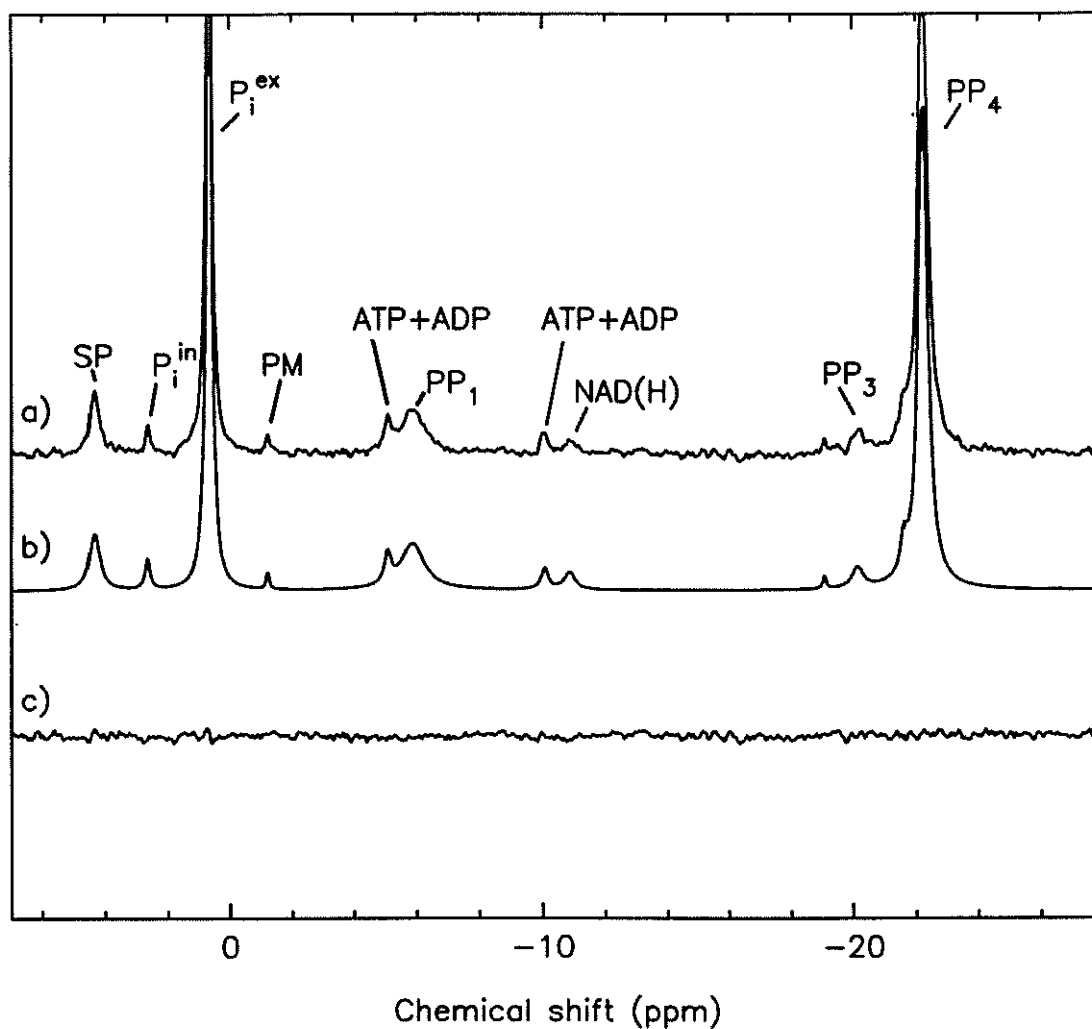


Figure 1: Low-cell density ^{31}P NMR spectra

Spectra obtained from adding 15 1-minute FIDs of a 5% (v/v) yeast suspension conducting steady-state glucose catabolism (signal-to-noise = 162). a) phase-corrected FFT spectrum of the experimental FID, b) spectrum calculated from the FID reconstructed from LPSVD parameters, c) residual obtained by Fourier-transforming the difference between the experimental FID and the LPSVD-reconstructed FID. (SP: sugar phosphates, P_i^{in} : intracellular inorganic phosphate, P_i^{ex} : extracellular inorganic phosphate, PM: phosphomannan, PP_1 , PP_3 and PP_4 : polyphosphates.)

TABLE I: Metabolite concentration estimation by FFT and by LPSVD using the low-cell density data.

Metabolite concentrations estimated using the fast Fourier transform (FFT) method and linear prediction singular value decomposition (LPSVD) method in a dilute yeast suspension conducting steady-state glucose catabolism. Fifteen 1-min FIDs were added at steady-state obtaining a spectrum with signal-to-noise=162. SP: sugar phosphates, P_i^{in} : intracellular inorganic phosphate, P_i^{ex} : extracellular inorganic phosphate, A(D)TP: adenosine di- and triphosphate.

	FFT (mM)	LPSVD (mM)	$\frac{\text{LPSVD}}{\text{FFT}}$
SP	14.8	15.4	1.04
P_i^{in}	10.3	9.7	0.94
P_i^{ex}	42.0	45.0	1.07
NAD(H)	2.5	2.7	1.08
A(D)TP	3.8	3.4	0.89

In order to obtain a sequence of spectra with different signal-to-noise ratios, two or more experimental FIDs were added to obtain FIDs corresponding to acquisition times of 2, 3, 4, 5, 6, and 7 minutes. The signal-to-noise ratios in the FFT spectra were 45, 63, 83, 92, 94, and 108, respectively. Each experimental FID was processed using the FFT and the LPSVD methods. Spectrum resonances were integrated and compared with the corresponding reference information of Table I. Figure 2 shows the percentage errors in intracellular concentrations of both methods relative to the reference data.

Most of the discrepancies in using FFT are around 20%, even for the 7 min scan (Figure 2-a). There is a systematic underestimation of all metabolite concentrations except for NAD(H), probably due to errors in setting the baselines in the spectra.

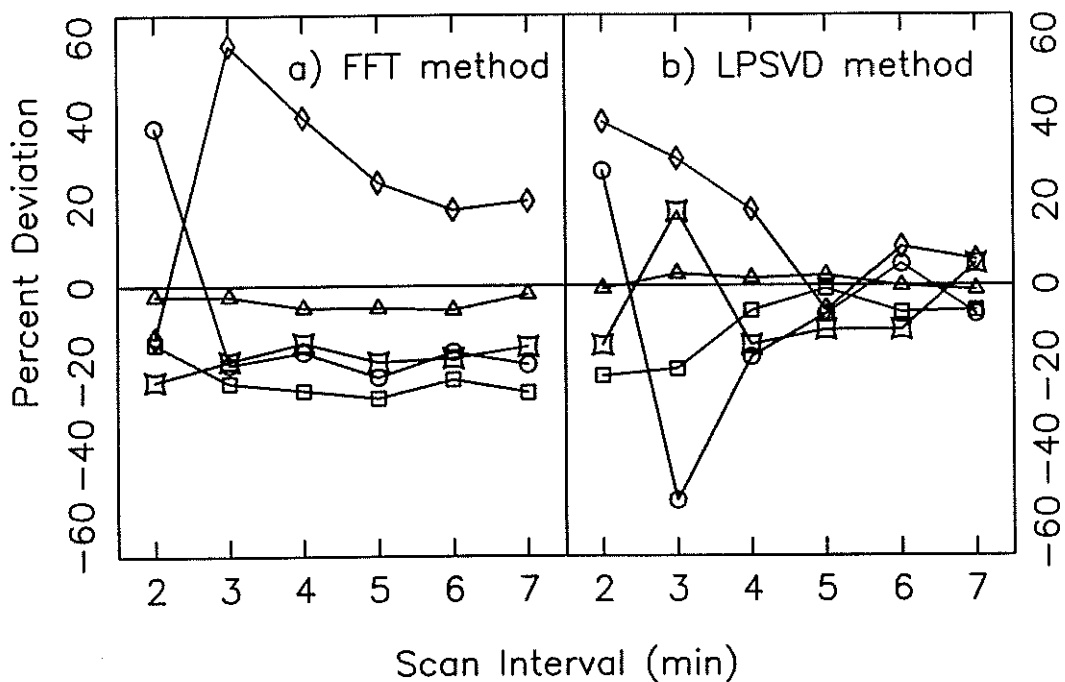


Figure 2: Percent deviation of metabolite concentrations from the low-cell density data.

The abscissa denotes the total scan interval used for accumulation of an FID which is then processed by two alternative procedures. a) FFT method, b) LPSVD method.

There is a good agreement between the reference spectrum results and the ones obtained by the LPSVD method (Figure 2-b). LPSVD provides estimates of metabolite concentrations within 10% of the reference values using acquisition times of 5 minutes.

Short time acquisition experiments

These experiments were performed in a fashion similar to those just described, but employed a higher cell concentration. 2 mL of a sample with 40% (v/v) cell concentration (*ca.* 80 g/L) were placed in a 10-mm-diameter NMR tube. Glucose was added to a final concentration of 200 mM. Once pseudo-steady state was reached after 15-16 min, a 240-scan FID was acquired for reference purposes. Then, FIDs were accumulated with different numbers of scans (15, 30, 60 and 120 scans) corresponding to 7.5, 15, 30 and 60 second intervals. The signal-to-noise ratios of the FFT spectra were 33, 34, 47, 88, and 122 respectively. The FID for reference was obtained by adding the initial 240-scan FID with a final 240-scan FID. The signal-to-noise ratio of the FFT spectrum of the reference FID was 221.

Table II shows the concentration values estimated from the reference FID using the FFT method and the LPSVD method. The ratio of LPSVD concentration estimates to concentrations estimated by FFT has a mean value of 1.004 and a standard deviation of 0.032. The agreement between the two methods is slightly better in this case than in the low cell density experiments because the signal-to-noise ratio of the reference signal is higher. Hence both the LPSVD and the FFT methods have better performance.

TABLE II: Metabolite concentration estimation by FFT and by LPSVD using the 15-sec scan data.

Metabolite concentrations estimated using fast Fourier transform (FFT) method and linear prediction singular value decomposition (LPSVD) method in a 40% (v/v) yeast suspension. Two 2-min FIDs were added at steady-state obtaining a FFT spectrum with signal-to-noise = 221. Abbreviations as in Table I.

	FFT (mM)	LPSVD (mM)	$\frac{\text{LPSVD}}{\text{FFT}}$
SP	16.1	16.2	1.01
P_i^{in}	11.9	12.0	1.01
P_i^{ex}	25.6	26.0	1.02
NAD(H)	2.2	2.1	0.95
A(D)TP	3.6	3.7	1.03

Figure 3 shows a visual comparison of the sugar phosphate region (SP) between the FFT and the LPSVD spectra obtained from the FID with 15-sec acquisition time (30 scans). The SP and intracellular phosphate resonances are much more clearly delineated in the LPSVD results than in the FFT spectrum. The concentrations of SP and intracellular phosphate estimated by FFT in this experiment deviate 30% (Figure 4) from the reference concentrations (Table II). On the other hand, using the LPSVD method, deviations from the reference concentration are less than 10%.

Relative errors for all metabolites obtained using both methods are shown in Figure 4 as a function of the acquisition time used. While there is a good agreement between the values obtained by the LPSVD method and the reference values of Table II, the agreement using the traditional FFT method is well above 30% for acquisition times lower than 15 seconds.

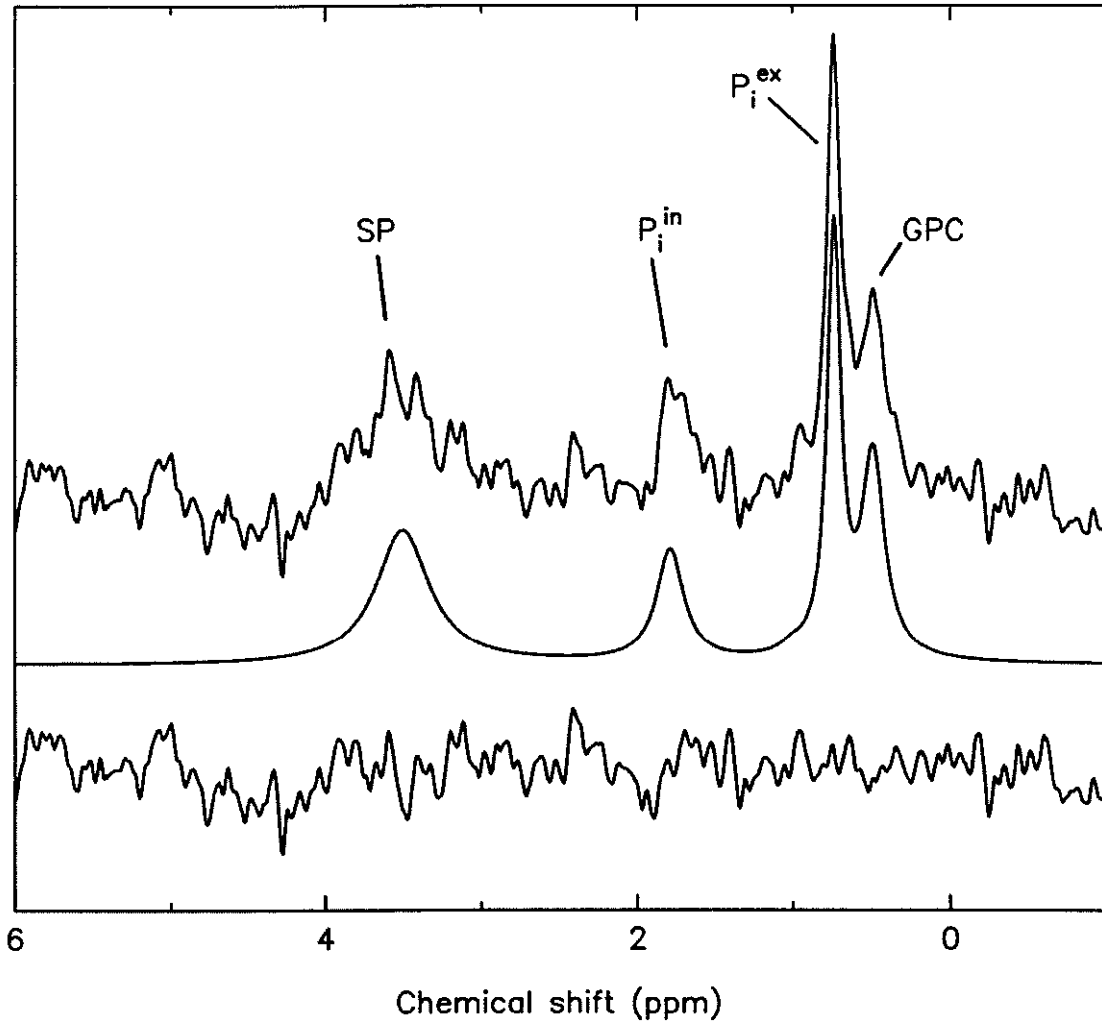


Figure 3: Comparison of the downfield region of the 15-sec scan data.

Comparison of the downfield region of a 15-sec scan of a 40% (v/v) yeast suspension conducting steady-state glucose catabolism. (Signal-to-noise = 33.9) (SP: sugar phosphates, P_i^{in} : intracellular inorganic phosphate, P_i^{ex} : extracellular inorganic phosphate, GPC: glycerol phosphorylcholine.)

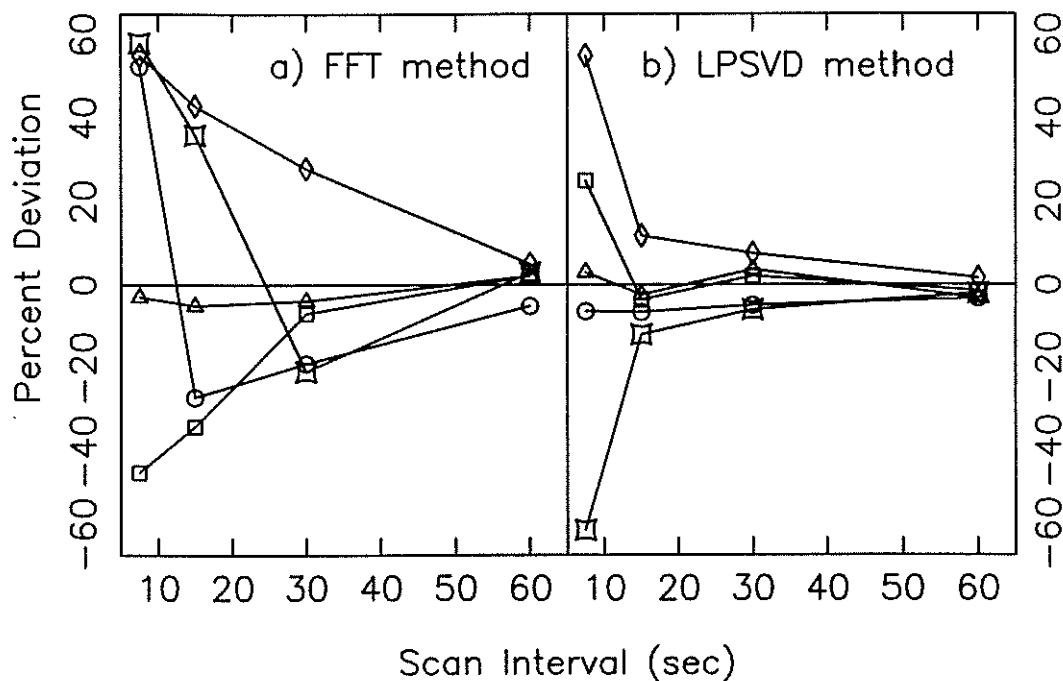


Figure 4: Percent deviation of metabolite concentrations for the 15-sec scan data.

Percent deviation of metabolite concentrations from the reference values of Table II. The abscissa denotes the total scan interval used for accumulation of an FID which is then processed by two alternative procedures. a) FFT method, b) LPSVD method. Symbols as in Figure 2.

DISCUSSION

LPSVD has proven to be a superior method to retrieve quantitative information from FIDs with poor signal-to-noise ratio. This allows NMR analysis of diluted cell samples more closely resembling bioreactor conditions. The method should be very useful in future NMR studies of growing cells. Also, LPSVD can be used to monitor rapidly changing processes where short acquisition times are essential. The main drawback of LPSVD, besides the need to assume a model for the FID, is the extensive computing time required to process the data. FFT is still a very powerful and fast technique that will continue to have a role in *in vivo* NMR data processing. FFT methods can be used in conjunction with more sophisticated but computationally slower techniques like LPSVD in order to monitor, control, and analyse NMR studies of metabolizing cells.

Acknowledgements

This research was sponsored by the Energy Conversion and Utilization Technology (ECUT) Program of the U.S. Department of Energy. NMR1 software was provided by the NIH Resource Laboratory at Syracuse University (Grant RR-01317). We thank S. Sibisi for providing the LPSVD programs written by H. Barkhuijsen and R. de Beer.

REFERENCES

1. London R., *Prog. in NMR Spect.*, **20**, 337 (1988).
2. Fernandez E., and Clark D., *Enzyme Microb. Technol.*, **9**, 259 (1987).
3. Burk S., and Shulman R., *Ann.Rev. Microbiol.*, **41**, 595 (1987).
4. Gadian D., In: "*Nuclear Magnetic Resonance and its Applications to Living Systems*", Clarendon Press, Oxford, pp. 8-10, (1982).
5. Galazzo J., and Bailey J., *Biotech. Bioeng.*, in press (1988).
6. Shanks J., and Bailey J., *Biotech. Bioeng.*, **32**, 1138 (1988).
7. Burk S., Jones K., and Shulman R., *Biochemistry*, **26**, 7483 (1987).
8. Nicolay K., Scheffers W., Bruinenberg P., and Kaptein R., *Arch. Microbiol.*, **133**, 83 (1982).
9. Mendez R., Wemmer D., Halm G., Jardetzky N., and Jardetzky O., *Biochim. Biophys. Acta*, **720**, 274 (1982).
10. Kay S., and Marple S., *Proc. IEEE*, **69**, 1380 (1981).
11. Barkhuijsen H., de Beer R., Boveé W.M.M.J., and van Ormondt D., *J. Mag. Res.*, **61**, 465 (1985).
12. Laue E., Skilling J., Staunton J., Sibisi S., and Brereton, *J. Mag. Res.*, **62**, 437 (1985).
13. Johnson B., Malikayil J., and Armitage I., *J. Mag. Res.*, **76**, 352 (1988).

14. Gesmar H., and Led J., *J. Mag. Res.*, **76**, 183 (1988).
15. Gull S., and Skilling J., *Proc. IEE(F)*, **131(F)**, 646 (1984).
16. Galazzo J., Shanks J., and Bailey J., *Biotech. Techniques*, **1**, 1 (1987).
17. LAB ONETM NMR1 Spectroscopic Data Analysis Software, Ver. 2.7, Syracuse University, New Methods Research Inc., (1985).
18. Redfield A., and Kunz S., *J. Mag. Res.*, **19**, 250 (1985).
19. Gancedo J., and Gancedo C., *Biochimie*, **55**, 205 (1973).
20. Barkhuijsen H., de Beer R., and van Ormondt D., *J. Mag. Res.*, **67**, 371 (1986).

APPENDIX B

**COMPARISON OF INTRACELLULAR SUGAR PHOSPHATE LEVELS
OF INTACT CELLS AND PERCHLORIC CELL EXTRACTS
USING PHOSPHORUS-31 NMR**

ABSTRACT

Phosphorus-31 NMR experiments were performed for cells in suspension and cell extracts of *Saccharomyces cerevisiae* ATCC 18790 and *S. cerevisiae* D603. The assay was performed by monitoring the cell suspension metabolism using ^{31}P NMR. At the desired time, the metabolism of the cell suspension was stopped by freezing the cells with liquid nitrogen and the intracellular components were extracted by adding perchloric acid. Subsequently, the cell extracts were analyzed using ^{31}P NMR. In this way, *in vivo* and *in vitro* spectra were taken at the same time in glucose catabolism. Thus, the sugar phosphate values obtained by the deconvolution method described in Chapter 2 may be compared with the values obtained from the cell extracts. This work was done in collaboration with Jackeline Shanks.

INTRODUCTION

The estimation of intracellular metabolite levels is of fundamental importance to characterize the cell metabolic processes and their regulation. *In vivo* estimation of intracellular components is now possible using nuclear magnetic resonance spectroscopy (NMR), a technique that allows the estimation of intermediates within the cells noninvasively. Phosphorus-31 (^{31}P) NMR resolves small phosphate-containing metabolites in different compartments within the cell, as well as extracellular compounds. Using *in vivo* ^{31}P NMR, the intracellular sugar phosphates in glucose metabolism in yeast appear as a single broad peak, which is mainly composed of overlapping peaks of glucose-6-phosphate, fructose-6-phosphate, fructose-1,6-biphosphate and 3-phosphoglycerate. This peak can be deconvoluted in its individual components by spectral analysis methods as described in Chapter 2.

The sugar phosphate concentration values obtained from the deconvolution method analysis of *in vivo* ^{31}P NMR are compared with the values obtained by analyzing ^{31}P spectra of cell extracts.

MATERIALS AND METHODS

Yeast strains

Saccharomyces cerevisiae ATCC 18790 and D603 were the yeast strains

used. *S. cerevisiae* 18790 is a standard diploid strain and has no known mutations. *S. cerevisiae* D603 is the homozygous diploid version of YM603 (*ade2-101*, *ura3-52*, *his3*, *met*, *lys2-801*, *reg1-501*). The *reg1* mutation inhibits catabolic repression by glucose.

Culture and NMR preparation

The strains were grown to mid-exponential phase in liquid medium containing 1% yeast extract, 2% bacto-peptone, and 2% glucose, at pH 4.5. The cultures were chilled on ice, then harvested by low speed centrifugation at 4°. The cells were washed twice in an ice-cold sterile buffered salt solution: 0.85 g/L KH₂PO₄, 0.15 g/L K₂HPO₄, 0.5 g/L MgSO₄, and 0.1 g/L NaCl in 50 mM MES buffer, pH adjusted to 6. The cells were resuspended in wash medium supplemented with an additional 15 mM of inorganic P at a 1:1 ratio of cell pellet volume to resuspension volume. Cell suspensions (2 mL) in the NMR tubes were tightly capped, and kept on ice until used for the NMR experiment (less than 2 hours).

Assay

³¹P NMR spectra of the cellular suspensions were obtained in the Fourier-transform mode at 202.46 MHz on a Bruker AM-500 NMR spectrometer at 20°. The pulse interval and angle were 0.5 s and 70°, respectively. Free induction decays (FIDs) were accumulated in consecutive 1 min blocks (120 scans, 8K files). Sample spinning and ¹H decoupling were not employed.

The yeast suspension was warmed to 20° inside the magnet for 15 min. An initial spectrum was taken of the cellular suspension, then 75 μL of a 40 % (wt) glucose solution was added to the cells and a sequence of spectra was collected during subsequent 1 min intervals. The spectra were monitored at the console while the experiments were in progress. The *in vivo* experiment was stopped when the levels of metabolites in the *in vivo* spectrum indicated that the cells were near quasi-steady-state period, between 10-20 min after addition of glucose. The yeast suspension was immediately poured into a mortar that had been precooled and filled with liquid nitrogen. 1 mL of concentrated perchloric acid was added to the frozen yeast suspension. The mixture was ground to a powder with a pestle. Liquid nitrogen was added to the frozen yeast pellet so that the pellet was always immersed while grinding.

The powder sample was then transferred to a Nalgene test tube that had been precooled in dry ice-ethanol. The test tube was placed in a dry ice-ethanol bath for 30 min, then thawed in an ice bath (*ca.* 5 min). This cycle was repeated two more times, with the freeze period and thaw period about 5 min each.

The sample was centrifuged for 15 min at 10,000g at 4° to separate the cell debris. The supernatant was transferred to another precooled test tube and neutralized with cold 2 M KHCO_3 . The pH was checked with Litmus paper. The step of adding KHCO_3 was performed in a cold room (8°) to minimize sample degradation. The sample containing precipitate was set in an ice bath for 10 min, the centrifugation was performed as before to remove the precipitate. The supernatant was passed through a Chelex

100, 200-400 mesh, Biorad Poly-Prep column to remove paramagnetic cations. The sample was then lyophilized overnight in a freeze-dryer. Freeze-dried samples were stored in a -20°C freezer until NMR spectroscopy was applied.

For NMR spectroscopy of extracts, the lyophilized sample was redissolved in 20 mM EDTA equal in volume to the original sample, and placed in 10-mm-diameter NMR tubes. D_2O was added to 10% final volume. The sample was kept on ice until used for the NMR experiment. ^{31}P NMR spectra of cell extracts were obtained at 8°C , using a pulse interval of 5.5 sec and pulse angle of 90° . FIDs were accumulated for 1,000 scans in 8K files. Inverse-gated broad band decoupling of ^1H with a power of 2 W and sample spinning of 14 Hz were employed.

Identification of compounds in the sugar phosphate region was determined by adding the individual sugar phosphate compounds and taking an additional spectrum, and by peak position vs. pH curves.

Data processing

The 8K FID files taken by the Bruker Aspect-3000 computer were transferred to a VAX 11/780 computer for analysis using the LAB ONE (TM) NMR1 Spectroscopic Data Analysis Software System. All subsequent processing was performed by the software system on the VAX computer. The FIDs were multiplied by an exponential apodization function corresponding to a line broadening of 10 Hz for the cellular spectra and 3 Hz for the cell-free extract spectra, Fourier transformed, phased, and baseline flattened (4^{th} degree polynomial).

Estimation of sugar phosphate concentrations

Estimates of the levels of the sugar phosphates were determined by a systematic procedure based upon ^{31}P NMR measurements. The sugar phosphate region of the ^{31}P NMR spectrum was first decomposed by computer analysis (NMR1 software), and the decomposition consistency and identification of individual sugar phosphate resonances was established based on *in vitro* chemical shift calibrations determined in separate experiments.

Calibration experiments were performed to take into account the saturating pulsing conditions of the NMR experiments by alternating fully relaxed spectra with partially saturated spectra as described previously. Relative concentrations can be determined within $\pm 5\%$. For estimation of intracellular concentrations, 1.67 g wet weight/mL intracellular volume and 0.2 g dry weight/g wet weight were assumed.

RESULTS

^{31}P NMR experiments were performed for cell suspension and cell extracts of *Saccharomyces cerevisiae* ATCC 18790 and D603. The assay was performed by monitoring the glucose metabolism of the cell suspension using ^{31}P NMR, stopping the metabolism of the cell suspension while glucose was still being catabolized at constant rate by freezing the cells with liquid nitrogen and perchloric acid, preparing the cell extract, and then using ^{31}P NMR to determine

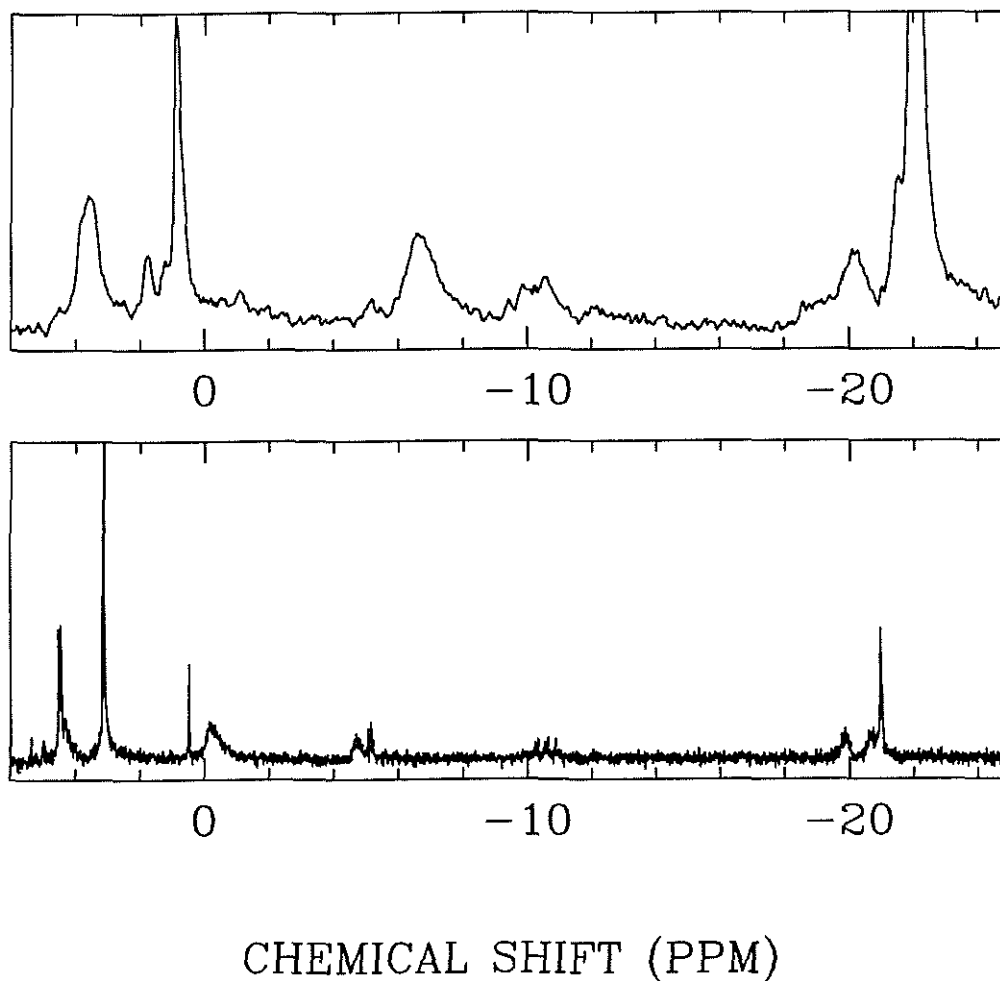


Figure 1: *In vivo* and perchloric acid extract ^{31}P NMR spectra of *S. cerevisiae* ATCC 18790.

^{31}P NMR spectra of *S. cerevisiae* ATCC 18790 cells in suspension (top frame) and of perchloric acid extracts of the same suspension (bottom frame) 18 min after addition of glucose to starved cells.

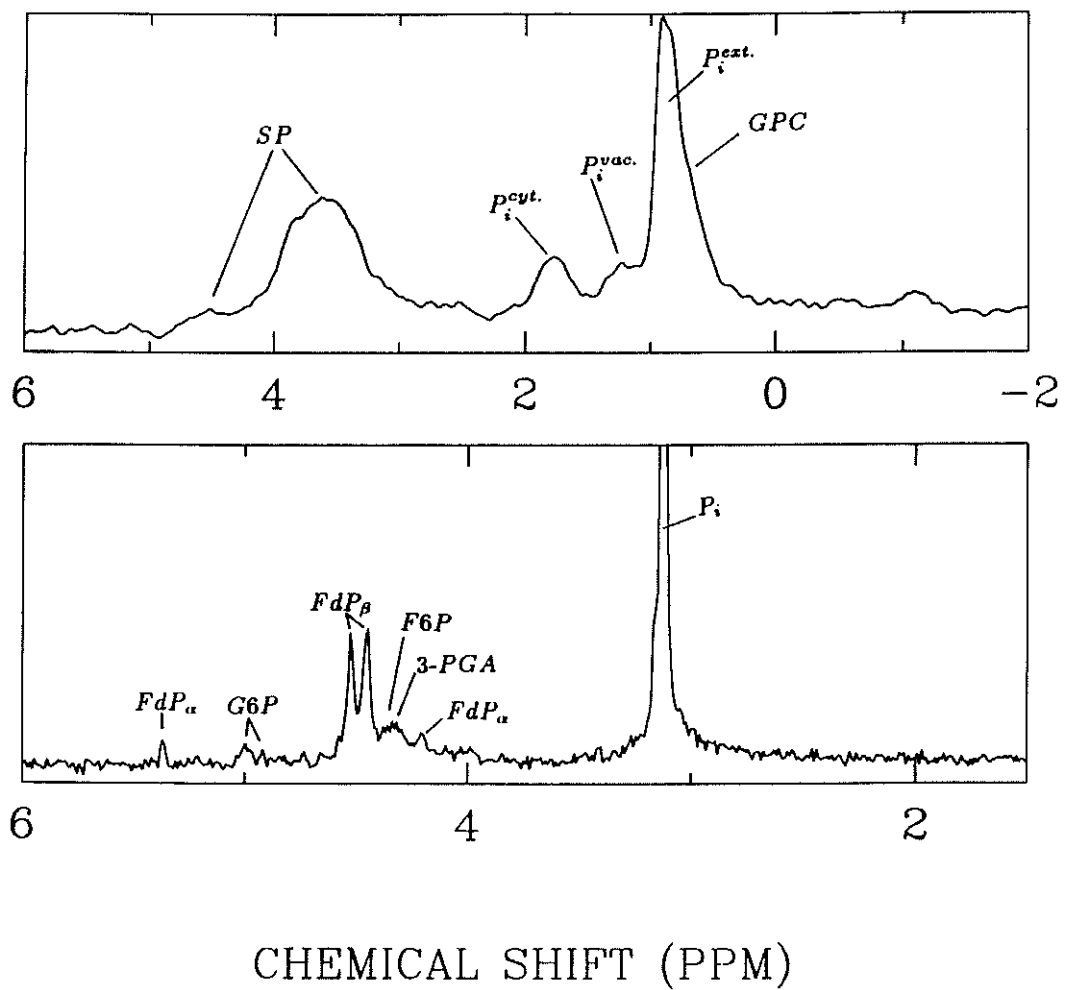


Figure 2: Downfield region of *in vivo* and perchloric acid extract ^{31}P NMR spectra of *S. cerevisiae* ATCC 18790 cells.

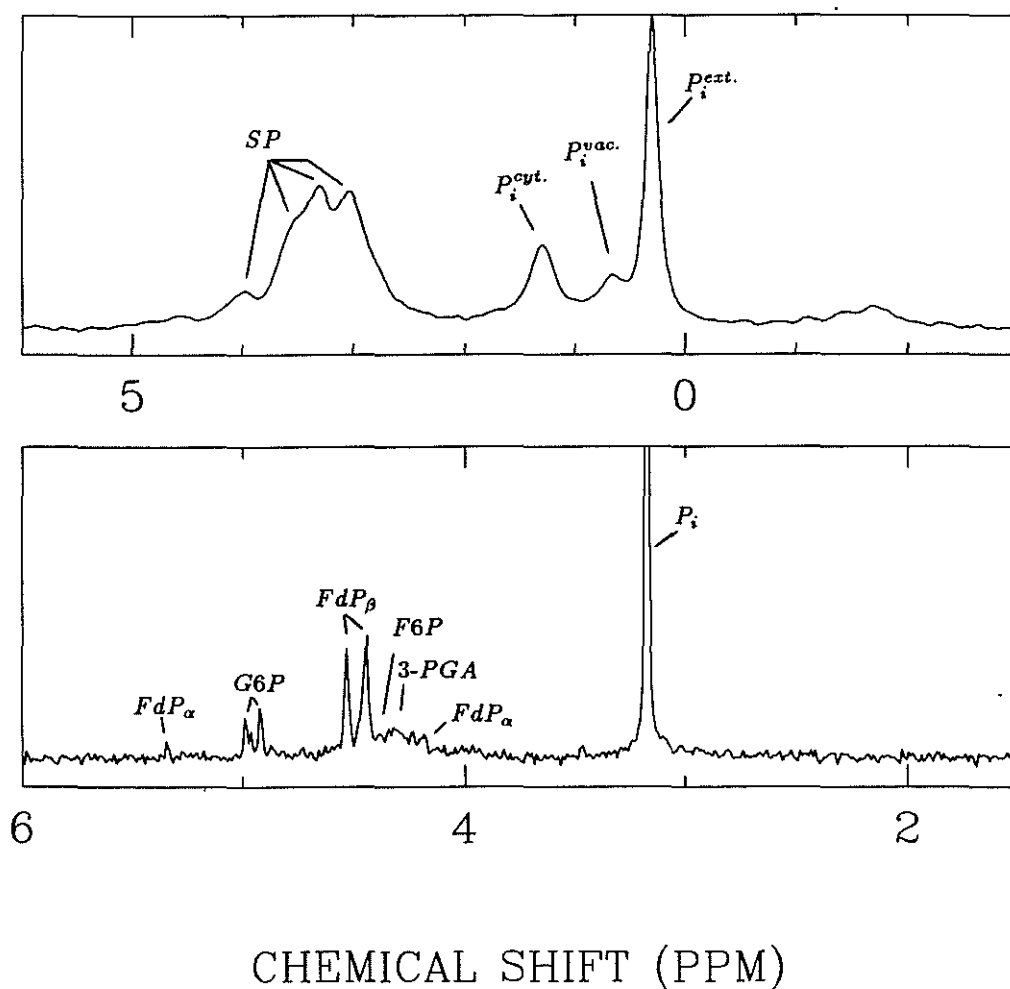


Figure 3: Downfield region of *in vivo* and perchloric acid extract ^{31}P NMR spectra of *S. cerevisiae* D603 cells.

Downfield region ^{31}P NMR spectra of *S. cerevisiae* D603 cells in suspension (top frame) and of perchloric acid extracts of the same suspension (bottom frame).

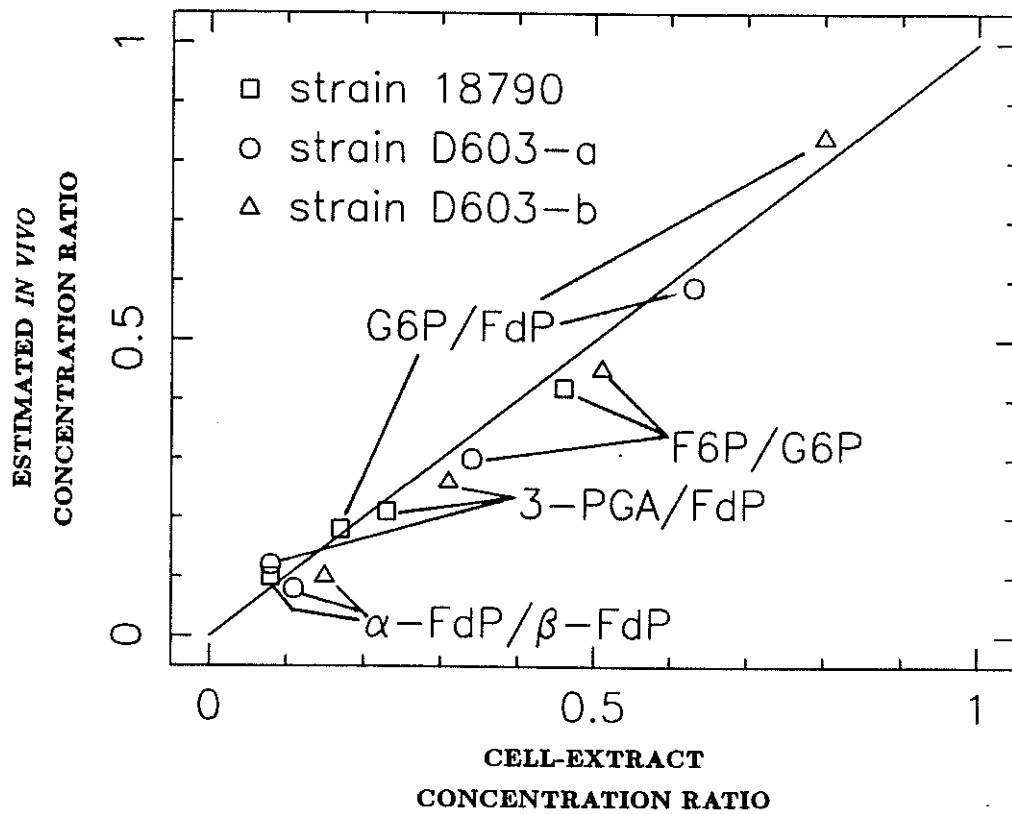


Figure 4: *In vivo* vs. *in vitro* relative levels of various sugar phosphate compounds.

In vivo levels were determined from cell suspension spectra using the deconvolution method described in Chapter 2. *In vitro* sugar phosphate levels were determined by integration of the peaks in the sugar phosphate region of spectra of cell extracts.

the compounds in the cell extract. In this way, *in vivo* and *in vitro* spectra were taken at the same time in catabolism of glucose.

Figure 1 shows the ^{31}P NMR spectra of *S. cerevisiae* ATCC 18790 and of perchloric acid extract of the same sample 18 minutes after addition of glucose.

The resonances in the cytoplasm and in the vacuolar compartments corresponding to inorganic phosphorus, have collapsed in only one resonance in the cell extract. This can be more clearly observed in Figure 2 where the sugar phosphate region has been expanded.

It is interesting to note the similarity between the shape of the SP peak in the *in vivo* spectrum with the sum of all the SP resonances in the *in vitro* spectrum. This indicates that the cell extract is qualitative consistent with the *in vivo* state. Thus, the extraction procedure was performed satisfactorily. In several initial tries, the cell extract spectrum was considerably different from the *in vivo* spectrum not only in the SP region but also in the adenosine nucleotide region. This indicated that something went wrong in the extraction procedure. It was necessary to optimize the methodology in order to obtain cell extracts that were representative of the intracellular content. Similar spectra, but for *S. cerevisiae* D603 are shown in Figure 3.

Concentration ratios for the cell extract and for the *in vivo* determination using the deconvolution method are shown in Table 1 and in Figure 4. The correlation coefficient is $r^2 = 0.96$ indicating a good agreement between the two methods.

TABLE I: Comparison of cell extract vs. *in vivo* determinations.

	F6P/G6P	3-PGA/FdP	G6P/ <i>beta</i> -FdP	α -FdP/ β -FdP
18790 <i>in vivo</i>	0.42	0.21	0.18	0.10
cell extract	0.46	0.23	0.17	0.08
D603-a <i>in vivo</i>	0.30	0.12	0.59	0.08
cell extract	0.034	0.08	0.63	0.11
D603-b <i>in vivo</i>	0.45	0.26	0.84	0.10
cell extract	0.51	0.31	0.80	0.15
